Medial Olivocochlear Efferent (MOC) Effects on Stimulus Frequency Otoacoustic Emissions (SFOAEs) and Auditory-Nerve Compound Action Potentials (CAP) in Guinea Pigs

by

Maria Andrey Berezina

B.S. Electrical Engineering

University of Massachusetts Lowell, 2008

Submitted to the Harvard-MIT Division of Health Sciences and Technology in partial fulfillment of the requirements for the degree of

Doctor of Philosophy in Biomedical Engineering

at the

MASSACHUSETTS INSTITUTE OF TECHNOLOGY

February 2015

Signature of Author: Signature redacted

Harvard-MIT Division of Health Sciences and Technology
October 31st, 2014

Certified by: Signature redacted

John. J. Guinan Jr.,PhD
Professor of Otology and Laryngology, Harvard Medical School
Thesis Supervisor

Accepted by: Signature redacted

Emery N. Brown, MD, PhD
Professor of Computational Neuroscience and Health Sciences and Technology
Director, Harvard-MIT Program in Health Sciences and Technology

Medial Olivocochlear Efferent (MOC) Effects on Stimulus Frequency Otoacoustic Emissions (SFOAEs) and Auditory-Nerve Compound Action Potentials (CAP) in Guinea Pigs

by

Maria Andrey Berezina

Submitted to the Harvard-MIT Division of Health Sciences and Technology on October 31st, 2014, in partial fulfillment of the requirements for the degree of Doctor of Philosophy in Biomedical Engineering

Abstract

In humans, SFOAEs can non-invasively assess MOC strength and, may predict the MOC reduction of damage from traumatic sounds. However, the functionally important MOC effect is inhibition of auditory-nerve (AN) responses. Understanding the relationship between MOC effects on SFOAEs and AN CAPs is important for understanding SFOAE generation and for development of clinical tools that use these measures. This thesis presents several novel data sets that address MOC effects on SFOAEs, CAPs and the relationship between them in guinea pigs.

Classic theory indicates that SFOAEs come from cochlear irregularities that coherently reflect energy at the peak of the traveling wave (TW), and that reflected energy arrives in the ear canal as a single wave at certain delay. Contrary to theory, in humans and chinchillas there have been reports of SFOAEs having multiple components with different delays, and that low-frequency SFOAE delays are too short. The first thesis aim used time-frequency analysis to show that guinea pigs have frequency regions over which SFOAEs appear to have multiple components. However, we argue that the multiple components can be a simple result of variations in the patters of irregularities near the TW peak and are not necessarily indicative of multiple SFAOE sources. From comparison of our SFOAE delays with previously reported neural delays, we hypothesize that short SFOAE delays at low frequencies arise from a cochlear motion with a group delay shorter than the TW group delay.

Aim 2 investigated how SFOAEs are affected by brainstem electrical stimulation of MOC fibers and found that MOC activation sometimes inhibited and sometimes enhanced SFOAEs. MOC stimulation always decreased CAP sensitivity which rules out SFOAE enhancement from increased cochlear amplification. We propose that shock-evoked MOC activity increases cochlear irregularity which results in increased SFOAE amplitudes.

Aim 3 investigated the relationship between MOC effects on SFOAEs and tone-pip-evoked AN CAPs at same frequency and sound level. The ratio of the MOC effect on the SFOAE to the MOC effect on the CAP showed a highly-significant decrease ($p<0.001$) as the strength of MOC stimulation was increased. Although this observation was unexpected, several hypothesis to explain it are presented.

Thesis Supervisor:
John J. Guinan Jr., PhD
Title: Professor of Otology and Laryngology and Health Sciences & Technology, HMS

Acknowledgments

This work could not have been completed without support and advice from number of people and agencies.

First and foremost I would like to thank my adviser Dr. John J. Guinan Jr.who has kindly and generously shared his knowledge with me over the last six years. I feel honored to have been able to conduct my thesis work under his supervision and will forever be grateful to him for the effort and time he has put into making me a better scientist.

I would also like to thank my thesis committee Dr. Christopher A. Shera, Dr. M. Christian Brown and Dr. David Mountain. These people have provided valuable feedback over number of years and I could not be more grateful for their time and advice.

Some of this work is based on simulated SFOAE data and chinchilla SFOAE data that were generously provided by Dr. Christopher A. Shera and Dr. Jonathan Siegel respectively. I want to thank them for sharing these data.

Over the years I have been supported by NSF Graduate Research Fellowship and SHBT Training Grant (T32 DC00038). This work was also supported by R01 DC000235 and P30 DC005209.

I want to thank my family for their endless support and love. My parents have always been there for me. I have also been blessed with most amazing brothers who have supported and encouraged me on over the years and I will always be grateful to them.

Last but not least, I could not have done any of this work without the inspiration, love and happiness that my husband, Matt, and my kids, Gambit and Vivian, bring me. I also cannot imagine completing this work without the clarity, reason and calmness that Matt gives me.

Table of Contents

List of Figures

Chapter 1: Introduction

1.1 General Background

Basic Hearing Anatomy and Physiology

The peripheral hearing system consists of the outer, middle and inner ear. The outer ear leads to the boney ear canal that terminates with the tympanic membrane. The tympanic membrane is connected to the malleus, one of the three middle ear ossicles. The malleus is connected to the incus which is connected to the stapes. Finally, the stapes is connected to inner ear or cochlea. The cochlea is a fluid filled organ that consists of three spaces, called scale: scale vestibuli, scale media and scale tympani. The end of cochlea that interfaces with middle ear is called the basal end, while the other end is called the apex. Scala vestibuli in the basal end of the cochlea contains the oval window which holds the stapes footplate. The stapes footplate's contact with scala vestibuli enables middle-ear vibrations to be transmitted to the cochlear fluid. Scala tympani in the basal end of cochlea contains the round window which is covered by a thin, elastic membrane. In the apex of the cochlea, scala vestibule and scala tympani are connected through a passage called the helicotrema. Scala vestibuli and scala media are separated by Reissner's membrane, which is a thin membrane that provides electrical and chemical separation, but allows these two compartments to act as a single chamber for sound-frequency pressure waves and fluid displacement. Scale media and scala tympani are separated by the basilar membrane (BM), a thick membrane whose stiffness is a dominating feature in the cochlear mechanical response to sound. The sensing organ of hearing, the organ of Corti (Fig 1), is located along the top (the scala media, scala vestibuli side) of the basilar membrane.

When a sound pressure wave reaches the ear, it causes a displacement of the ear drum, which propagates along middle ear ossicles and causes the displacement of the stapes, which, results in a pressure wave inside the inner ear. The high compliance of the round-window nulls (or shunts out) the fast pressure wave near the round window, which causes a pressure difference across the BM that initiates a slow traveling wave (TW) along the BM.

The mechanical properties of BM (primarily its stiffness) vary along the cochlear length so that different locations are tuned to different frequencies. The cochlear base is tuned to high frequencies and more apical cochlear locations are tuned to lower frequencies. For all

frequencies the TW propagates to, and peaks at, the location that is best tuned to the frequency of the sound; past that point the TW rapidly decays. The TW at the best frequency place is referred to as the peak of the TW, while the region of TW basal to the peak region is referred to as basal part of TW. Since the TW decays rapidly apical to the peak region, there is nothing called the apical TW.

A cross section of organ of Corti is illustrated in Figure 1. Two types of sensing hair cells are involved in hearing: inner hair cells (IHCs) and outter hair cells (OHCs). IHCs have a sensing stereocilia bundle on the apical part of the cell and are innervated by auditory nerve fibers at basal part of the cell. These cells are responsible for sending information about sound to the brain. Mechanical stimulation of the stereocilia of an IHC results in IHC neurotransmitter release and excitation of the auditory nerve fibers that innervate the IHC. Like IHCs, the apical parts of OHCs have steroecilia bundles, however unlike IHCs, the tallest stereocillia of an OHC's hair bundles are embedded into the tectorial membrane, a gelatinous membrane atop of organ of Corti (Fig 1). The cell wall of OHCs contains a unique protein, prestin, which changes its conformation when the membrane voltage of the OHC is changed. When the stereocillia of OHCs are deflected and the OHC membrane voltage is changed, OHCs change their length, a phenomenon called "electromotility". During sound stimulation, in the peak region of the traveling wave, OHC electromotility actively couples energy into BM motion and amplifies the traveling wave. This phenomenon is called "cochlear amplification" and is critical for the normal sensitivity of hearing. The basal parts of OHCs are innervated by medial olivocochlear (MOC) efferent neurons, neurons that originate in the brainstem and allow the brain to control the sensitivity of the cochlea. Activation of MOC neurons results in a decrease of OHC motility and a resultant decrease of cochlear amplification.

Otoacoustic Emissions

Otoacoustic emissions (OAEs) are sounds generated within the cochlea that can be recorded in the ear canal as acoustic signals. OAEs were first discovered by Kemp (Kemp 1978) and since then have become a widely used clinical and research tool. In addition to emissions that occur without any sound stimulus, called spontaneous otoacoustic emissions (SOAEs), there are three types of sound-evoked OAEs emissions: distortion product OAEs (DPOAEs), stimulus frequency OAEs (SFOAEs) and transient evoked OAEs (TEOAEs). DPOAEs arise from

cochlear non-linearities when two primary probe tones f1 and f2 are presented (f2 > f1). Cubic distortion at the frequency 2f1-f2 is the most prominent distortion product and the one most commonly used both scientifically and clinically (e.g. for hearing screening). SFOAEs are produced by presenting a single probe tone to the ear and recording an emission of that same frequency in the ear canal. TEOAEs are evoked using a click or a brief tone-burst stimulus. All of these emission types arise via two generating mechanisms: distortion and reflection (Shera and Guinan, 1999). Distortion emissions arise from nonlinearities in the mechanical properties of cochlea, in particular, from the non-linearity in the mechanical-to-electrical transduction (MET) of OHC stereocilia. Stimulation of OHCs by a sound that produces MET distortion, results in the OHCs acting as source of backward-traveling waves that course backwards through the middle ear and create DPOAEs. Reflection emissions, according to "coherent reflection theory", arise as a result of the coherent reflection of energy in the traveling wave due to reflections from many mechanical irregularities along the cochlea (Zweig and Shera, 1995). These irregularities include both random perturbations in cochlear anatomy and irregularities associated with differences in the motility of individual OHCs (which may be the main contributors to the irregularities that produce coherent reflection). Irregularities are present throughout entire length of the cochlea and produce many reflected wavelets. Most reflections combine out-of-phase and cancel each other out, however in the peak region of the envelope of traveling wave there usually exists a region over which the effective scatter produces reflected energy that coherently combines to produce a reflected wave that can be recorded as an otoacoustic emission in the ear canal (Zweig and Shera, 1995).

The phases of evoked OAEs vary in systematic ways with frequency. The phase gradient across frequency yields a metric referred to as the "OAE latency" which contains information about the mechanisms underlying the otoacoustic emission. Emissions generated by distortion sources are sometimes referred to as "wave-fixed" emissions and they have a characteristic shallow slope of their phase gradient which is equivalent to a near-zero group delay and produces only a small accumulation of phase across frequencies. Distortion sources follow the traveling wave (TW) and because the TW shape does not change much with stimulus frequency, the phase of the OAE generated by a distortion source does not change much with frequency. If the cochlea were perfectly scaling symmetric, then distortion-component group delays would be

zero (Shera and Guinan, 1999). However, the cochlea is not perfectly scaling symmetric so distortion component group delays are near, but not exactly, zero. In contrast, emissions generated by reflection sources are sometimes referred to as place-fixed emission because the reflection points don't move as the peak of the traveling wave moves, and they have a characteristic rapid accumulation of phase (i.e. a steep phase-gradient) as stimulus frequency is changed. Reflection sources are due to scatter of TW energy from placed-fixed irregularities. As stimulus frequency is lowered and the TW peak is swept across irregular reflectors along the cochlea, the delay increases at which the wavelet phases coherently add, primarily because the TW amplitude and phase shapes change little and lower frequencies have longer periods.

The relationship between evoking stimuli and OAE generating mechanisms are well defined theoretically, i.e. DPOAEs are generated by distortion sources, while SFOAEs and TEOAEs are generated by reflections sources. However, in real ears emissions are often generated by a mixture of sources. Most prominently, 2f1-f2 DPOAEs in humans have been shown to be generated by the combination of a distortion source near the f2 place and a reflection source at the 2f1-f2 place (Shera and Guinan, 1999, Talmadge et al., 1999). These two types of DPOAE sources have different group delays and in humans their amplitudes are nearly equal so their addition results in interference that produces a prominent fine structure in DPOAE magnitude across frequency. Because the components have different group delays, time-frequency analysis techniques can be applied to DPOAEs to separate emission components that arise via different generating mechanisms (Dhar et al., 2011, Long et al., 2008). Similarly, SFOAEs and TEOAEs can have emission components that are produced by a distortion source, particularly for tones or transient sounds at high sound levels that can push OHC stereocilia far into the saturating regions of their transduction functions (Talmadge et al., 2000).

Both distortion and reflection sources are closely associated with OHC motility, which is believed to be main motor for cochlear amplification of the traveling wave. Irregularities in the strengths of individual OHCs are thought to be one of the main sources of energy reflection for emission arising via reflection sources. Distortion sources arise from the non-linear transduction of OHCs and this transduction is driven by the motion of the organ of Corti, so DPOAEs are also dependent on cochlear amplification. Because their amplitudes depend on cochlear amplification, OAEs can thus be potentially used to study cochlear amplification.

Medial Olivocochlear Efferents

Medial olivocochlear (MOC) fibers originate in the medial part of the superior olivary complex in the brainstem and terminate on OHCs in the cochlea. Each cochlea receives MOC fibers originating from the ipsilateral brainstem via the uncrossed olivocochlear bundle and MOC fibers originating from the contralateral brainstem via the crossed olivocochlear bundle. Activation of MOC neurons results in hyperpolarization of OHCs which decreases their effective motility and translates into a decrease of cochlear amplification. MOC neurons can be activated by sound stimulation in the contralateral or ipsilateral ears or by electrical stimulation at the midline of the floor of 4^{th} ventricle in the brainstem. Activation of MOC neurons turns down the gain of the cochlear amplifier (Murugasu and Russell 1996, Dolan et al., 1997, Guinan and Cooper 2003, Cooper and Guinan 2006) and results in inhibition of auditory nerve fiber responses (Guinan and Gifford 1988a, Guinan and Stankovic 1996). Activation of MOC efferents provides a way to change the mechanical properties of the cochlea reversibly and through action on a known part (OHCs).

1.2 Thesis Aims and Motivation

OAEs are widely used in both research and in the clinic. As a non-invasive measure that indirectly represents active cochlear amplification, there is value in trying to understand the mechanisms of OAE generation so that they can be effectively used for diagnostic and research purposes. In particular, there has been great effort aimed at understanding the different sources that generate emissions and methods for effectively separating them.

We are concerned in this thesis with several interrelated scientific issues pertaining to OAE generation. First, in the apical part of the cochlea the SFOAE group delay predicted by coherent-reflection theory is longer than the SFOAE group delay experimentally measured in animals. Measured SFOAE delays at low frequencies in guinea pigs and cats are shorter than predicted (Shera and Guinan 2003). The discrepancy has also been shown to exist in chinchilla ears (Siegel et al., 2005, Shera et al., 2008). A second issue is where SFOAEs originate relative to the traveling wave (TW) peak. SFOAEs are often measured by suppressing them with a second tone called a "suppressor tone". When the second tone is more than an octave higher than the SFOAE generating probe tone, it still produces a probe-tone-frequency residual. To explain this, it has been hypothesized that SFOAEs are generated over a broad cochlear region that includes the

basal (non-amplified) part of the TW (Guinan 1990, Siegel et al., 2003). An alternate interpretation for far-basal suppressor-tone-residuals is that they are due to nonlinear effects at the peak of the suppressor-tone response that are present only when the suppressor is present (Shera et al., 2004). Large SFOAEs components that originate far basal of the traveling-wave peak can be produced in a model if the irregularities are spatially low-pass filtered (Choi et al., 2008). The presence of small SFOAE components that originate far basal of the traveling wave peak is expected from coherent reflection theory, however, the existence in live animals of large SFOAE components that originate far basal of the traveling wave peak has not been convincingly demonstrated experimentally. Finally, models predict, and some data suggest, that when the sound pressure level is raised sufficiently, cochlear nonlinearity will create wave-fixed distortion at the SFOAE frequency, and that these distortion components have near zero group delay (Goodman et al., 2003, Goodman et al., 2011, Talmadge et al., 2000).

Another issue revolves around whether, at some frequencies, SFOAE and TEOAE energy arrive in the ear canal not at a single delay but with multiple delay peaks (or components). In humans, a time-frequency analysis of SFOAEs and TEOAEs has suggested the presence of long latency and shorter latency components (Moleti et al., 2013; Sisto et al., 2013; Goodman et al., 2011). It has also been suggested that in chinchillas the discrepancy between measured and predicted group delay at low frequencies may be the result of the presence of two components with different group delays (Shera et al., 2008). The link between these two issues comes from the hypothesis that in the cochlear apex measured SFOAE delays are shorter than the delays predicted by theory because of the presence of an additional short-latency reflection component, i.e. as a result of apical SFOAEs having multiple components.

The first two aims of this dissertation address the issues pertaining to SFOAE generation that are described above. The goal of the first aim is to understand whether SFOAEs in guinea pigs show evidence of having multiple reflection components, as was reported in humans (Moleti et al., 2013). This goal was achieved by collecting an extensive body of SFOAE data in guinea pigs and developing a time-frequency analysis technique that, unlike the traditional phase-gradient method, can reveal multiple SFOAE components with different delays. The goal of the second aim was to try to understand the generating mechanisms for SFOAEs and SFOAE components. This was done by collecting SFOAE data with electrical stimulation of MOC efferent fibers that

turn down the gain of cochlear amplification. As was mentioned above, it has been proposed that, contrary to coherent reflection theory, substantial SFOAE energy is generated by reflection of energy from the basal part of the traveling wave (TW), a part of the TW that is not amplified. Considering this, determining whether SFOAEs and SFOAE components are affected by turning down cochlear amplification via MOC stimulation will be informative as to whether some of SFOAEs are generated in the basal part of the TW that does not receive cochlear amplification.

Understating how MOC activity affects SFOAEs also has clinical value. There is evidence that MOC efferents have an important role in the protection of hearing from damage due to traumatic sounds. Loud sounds can result in permanent elevation of hearing thresholds due to mechanical damage to the stereocilia of outer hair cells (Liberman and Dodds 1984) which results in a decrease in cochlear amplification. In animals it has been shown that MOC efferents can protect from such damage. Across a population of animals the amount of damage is negatively correlated with the strength of the MOC acoustic reflex (Maison and Liberman 2000). Because this protection depends on the strength of the MOC reflex, the development of clinical techniques for evaluating the strength of the MOC reflex is of interest. MOC effects on SFOAEs can be used as a non-invasive measure of the strength of the MOC effect. DPOAEs have been used to study MOC effects in laboratory animals (Maison and Liberman 2000, Liberman et al., 1996). In animals, DPOAEs are predominantly due to the distortion component (Zurek, 1985; Withnell et al., 2003). However, MOC-induced changes in DPOAEs in humans can be difficult to interpret because, in humans DPOAEs are generated by two mechanisms, distortion and reflection, each with nearly equal contributions to the DPOAE, and these two components can cancel in the ear canal. In contrast, at low sound levels, SFOAEs are generated by a single mechanism (reflection) and may be better suited for quantifying the effects of MOC stimulation; this, however, is something that needs to be determined experimentally and is one of the motivations for Aim 2.

Recently it has been shown that exposure to sounds that result in temporary elevations in the threshold of hearing (temporary threshold shifts, or "TTS") can result in long-term permanent loss of auditory nerve fibers (auditory neuropathy) (Kujawa and Liberman, 2009; Liberman et al., 2014). In animals electrical stimulation of MOC efferents produces a reduction of TTS, and since TTS can lead auditory neuropathy, this suggests that MOC activity may protect from

auditory neuropathy (Rajan 1988, Liberman et al., 2014). If the relationship between MOC effects on SFOAEs and MOC effects on auditory nerve fibers is understood (the goal of Aim 3), then this may enable MOC effects on SFOAEs to be used to estimate how well MOC activity protects from auditory neuropathy.

The goal of the third aim was to systematically compare MOC effects on SFOAEs and auditory-nerve compound action potentials (CAPs) at various frequencies. This aim was done by collecting SFOAE level functions and tone-pip CAP level functions, both with and without MOC stimulation. Tone-pip CAPs are gross neural responses that, at low sound levels, originate from the cochlear frequency region of the tone-pip. In experimental animals, CAPs can be measured with silver wire placed near the round window of the cochlea. The CAP is a gross neural measure that integrates neural responses across the auditory nerve fibers that respond to the stimulus. Thus, the results of this aim will allow comparison of MOC effects on mechanical and neural responses.

The results from the third aim can also be useful in understanding backward propagation of the traveling wave. In some cochlear models the cochlear-amplifier gains imparted to the forward and backward traveling waves are assumed to be nearly equal (e.g. Zweig, 1991, Zweig and Shera, 1995), while in others the gain received by the backward traveling wave is different from gain received by forward traveling wave (e.g. Yoon et al., 2011). The MOC effect on N1-CAPs at threshold levels is representative of the gain reduction that the forward traveling wave receives. SFOAEs recorded in ear canal are a product of both forward and backward traveling waves and will be affected by whatever cochlear-amplifier gain these traveling waves receive. Because of this, the MOC effect on SFOAEs, at low sound levels where SFOAEs grow linearly, is expected to show how much the MOC activity reduced the cochlear amplifier gain of both forward and backward traveling waves.Thus, a comparison of the MOC induced level shifts in auditory-nerve CAPs and in SFOAEs at threshold levels can potentially be used to determine whether and how much backward traveling waves are amplified.

It is important to note that evaluating MOC effects on OAEs has clinical value beyond determining the strength of the MOC effect. MOC effects on OAEs can be potentially used to monitor clinical conditions in humans, e.g. monitoring changes in hearing due to drug administration. MOC effects on OAEs may also be useful in cognitive research as a means of

monitoring effects of attention and learning on auditory task performance. Results from the second and third aims of this thesis provide basic knowledge that should help interpretation of data in these clinical applications.

1.3 References

Choi Y.S., Lee S.Y., Parham K., Neely S.T., Kim D.O., 2008. Stimulus-frequency otoacoustic emission: measurements in humans and simulations with an active cochlear model. J Acoust Soc Am 123, 2651–69

Cooper N.P., Guinan J.J., Jr., 2006. Efferent-mediated control of basilar membrane motion. J Physiol. 576, 49–54

Dhar, S., Rogers, A., and Abdala, C., 2011. Breaking away: Violation of distortion emission phase-frequency invariance at low frequencies. J. Acoust. Soc. Am. 129, 3115–3122.

Dolan D.F., Guo M.H., Nuttall A.L., 1997. Frequency-dependent enhancement of basilar membrane velocity during olivocochlear bundle stimulation. J Acoust Soc Am. 102, 3587–3596.

Fettiplace R., Hackney C.M., 2006 The sensory and motor roles of auditory hair cells. Nat. Rev. Neurosci., 7, 19–29

Goodman, S.S., Withnell, R.H., Shera, C.A., 2003. The origin of SFOAE microstructure in the guinea pig Hear Res 183, 7–17

Goodman, S.S., Mertes, I.B., Scherer, M.P., 2011. Delays and growth rates of multiple TEOAE components In: Shera CA, Olson ES, (eds) What Fire is in Mine Ears: Progress in Auditory Biomechanics, Vol 1403 American Institute of Physics, Melville, New York, USA pp. 279–285

Guinan, J.J. Jr, 1990. Changes in stimulus frequency otoacoustic emissions produced by two-tone suppression and efferent stimulation in cats In: Dallos, P, Geisler, CD, Matthews, JW, Steele, CR, (Eds), Mechanics and Biophysics of Hearing, Springer Verlag, Madison, Wisconsin, pp. 170–177

Guinan J.J., Jr, Cooper N.P., 2003. Fast effects of efferent stimulation on basilar membrane motion. In: Gummer AW, editor. The Biophysics of the Cochlea: Molecules to Models. Singapore: World Scientific; pp. 245–251.

Guinan J.J., Jr, Gifford M.L., 1988 Effects of electrical stimulation of efferent olivocochlear neurons on cat auditory-nerve fibers. III. Tuning curves and thresholds at CF. Hear Res. 37, 29–45.

Guinan, J.J., Jr., Stankovic, K.M., 1996. Medial efferent inhibition produces the largest equivalent attenuations at moderate to high sound levels in cat auditory-nerve fibers. J Acoust Soc Am 100, 1680-90.

Kemp, D. T., 1987. Stimulated acoustic emissions from within the human auditory system. J Acoust Soc Am 64, 5-1386.

Kujawa S.G., Liberman M.C., 2009. Adding insult to injury: cochlear nerve degeneration after "temporary" noise-induced hearing loss. J Neurosci. 29(45):14077–14085.

Liberman M.C., Dodds L.W., 1984 Single-neuron labeling and chronic cochlear pathology. III. Stereocilia damage and alterations of threshold tuning curves. Hear Res 16:55–74.

Liberman M.C., Puria S., Guinan J.J., 1996. The ipsilaterally evoked olivocochlear reflex causes rapid adaptation of the 2f1–f2 DPOAE. J Acoust Soc Am 99:3572–3584.

Liberman MC, Liberman LD, Maison SF, 2014. Efferent Feedback Slows Cochlear Aging. J Neurosci. 34(14):4599–4607.

Long, G.R., Talmadge, C.L., and Lee, J., 2008. Measuring distortion product otoacoustic emissions using continuously sweeping primaries. J. Acoust. Soc. Am. 124, 1613–1626.

Maison S.F., Liberman M.C., 2000. Predicting vulnerability to acoustic injury with a non-invasive assay of olivocochlear reflex strength. J Neurosci 20: 4701–4707

Moleti, A, Mohsin Al-Maamury, A, Bertaccini, D, Botti, T, Sisto, R 2013. Generation place of the long-and short-latency components of transient-evoked otoacoustic emissions in a nonlinear cochlear model. J Acoust Soc Am 133, 4098–108

Murugasu E, Russell I.J., 1996. The effect of efferent stimulation on basilar membrane displacement in the basal turn of the guinea pig cochlea. J Neurosci. 16, 325–332.

Rajan R., 1988 Effect of electrical stimulation of the crossed olivocochlear bundle on temporary threshold shifts in auditory sensitivity. I. Dependence on electrical stimulation parameters. J Neurophysiol 60:549 –568.

Shera, C.A., Guinan, J.J. Jr 1999. Evoked otoacoustic emissions arise by two fundamentally different mechanisms: A taxonomy for mammalian OAEs. J Acoust Soc Am 105, 782–798

Shera, C.A., Guinan, J.J. Jr 2003. Stimulus-frequency-emission group delay: a test of coherent reflection filtering and a window on cochlear tuning. J Acoust Soc Am 113, 2762–72

Shera, C.A., Tubis, A, Talmadge, C.L., Guinan, J.J. Jr., 2004. The dual effect of "suppressor" tones on stimulus-frequency otoacoustic emissions Assoc Res Otolaryngol Abstr 27, Abs 776

Shera, CA, Tubis, A, Talmadge, C.L., 2008. Testing coherent reflection in chinchilla: Auditory-nerve responses predict stimulus-frequency emissions. J Acoust Soc Am 123, 3851

Siegel, J.H., Temchin, A.N, Ruggero M., 2003. Empirical estimates of the spatial origin of stimulus-frequency otoacoustic emissions J Assoc Res Otolaryngol 26, 172 (#679)

Siegel J.H., Cerka A.J., Recio-Spinoso A., Temchin A.N., van Dijk P., Ruggero M., 2005. Delays of stimulus-frequency otoacoustic emissions and cochlear vibrations contradict the theory of coherent reflection filtering. J Acoust Soc Am 118, 2434–2443

Sisto R, Sanjust F, Moleti A., 2013. Input/output functions of different-latency components of transient-evoked and stimulus-frequency otoacoustic emissions, J Acoust Soc Am 133, 2240–53

Talmadge, C. L., Long, G. R., Tubis, A., and Dhar, S., 1999. Experimental confirmation of the two-source interference model for the fine structure of distortion product otoacoustic emissions. J. Acoust. Soc. Am. 105, 275–292.

Talmadge, C.L., Tubis, A., Long, G.R., Tong, C., 2000. Modeling the combined effects of basilar membrane nonlinearity and roughness on stimulus frequency otoacoustic emission fine structure. J Acoust Soc Am 108:2911–2932

Withnell, R. H., Shaffer, L. A., & Talmadge, C. L. 2003. Generation of DPOAEs in the guinea pig. Hear Res *178*(1), 106-117.

Yoon, Y.J., Steele, C.R., Puria, S. 2011. Feed-forward and feed-backward amplification model from cochlear cytoarchitecture: an interspecies comparison. Biophys J 100, 1-10.

Zurek, P.M. 1985. Acoustic emissions from the ear: A summary of results from humans and animals. J. Acoust. Soc. Am. 78, 340-344.

Zweig, G. 1991. Finding the impedance of the organ of Corti. J. Acoust. Soc. Am. 89, 1229-1254.

Zweig G, Shera C.A., 1995. The origin of periodicity in the spectrum of evoked otoacoustic emissions J Acoust Soc Am 98, 2018–2047

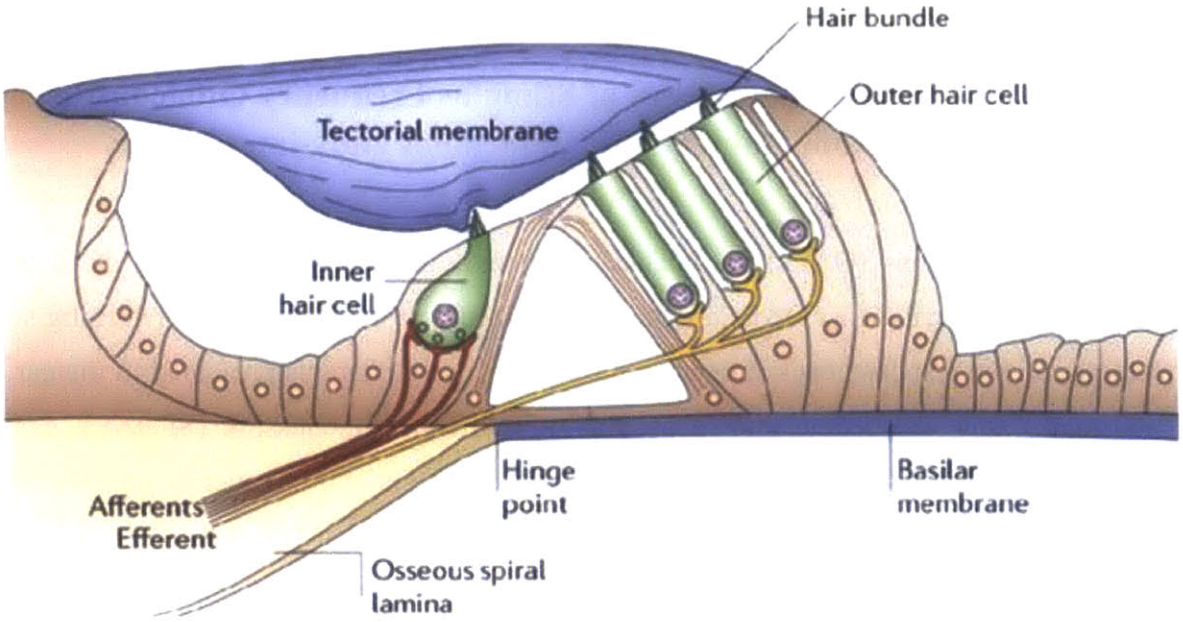

Figure 1.1: A cross-section of the organ of Corti

A transverse section through a middle turn of the cochlea, From Fettiplace and Hackney 2006)

Chapter 2: Time-Frequency Analysis of Stimulus Frequency Otoacoustic Emissions (SFOAEs) from Guinea Pigs, Chinchillas and Simulations.

2. 1 Introduction

Otoacoustic emissions (OAEs) are cochlear responses in the form of sounds that can be recorded in the ear canal. Most OAEs are the result of cochlear active processes returning some of the energy in the response back into ear canal. When a single tone is presented to the ear, an emission at the tone frequency, known as a stimulus frequency emission (SFOAE), can be recorded. The amplitudes and phases of SFOAEs vary with stimulus frequency and provide a non-invasive way to assess the cochlea and its mechanics. The change in SFOAE phase with frequency, quantified as a group delay, has been used for a number of applications, e.g. to understand SFOAE generation mechanism (Shera & Guinan, 1999) or to determine characteristics of peripheral frequency selectivity (Shera et al., 2002, 2010).

SFOAE group delays have traditionally been obtained from the gradient across frequency of the rotating SFOAE phase. Various optimizations for obtaining phase-gradient delays have been used, such as applying different weights to individual phase points depending on the corresponding SFOAE amplitude, or calculating average phase-gradient delays only near the peaks of the emissions (Shera and Bergevin, 2012). Although, methods for obtaining SFOAE delay from phase-gradients sometimes use the SFOAE magnitude, this information is not used as much as it could be and most methods are constrained to produce a single delay value per frequency.

A broader picture of the time-course of the arrival of SFOAE energy in the ear canal can be revealed using a time-frequency analysis of SFOAE data. The basic idea of an SFOAE time-frequency analysis is that the SFOAE distribution across frequency can be thought of as the ***transfer function*** of the mechanical processes involved in SFOAE generation. The transfer function of a system is the ratio of the output of a system to the input to the system as a function of frequency, with the output and input expressed as complex numbers (i.e. numbers that include both amplitude and phase). The SFOAE at each frequency is experimentally obtained by presenting a probe tone to the ear and measuring the ear's SFOAE response at the probe-tone frequency. The SFOAE at a given frequency can thus be thought of as the value of the transfer

function of the ear at that frequency. With this reasoning in mind, the inverse Fourier Transform (IFFT) of a segment of the complex SFOAE frequency response, a transformation from the frequency domain into the time domain, yields the impulse response function for that frequency segment. This impulse response provides information about the timing and amplitude of the energy in the SFOAE from this frequency segment. Unlike a group delay from the phase-gradient, a time-frequency analysis can reveal energy arriving at different delays.

According coherent reflection theory, SFOAEs are generated from cochlear irregularities that coherently reflect energy in the broad, tall peak of the traveling wave (Zweig and Shera 1995). This coherently reflected energy normally arrives in the ear canal as a wave with a single latency that increases as tone frequency decreases (Zweig and Shera 1995). Measurements of SFOAEs and their group delay, however, show a more complicated picture. Although data from the base fits the theory well (Shera and Guinan 2003, Shera et al., 2008), in the apical half of the cochlea the SFOAE phase-gradient delays are shorter than predicted by coherent reflection theory in cats, guinea pigs (Shera and Guinan 2003) and chinchillas (Siegel et al., 2005). It has been suggested that the short apical SFOAE delays may be due to energy that travels backward in the cochlea by fast pressure waves (Ren 2004, Ruggero 2004), however some SFOAE phase-gradient delays are too short for this (Siegel et al., 2005), and there is no evidence for backward fast waves. A suppressor tone an octave or more above the SFOAE tone elicits a residual at the SFOAE frequency and this has been taken to mean that some SFOAEs components are generated far basal of the traveling wave peak (Guinan 1990; Siegel et al., 2003). An alternate interpretation of far-basal suppressor-tone-residuals is that they are due to nonlinear effects at the peak of the suppressor-tone response that are present only when the suppressor is present (Shera et al., 2004). Large SFOAEs components that originate far basal of the traveling-wave peak can be produced in a model if the irregularities are spatially low-pass filtered (Choi et al., 2008). The presence of *small* SFOAE components that originate far basal of the traveling wave peak is expected from traditional coherent reflection theory (Zweig and Shera 1995). However, the existence in live animals of *large* SFOAE components that originate far basal of the traveling wave peak has not been convincingly demonstrated experimentally. Finally, models predict that when the sound pressure level is raised sufficiently, cochlear nonlinearity will create wave-fixed distortion at the SFOAE frequency, and that these distortion components have near zero group

delay (Goodman et al., 2003; Goodman et al., 2011; Talmadge et al., 2000). This nonlinear distortion is another possible source of the short-latency SFOAEs found in the apex.

Another kind of explanation for short-latency SFOAE group delays from the cochlear apex is that these SFOAE components arise from coherent reflection from an apical cochlear motion that has a shorter group delay than the basilar-membrane traveling wave. Evidence for a short latency motion in the cochlear apex comes from (1) the shorter group delays found in the side-lobes (re the main lobe) of tuning curves from low-frequency auditory nerve fibers (Kiang, 1984), and (2) the short latency of the Auditory-Nerve-Initial-Peak (ANIP) response that has been shown to be a separate motion from the traveling wave by its strong selective inhibition by stimulation of medial olivocochlear efferents (Guinan et al., 2005; Guinan and Cooper, 2008).

In humans, a time-frequency analysis of SFOAEs has suggested that there is a long-latency component that grows compressively and originates near the traveling-wave peak, as well as a shorter-latency component that grows more linearly and is estimated to originate 2 mm (~1/3 octave) basal to the traveling-wave peak (Moleti et al., 2013; Sisto et al., 2013). Both of these components originate from the peak region of the traveling wave, despite one being called "basal". Although two peaks can be distinguished in some subjects, it is not clear how distinct these peaks are across subjects. Cochlear regions an octave or more basal to the traveling wave peak do not receive cochlear amplification so any SFOAE components that originate from these basal regions should grow linearly with sound level. The more apical SFOAE component distinguished in humans grew compressively and was presumed to arise from the peak region of the traveling wave (Sisto 2013). In contrast, the more-basal SFOAE component grew more linearly, which is consistent with it originating somewhat basal to the traveling wave peak.

Understanding the mechanisms of SFOAE generation is valuable for at least two reasons. First, SFOAEs have the potential of being used in clinical settings because they provide information about cochlear amplification and are easily and non-invasively measured in humans. Second, SFOAEs can be used to study medial olivocochlear (MOC) efferent effects in humans. Historically, DPOAEs have used in animals to study MOC effects for clinically relevant issues (Maison and Liberman 2000, Liberman et all 1996). However, the fact that DPOAEs are generated by two mechanisms obscures the interpretation of results using DPOAEs when DPOAEs are used in humans because in humans components from both mechanisms are

important and may cancel. According to coherent-reflection theory, SFOAEs are generated by single mechanism which should make them better suited for use with MOC stimulation. However this is something that needs to be determined experimentally and determining whether SFOAEs are generated by a single mechanism is the main motivation for the work presented in this chapter.

To help shed light on the mechanisms that produce SFOAEs, and why their group delays are shorter than expected in the apex, we (1) measured SFOAEs in guinea pigs at closely-spaced frequencies, (2) did time-frequency analyses of the results, and (3) looked for evidence for multiple SFOAE components that might be distinguished by their delays. For comparison, we did a similar time-frequency analysis on SFOAEs from chinchillas (using the data of Siegel et al., 2005) and on SFOAEs from a simple cochlear model (the model described by Shera and Bergevin, 2012).

2. 2 Methods

2. 2.1 General Methods

SFOAEs were collected using the suppression method (Fig. 2.1, see Guinan, 1990; Shera and Guinan 1999) over a frequency range 0.5 to 10-12 kHz in 83 Hz steps. Suppressor tones (50 ms every 100 ms, 60 dB SPL) at 50 Hz above the probe frequency were superimposed on continuous, 40 dB SPL probe tones. At each probe frequency, responses were averaged over 6-8 s and SFOAEs were calculated from the vector difference between the probe-frequency part of the probe-alone and the probe-plus-suppressor responses. The probe-frequency part of each response was obtained from a Fast Fourier Transform (FFT) of the time-waveform. For each probe frequency, the FFT amplitudes at eight frequencies below and eight frequencies above the probe frequency were averaged as measures of the noise floor. SFOAE vs. probe-tone frequency functions (e.g. Fig. 2.2A) were measured in 26 animals, mostly from one ear in each. Some ears had frequency regions with hearing thresholds at or over 40 dB SPL and were not included in the data analysis. In two animals we obtained data over the 0.5-9 kHz frequency range at sound levels that were varied from 35 to 55 dB SPL in 5 dB steps.

Albino guinea pigs were anesthetized with Nembutal, followed by Fentanyl and Haloperidol (initial dose of 25mg/kg, 0.2 mg/kg and 10mg/kg respectively). Additional doses were given as necessary as judged by reflex withdrawal from toe pinch or change in heart rate. Animals were

tracheotomized and when necessary, mechanically ventilated. Soft tissue around the skull was removed and a head holder bar was cemented to the skull, the ear-canals were truncated and acoustic assemblies were inserted. The heart rate, breath rate, expired CO_2, rectal temperature and electroencephalogram (EEG) were continuously monitored. The rectal temperature was maintained at approximately 37-38 degrees C. The bulla was opened dorso-laterally and a silver wire electrode was placed near round window to monitor the auditory-nerve compound action potential (CAP). Cochlear thresholds were estimated from CAPs in response to tone pips (5 ms duration, 0.5 ms raised-cosign-shaped rise/fall) by an automated up/down procedure which determined the sound level needed to produce 10 μV p-p CAPs at frequencies 1-32 kHz in octave, or less, steps. Experimental protocols were approved by the Mass. Eye & Ear Animal Care Committee.

The chinchilla SFOAE data are from Siegel et al. (2005) and were collected using the suppression method over a frequency region 0.3 to 12 kHz. The probe and suppressor tones had 30 and 55 dB SPL sound pressure levels, respectively, and the frequency of the suppressor was always 43 Hz below the probe tone frequency. The frequency spacing was 21.83 Hz for frequencies from 0.3 to 2 kHz and 43.06 Hz for higher frequencies.

2. 2.2 Time-Frequency Analysis of SFOAEs

A time-frequency analysis based on short-term Inverse Fourier Transforms (stIFFTs), as detailed below, was used to obtain SFOAE components. The analysis was implemented using custom software written in MATLAB (version 7.6.0 R2008a, The MathWorks,Inc.).

The time-domain responses that corresponded to the SFOAEs that originated from restricted cochlear frequency regions were obtained in the following way:

(1) The complex SFOAE vs. probe frequency data were windowed along the frequency axis using the magnitude of a Butterworth-filter transfer function set to have an effective pass-band (i.e. a frequency "window") of 500 Hz (e.g. thin lines in Fig. 2.2 A). This window shape was chosen to reduce time-domain ripple after step 2 (see Section 2.2.3). Response phase values were not changed. Amplitudes more than 850 Hz from the center frequency of each window were set to zero over the range 0-16 kHz. This window was moved along the frequency axis in 83 Hz steps so that it was centered on each frequency in the original data acquisition (the windows overlapped) and each window's result was attributed to that window's center frequency.

(2) Each set of windowed data was Inverse Fast Fourier Transformed (IFFTed) using Matlab's *ifft* function. The magnitude of the complex output of the IFFT was divided by the square root of two to obtain the magnitude (in rms Pascals) vs. latency function or "impulse response" (e.g. Fig. 2.2 D1-D4). This impulse response function represents the arrival over time of SFOAE energy in the ear canal. Energy with a latency over 5 ms was removed with a recursive exponential filter (Kalluri and Shera 2001) because it was mostly noise.

Peaks that may correspond to SFOAE components were identified in each impulse response in the following way:

(1) The change in the sign of the first derivative of the impulse response function was used to detect peaks in the impulse response. Two criteria were then applied to select peaks that may represent SFOAE components. Identified peaks needed to be at least ¼ the size of the maximum IFFT peak and to have a signal-to-noise ratio of at least 15 dB (the noise floor impulse response function was obtained by applying steps 1 and 2 to the noise measurements). We decided on the above criteria by applying the analysis to a number of ears, observing where the noise floors for the two measures were, and then selecting a threshold so that the resulting components were above the noise floor. Example delays of impulse response peaks that passed the criteria are shown in Figure 2.2 C.

(2) The equivalent dB SPLs of the SFOAE components that corresponded to the peaks in (Fig 2.2 B) were obtained from the impulse response plots by separating the peaks with recursive exponential filters set to the time of the dips between the peaks, and then transforming the peaks separated in the time domain back to the frequency domain by an FFT. If, at any center frequency, conversion of a peak from the time domain to the frequency domain produced a SFOAE component with a signal-to-noise ratio (SNR) lower than 6 dB, then for that window frequency, the peak at that latency was removed from being considered a separate peak. Then, transforms of other peaks were repeated without the separation of the removed peak.

Note that Figure 2.2C shows only peaks that satisfied the criteria in the time domain (step 1) and produced component of SNR greater than 6 dB in frequency domain (step 2). Also shown in Figure 2.2 C, is the phase gradient delay obtained from a regression line fit to the phases of the windowed SFOAEs in that segment. The equivalent dB SPLs of the SFOAE peaks in Fig 2.2 C are shown in Fig 2.2 B.

2. 2.3 Selection of Window Shape and Length

Selection of the Analysis Window Shape

To select frequency windows whose IFFTs would yield impulse responses with relatively little time-domain energy splatter, we filtered the SFOAE vs. frequency functions with the magnitude of a band-pass Butterworth filter. The filters were designed using the "*fdesign. bandpass*" and "*design*" functions in Matlab by specifying the following parameters:

- Low- and high-pass frequencies, i.e. frequencies between which the signal received approximately 0 dB attenuation. The frequency region between the pass frequencies is referred to as the pass-band and is effectively the width of the analysis window.
- Low and high stop frequencies: one below the low-pass frequency and one above the high-pass frequency. The frequency region between stop and pass frequencies on either side of the pass-band is referred to as the "attenuation-band".
- Attenuation gain, which is how many dB the signal will be attenuated at the high and low stop frequencies.

The above parameters specified the shape of the transfer function of the Butterworth filter which was then modified to have zero values outside of the attenuation bands. The magnitudes of the modified transfer functions of a series of Butterworth filters centered at each experimental frequency point were used to select the SFOAE segments to be IFFTed.

The shape of the frequency-selection window greatly impacts the resulting impulse response functions as is illustrated in Fig. 2.3 and 2.4. To understand the effects of window shape on the resulting impulse response functions, windows of varying lengths and varying shapes were applied to simulated SFOAEs (SFOAEs with constant 25 dB SPL magnitudes and a constant phase slope of 1.3 ms). The effects of using a Butterworth-shaped window vs. a rectangular window, for windows with 0.5, 0.75 and 1 kHz pass bands, are demonstrated in Fig. 2.3. The important thing to notice in Fig 2.3 is that the rectangular window produces significant ripple, i.e. peaks at times where the signal has no energy, while the Butterworth-shaped windows have reduced ripple patterns.

The attenuation also needs to be optimized for a given window pass-band width. The effects of different attenuation gains, for a window with a 0.5 kHz pass band and 0.6 kHz attenuation-band, are illustrated in Fig. 2.4. Again, the Butterworth-windowed data have less energy at

frequencies far from the center frequency than the rectangular-windowed data. The analysis presented in Figures 2.3 and 2.4 was used in deciding the parameters for the Butterworth filter used to analyze the SFOAEs. All of the data presented in this chapter were analyzed with 0.5 kHz wide frequency windows that had 0.6 kHz attenuation bands with 30 dB attenuation, unless specified otherwise.

Should the Window Length Change as a Function of Frequency?

One of the central methodological issues of time-frequency analysis is how the choice of the analysis window affects the results and whether the window duration should change with frequency. Short-term Fourier transforms and inverse Fourier transforms (stFFTs, and stIFFTs) typically use fixed window lengths. In contrast, Wavelet Transform (WT) methods effectively have variable window lengths. The fundamental difference between two methods is that the stIFT provides constant time-frequency resolution across frequencies, while the WT allows for time-frequency resolution to vary across frequencies. The WT can have good time resolution at high frequencies and good frequency resolution at low frequencies, i.e. wavelets can select narrow frequency regions at low frequencies and select wider frequency region at high frequencies. With this said, the benefits that WT provides over stIFT can be achieved by performing stIFT with analysis windows that vary in length across frequencies. An alternate is to apply the stIFT method multiple times, each with a different frequency window. When the stIFFT analysis is swept across frequencies, a way of varying the window length across frequencies that would keep it in line with the data is to set the analysis window length to be equal to some integral number of phase cycles, rather than a constant value in Hz. The phase of SFOAEs rotates more rapidly at low frequencies compared to high frequencies, so if an analysis window is set to be a single SFOAE cycle, for example, than the analysis window will be narrower in frequency at low frequencies and wider in frequency at high frequencies.

To understand whether it is necessary to vary the analysis window length with frequency, an analysis of the accumulation of SFOAE phase across frequency was done for the SFOAEs from 17 guinea pig ears. In every ear, unwrapped SFOAE phase was plotted from low to high frequency and for each successive one-cycle segment, the center frequency and width of the segment in kHz were obtained. The widths of the segments over which SFOAE phase accumulated one cycle are plotted vs. the center frequencies of the segments in Figure 2.5. This

plot demonstrates how the width of an analysis window would change across frequency if we set the analysis window to be equal to the frequency interval over which a single cycle of SFOAE phase was accumulated. For most ears, we collected SFOAEs for probe tones in the 0.5 to 9 kHz frequency region. As can be seen in Figure 2.5, the width of window over which a single cycle of phase was accumulated over this frequency region changes roughly by a factor of 2. Across all center frequencies, the average width of the window over which a single cycle of phase was accumulated is 0.7 kHz (dotted line in Fig. 2.5).

Overall, this analysis suggests that for the frequency region over which most of our data were collected, there is no strong need to vary the width of analysis window. It should be noted that although 0.7 kHz is the average width of the one-cycle phase changes across all center frequencies, for center frequencies below 8 kHz there is a strong clustering of data points with widths between 0.4 and 0.7 kHz., which may indicate that an analysis window length shorter than 0.7 kHz may be desirable for analyzing most of the data that were collected. How time-frequency-analysis results are affected by using windows of different length (0.5, 0.75, and 1 kHz) is addressed next.

Time-Frequency Analysis Using Different Window Lengths

It is of basic interest to see how the results of the SFOAE time-frequency analysis change with analysis windows of different lengths. Group-delay vs. frequency plots with analysis window lengths of 0.5, 0.75 and 1 kHz are shown for SFOAEs from one guinea pig ear in Figure 2.6. For all window lengths, the attenuation band was 0.6 kHz and the attenuation gain was 30 dB. As the analysis window length increased, the regions over which the time-frequency analysis revealed multiple components extended over longer frequency regions (Fig 2.6 B vs. C vs. D). This observation is a natural result of the increase of analysis window length: as a window that covers larger frequency region slides along the frequency axis, it "sees" a region where multiple component are present earlier and later than a shorter length window would "see" this region. There were also slight changes in the latencies of the SFOAE components as the length of the analysis window increased, which is a result of peaks becoming higher in energy and sharper as the analysis window length increased. As a whole, the general pattern seen using all three of these time-frequency-analysis windows, i.e. multiple components centered at SFOAE amplitude dips (see Results), does not appear to be an artifact or result of the choice of window length.

Based on this, we choose to use an analysis window length of 0.5 kHz, which, of the three window lengths tested, gives the most frequency-specific picture of the multiple components.

2.3 Results

We collected data in 26 ears, of which 20 had normal hearing (no frequency regions with hearing CAP thresholds ≥40 dB SPL) across the entire frequency region over which SFOAEs were collected (i.e. 0.5 to 8–12 kHz). Representative SFOAE data from two guinea pigs are shown in Fig. 2.7. The SFOAE magnitudes show a pattern of broad peaks and sharp dips (Fig.2.7 A1 and A2), as previously reported (Goodman 2003). Many of the dips were accompanied by near half-a-cycle phase changes (not shown). Every ear had frequency regions in which the impulse response functions revealed energy at a single delay, as well as frequency regions over which impulse response functions had two peaks at different delays (across all frequencies of all ears, 1/3 of frequencies had two peaks). A few ears had small regions over which impulse response functions had three peaks (across all frequencies and ears only 1% of frequencies showed three peaks). When a single peak was detected, its group delay was almost always similar to the phase-gradient group delay. At frequencies where the SFOAE analysis revealed two peaks in the impulse response function, the delay of one of the components was similar to the phase-gradient group delay, while the delay of the other peak could be longer or shorter than the phase-gradient delay (Fig. 2.7 B1, B2). Two components almost always arose at frequencies near dips in the SFOAE magnitude (Fig. 2.7 B1-2, D1-2). Two components were not shown by our analysis near some dips because one of the components was below our component selection criteria (e.g. Fig. 2.7, left, 5.6 kHz). The presence of two components near an SFOAE dip is explained by coherent reflection theory which predicts that sometimes the pattern of irregularities will be such that the SFOAEs originating from the peak region of the traveling wave will cancel. Such a cancellation is what produced the dips in the SFOAE response. If the energy from the traveling wave peak region is cancelled, then what remains is energy coming from the edges of the traveling wave peak region and these form two peaks in our analysis.

2.3.1 Attempts to Classify SFOAE Components by Their Group Delays

It appears that guinea-pig SFOAEs are predominantly generated with either one or two delay components. For the purpose of understanding difference between multiple components, we have attempted to classify the components obtained by the SFOAE time-frequency analysis.

The first attempt at classifying the SFOAE components involved using the group delay obtained from the phase-gradient as a means of defining components (Figure 2.8). In each ear, the SFOAE group delays that passed our noise criteria were identified as either a component group delay that agrees with the phase-gradient delay (blue x's in Figure 2.8) or a component group delay that is longer than the phase-gradient delay (green x's in Figure 2.8) or a component group delay that is shorter than the phase-gradient delay (maroon-x's in Figure 2.8). As more data were collected and analyzed it became evident that this kind of grouping is ill-defined for the following reason. The phase-gradient delay usually follows the component with the largest energy (compare the phase gradient curves in Fig. 2.7 B1 and B2 to the high energy peaks in Fig. 2.7 D1 and D2). However, when two components are present they are often nearly equal in amplitude (Fig. 2.7 C1 and C2 and D1 and D2). As a result, when two components are present it is somewhat random which one of the two components agrees with phase-gradient delay. Due to this phenomenon, the classification of a component as being shorter or longer than component that agrees with phase-gradient is inappropriate and perhaps misleading.

Coherent reflection theory along with basilar-membrane traveling wave delays from simple cochlear models predict that the group delays of OAEs decrease with increasing frequency in a negative power law form. Sisto et al., (2013) used this theoretical prediction to classify the multiple components seen in time-frequency distributions of SFOAEs and TEOAEs from human ears. The curve that produced the optimal negative power law fit was defined as: the negative-power-law curve which yielded the maximum energy integrated across frequency in a narrow band around the curve. The fit can be thought of as the "maximum energy curve" of a negative-power-law form. A negative-power-law fit was obtained for emissions in every ear they studied. Sisto et al., (2013) observed that the emissions had components with both longer and shorter latency than were predicted by the theory. The longer latency component had approximately twice the latency of the main component and they identified it as being due to a SFOAE component that was reflected back into the cochlea at the stapes and therefore had twice the latency of the main SFOAE component. The shorter component was identified as arising from a region about 1/3 octave basal of the main component. We have replicated the method of Sisto et al. (2013) in guinea pig ears. An optimal negative power law fit was obtained for every guinea pig ear using the procedure of Sisto et al (2013) and each SFOAE group delay was identified

either as a component group delay that agreed with the fit (blue x's in Figure 2.9), as a component group delay that was longer than the fit (green x's in Figure 2.9), or as a component group delays that was shorter than the fit (maroon-x's in Figure 2.9). SFOAE delays are much longer in humans than in guinea pigs and human SFOAE delays appear to be well described by a negative power law fit (Sisto et al., 2013). In guinea pigs the negative power law fit appears to be less optimal: in 10 ears the fits yielded low values for the power parameter (mean = 0.31 ±0.11, compared to 0.6 to 0.8 in humans) suggesting that the change across frequency in SFOAE group delays is less well described by a power law. In addition, components classified using the fit suffered from same issue as components classified relative to the phase gradient delay. When there were two components present, the fit sometimes fell in-between the two components, making classification relative to the fit impossible, and at other times the fit agreed with one of the components but not in a uniform way. There was clear inconsistency across ears, and sometimes within an ear, as to how components were classified.

We also attempted to classify components manually from estimates of the traveling-wave latency as a function of frequency based on neural delays measured in guinea-pig single auditory nerve fibers. Versnel et al., 1990 collected PST histograms from single auditory nerve fibers of guinea pigs in response to clicks of 92 dB peSPL. The latency of the neural response was assessed by the latency of the highest PST peak of a fiber's response to the clicks. The SFOAE delay time to and from the location of fiber was taken to be twice the latency of the traveling wave calculated from the neural response (i.e. the neural latency minus a neural conduction time). Versnel et al. (1990) presented a distribution of the neural latencies vs. frequency, as well as equations for one-line and two-line fits to the data (the two-line fit matched the data better). We used the fits presented by Versnel et al., 1990 (doubled to approximate the expected SFOAE latencies) to classify SFOAE components. The components were manually classified as either a *main component* whose latency agreed with the double-line fit to the neural delays (blue x's in Figure 2.10) or a component longer than main component (green x's in Figure 2.10) or a component shorter than main component (maroon x's in Figure 2.10). In general, there was no good match between the group delays revealed by the SFOAE time-frequency analysis and the delays predicted by the neural latencies. This was especially true when time-frequency analysis revealed two delays in the impulse response, since sometimes neither agreed with the double-line

fit to the neural delays and other times one of the component delays did agree but not uniformly the component with the longer or shorter delay. Again there was inconsistency across ears, and sometimes within an ear, as to how components were classified. Overall, none of the methods provided a way to consistently classify cases in which there were two delay components. One possible reason these methods failed is because the different delay components are not from different origins, i.e. all of them originate from reflected energy from near the peak of the traveling wave.

2.3.2 Time-Frequency Analysis of Simulated SFOAEs

Dr. Christopher Shera kindly provided us with 10 sets of simulated SFOAEs vs. frequency functions that were derived from the very simple cochlear model described in Shera and Bergevin (2012). In this model the amplitude of the traveling wave was approximated by a Gaussian pulse with a bandwidth set to match guinea pig basilar-membrane tuning curves from the corresponding frequency region in a cochlear mechanical model. The phase of the model traveling wave was a straight-line phase vs. frequency function with a slope equal to twice the expected mechanical delay at that frequency. For each of the 10 models, a random irregularity function along the cochlea was added to produce SFOAEs which resulted in 10 sets of simulated emissions. These model data were analyzed in the same way as our guinea pig data. SFOAE group delays vs. frequency plots for three representative SFOAE simulations are shown in Figure 2.11, middle column. For comparison, the left column of Figure 2.11 shows three more examples of real data from guinea pigs. In both simulated and real ears, frequency regions around the SFOAE-magnitude dips show two delay peaks in the impulse response functions.

The SFOAE simulation model was constructed to have delays that match those predicted by Shera and Guinan (2003, Table 1) from guinea-pig mechanical measurements. A line showing this prediction, superimposed on a plot showing all of our guinea-pig SFOAE group delays vs. frequency, is shown in Figure 2.12. Below 2 kHz, the line predicts longer group delays than were observed in almost all guinea pigs. Another way to appreciate the difference between the measured and predicted delays at low frequencies is to note how in Figure 2.11 the model group delays bend upward at low frequencies more than the measured group delays.

2.3.3 Time-Frequency Analysis of Chinchilla SFOAEs

Dr. Jon Siegel kindly provided us with the chinchilla SFOAE data that were used in his 2005 paper. We analyzed the data from 10 chinchillas in exactly the same way as was done for the guinea-pig and model data. Group delays vs. frequency plots from the SFOAEs of three representative chinchilla ears are shown in Figure 2.11, right. These chinchilla SFOAEs show delay vs. frequency patterns very similar to those in guinea pigs, namely a pattern of long and short delays around frequencies that have sharp SFOAE dips. The chinchilla data also show another pattern, regions of near-zero group delays (Figure 2.11 top and bottom panel of the right column). Small regions like these were observed in guinea pigs, but rarely. Such regions are far more extensive in chinchillas.

2.3.4 The Growth of SFOAE Components with Sound Level

In two guinea-pig ears we collected SFOAE data across frequency for sound levels from 35-55 dB SPL in 5 dB steps. In all cases, the suppressor-tone level was kept 20 dB above the probe-tone level. The magnitudes and phases of SFOAEs at different sound levels are shown in Fig. 2.13. As expected, SFOAEs collected at higher levels accumulated less phase change than SFOAEs collected at lower sound levels. At various frequencies the SFOAE magnitudes had regions of compressive, near linear and expansive growth. In each ear, we applied time-frequency analysis to the SFOAE sweeps at different sound levels with the results shown in Figures 2.14 and 2.15. In general, group delay vs. frequency plots changed little with sound level so that it was usually possible to identify corresponding SFOAE components across level. However, in some cases components disappeared, or appeared, as level was changed.

We analyzed the growth of SFOAE energy with sound level averaged across all frequencies. Time-frequency analysis was applied to the SFOAEs collected at different sound levels. At every analysis frequency and level, the energy in the impulse response function (e.g. Fig. 2.2 right) was integrated across time. The average energy at each level was obtained by taking the average of the energies across all frequencies. The average slope of energy growth across levels, as well as standard error bars of the slopes are shown in Figure 2.16, top. In general, the slopes are less compressive than what would be expected if the growth of SFOAEs follows the compressive growth of mechanical motion (e.g. basilar membrane motion). In one of the ears (GP108), the growth of energy is near linear for sound levels above 40 dB SPL. At lowest sound levels, i.e.

from 35 to 40 dB SPL, the average slope of energy growth was compressive and agrees closely in the two ears.

We do not know the reason for the near linear, or weakly compressive, average growth of SFOAE energy at sound levels above 40 dB SPL, but this observation makes further time-frequency analysis at these levels questionable. The goal of collecting data at different levels was to be able to analyze how individual components grow with level, especially when there are multiple components. However only the analysis of the compressive growth from 35 to 40 dB SPL seems appropriate. As can be seen in Figures 2.14 and 2.15, at the two lowest sound levels most of the non-main components were present at one level but not at the other level. Because of this, there was not enough data to conclude anything about the relative growth of the components as probe-tone level was changed from 35 to 40 dB SPL. On the other hand, an analysis of the overall SFOAE energy growth at the lowest levels could be done for different frequency regions. Average SFOAE energy vs. level functions were obtained for four frequency blocks: 1-3 kHz, 3-5 kHz, 5-7 kHz and 7-9 kHz. The average slope of energy growth from 35 to 40 dB SPL for the four frequency blocks are shown in the bottom panel of Figure 2.16. As expected from mechanical measurements, the SFOAE energy grows less compressively for the low-frequency block than for higher-frequency blocks. However, for these higher-frequency blocks the average slopes are less compressive than expected from mechanical measurements (Cooper, 1998).

2.4 Discussion

The time-frequency analysis of guinea-pig, chinchilla and simulated SFOAEs has shown that across a wide range of frequencies (0.5–12 kHz), SFOAE often have multiple delay components. Multiple components appear near dips in SFOAE amplitude that have approximate phase reversals. Such dips are predicted by coherent reflection theory. Presumably, a common origin in coherent reflection is the reason why there are no dramatic differences in the patterns of the multiple components from different frequencies or from animal and simulated SFOAEs.

While the multiple components agree with coherent reflection theory, at low frequencies the overall latencies of the measured SFOAEs disagree with the overall latencies predicted by coherent reflection theory. Our measured guinea pig, low frequency, SFOAE latencies are very similar to those measured by Shera and Guinan (2003), and our conclusion that the measured latencies are shorter than expected by theory concurs with theirs. Shera and Guinan (2003) fitted

a straight line (in a log-log plot) to their mid- and high-frequency guinea pig SFOAE latency data (shown with our data in Fig. 2.2) and noted that the extension of this line to low frequencies agrees fairly well with twice the group delays of the available mechanical measurements from the cochlear apex (Cooper and Rhode, 1995; Khanna and Hao, 1999). The line, therefore, serves as a surrogate for the predicted guinea pig SFOAE latencies based on coherent reflection theory and available mechanical measurements, and it predicts SFOAE latencies longer, on average, than those actually observed (Fig. 2.2). One possibility is that at low frequencies the line and the mechanical measurements are wrong. The mechanical measurements from the cochlear apex have been done without the benefit of a good test for cochlear sensitivity at low frequencies (see Lichtenhan, et al., 2013). However, in the cochlear base, decreased sensitivity has a relatively small impact on mechanical group delays, so the explanation for the short SFOAE delays may be elsewhere. Several other hypotheses have been offered.

One hypothesis is that the disagreement at low frequencies in measured and predicted SFOAE latencies is produced by additional short-latency SFOAE components that originate at the basal end of the traveling wave (Siegel et al., 2003; Choi et al., 2008). This is unlikely to be true for two reasons. First, time-frequency analysis of model data (Fig 2.11), indicates that SFOAE components with latencies shorter than the expected SFOAE latency do not necessarily mean that the energy in these components came from a cochlear place far basal of the traveling-wave peak. Short latency components are seen in model SFOAEs despite the fact that the Gaussian pulses used in the model to approximate the traveling wave had very low amplitudes far basal of the traveling-wave peak, with the result is that the simulated SFOAEs had little energy coming from regions far basal of the peak. Second, in the following chapter we show that all SFOAE components are affected by MOC stimulation. Since MOC stimulation reduces cochlear amplification but there is no cochlear amplification far basal of the traveling wave peak, the MOC effects that were found further indicate that none of the SFOAE components originated from the far-basal end of the traveling wave.

Components with very short latencies at low-frequencies were found in chinchillas sometimes and in guinea pigs rarely (Fig 2.11). It could be argued that these very-short-latency components might come from the cochlear base. While it is possible that these SFOAE components originate from cochlear regions far basal of the traveling wave peak, in chinchillas

the regions with very short group delays have delays that are so uniformly short that we think it is much more likely that these are regions where distortion is producing the SFOAEs. Distortion is a wave-fixed process that produces group delays near zero (Shera and Guinan, 1999). The chinchilla data were obtained from 30 dB SPL tones and it is surprising to find distortion producing significant SFOAEs at such low sound levels, but that is what the data are telling us.

In humans, Sisto et al., (2013) identified two closely-spaced SFOAE components, one with a latency corresponding to the traveling wave latency and another with 2/3 that latency. Because guinea-pig SFOAE delays are much shorter than those in humans, in guinea pigs it is difficult to resolve SFOAE components with such close ratios.

It has been noted that in the low-frequency region, SFOAE data show somewhat oscillatory behavior as if there were two beating SFOAE components (Shera, 2008). Our analysis shows multiple components, but these are evident in high-frequency regions as well as in low-frequency regions. It appears that in low-frequency cochlear regions something is different other than the presence of dip-produced multiple SFOAE components.

One hypothesis for the short SFOAE delays at low frequencies is that these SFOAEs arise from coherent reflections from a motion that has a shorter group delay than the traveling wave group delay (Guinan 2012). In Figure 2.17 we compare the group delays from the time-frequency analysis of guinea-pig SFOAEs to the group delays calculated from responses of single auditory nerve fibers to high-level clicks (Versnel et al., 1990; see Results for a further description of these data). The 92 dB SPL clicks used by Versnel et al., are very similar to the clicks that evoked the efferent-inhibited ANIP response in cats (Guinan et al., 2005). It seems likely that for fibers with low best frequencies, Versnel et al's largest PST peak in guinea pigs is equivalent to the ANIP peak in cats. This would mean that the thick line in Figure 2.17 shows the expected SFOAE group delay that would result from the motion that produces the ANIP response. At low frequencies, the SFOAE latencies estimated from auditory-nerve fiber data fit well with many of the short group-delay SFOAE points (Fig. 2.17). This does not prove that the short-group-delay SFOAEs and the auditory-nerve fiber responses came from the same mechanical origin. However, the data show that a viable hypothesis is that the short group-delay, low-frequency SFOAE components originate from the same short group delay cochlear motion as the ANIP response.

We attempted to look at how SFOAE components grow with sound level, however the data that were obtained at different sound levels had a growth that was close to linear instead of the expected compressive growth (Fig. 2.16). We don't know why the data had this form and this has discouraged us from doing a more detailed analysis of these data, because we wouldn't know how to interpret details when we don't understand the overall pattern. One thing to note is that for the 55 dB SPL probe tone, the suppressor tone was 75 dB SPL. Perhaps this rather high suppressor-tone level made small temporary changes in the cochlea similar to those of the "intrinsic effect" reported by Liberman et al. (1996).

2. 5 Conclusions

Overall, our analysis suggests that multiple SFOAE components can be a simple result of variation in the pattern of irregularities near the peak of the traveling wave and are not necessarily indicative of additional SFOAE sources.

We also found that, at low frequencies, the overall measured SFOAE delays are shorter than the delays predicted by standard coherent reflection theory, as reported by Shera and Guinan (2003). It seems possible that the overall shorter SFOAE delays from the apex are due to coherent reflections from a motion that has a shorter group delay than the traveling-wave group delay.

2.6 References

Choi YS, Lee SY, Parham K, Neely ST, Kim DO, 2008. Stimulus-frequency otoacoustic emission: measurements in humans and simulations with an active cochlear model J Acoust Soc Am 123, 2651–69

Cooper, N.P. 1998. Harmonic distortion on the basilar membrane in the basal turn of the guinea-pig cochlea. J Physiol (Lond) 509, 277-88

Cooper, N.P., Rhode, W.S. 1995. Nonlinear mechanics at the apex of the guinea-pig cochlea. Hear Res 82, 225-243.

Dhar, S., Rogers, A., and Abdala, C., 2011. Breaking away: Violation of distortion emission phase-frequency invariance at low frequencies. J. Acoust. Soc. Am. 129, 3115–3122.

Goodman, SS, Withnell, RH, Shera, CA,2003. The origin of SFOAE microstructure in the guinea pig Hear Res 183, 7–17

Goodman, SS, Mertes, IB, Scherer, MP, 2011. Delays and growth rates of multiple TEOAE components In: Shera CA, Olson ES, (eds) What Fire is in Mine Ears: Progress in Auditory Biomechanics, Vol 1403 American Institute of Physics, Melville, New York, USA pp. 279–285

Guinan, JJ Jr, 1990. Changes in stimulus frequency otoacoustic emissions produced by two-tone suppression and efferent stimulation in cats In: Dallos, P, Geisler, CD, Matthews, JW, Steele, CR, (Eds), Mechanics and Biophysics of Hearing, Springer Verlag, Madison, Wisconsin, pp. 170–177

Guinan, JJ Jr, 2012. How are inner hair cells stimulated? Evidence for multiple mechanical drives Hear Res 292, 35–50

Guinan, J.J., Jr., Cooper, N.P., 2008. Medial olivocochlear efferent inhibition of basilar-membrane responses to clicks: evidence for two modes of cochlear mechanical excitation. J Acoust Soc Am 124, 1080-92.

Guinan, J.J., Jr., Lin, T., Cheng, H. 2005. Medial-olivocochlear-efferent inhibition of the first peak of auditory-nerve responses: Evidence for a new motion within the cochlea. J Acoust Soc Am 118, 2421-2433.

Kalluri, R., Shera, C.A., 2001. Distortion-product source unmixing:A test of the two-mechanism model for DPOAE generation. J. Acoust. Soc. Am. 109, 622-637.

Kalluri R., and Shera, C. A. 2007a. Comparing stimulus-frequency otoacoustic emissions measured by compression, suppression, and spectral smoothing. J. Acoust. Soc. Am. 122, 3562–3575.

Khanna, S.M., Hao, L.F. 1999. Reticular lamina vibrations in the apical turn of a living guinea pig cochlea. Hear Res 132, 15-33.

Kiang, N.Y.S. 1984. Peripheral neural processing of auditory information, Handbook of Physiology, Section 1: The Nervous System, Vol. 3 (Sensory Processes). Am. Physiological Soc., Bethesda, MD. pp. 639-674.

Liberman MC, Puria S, Guinan JJ. 1996. The ipsilaterally evoked olivocochlear reflex causes rapid adaptation of the 2f1–f2 DPOAE. J Acoust Soc Am 99:3572–3584.

Lichtenhan, J.T., Cooper, N.P., Guinan, J.J., Jr. 2013. A new auditory threshold estimation technique for low frequencies: proof of concept. Ear Hear 34, 42-51.

Long, G. R., Talmadge, C. L., and Lee, J. 2008. Measuring distortion product otoacoustic emissions using continuously sweeping primaries. J. Acoust. Soc. Am. 124, 1613–1626.

Maison SF, Liberman MC. 2000. Predicting vulnerability to acoustic injury with a non-invasive assay of olivocochlear reflex strength. J Neurosci 20: 4701–4707
Moleti, A, Longo, F., Sisto, R 2012b. Time-frequency domain filtering of evoked otoacoustic emissions. J. Acoust. Soc. Am. 132, 2455–2467.
Moleti, A, Mohsin Al-Maamury, A, Bertaccini, D, Botti, T, Sisto, R 2013. Generation place of the long-and short-latency components of transient-evoked otoacoustic emissions in a nonlinear cochlear model. J Acoust Soc Am 133, 4098–108
Ren, T. **2004**. Reverse propagation of sound in the gerbil cochlea. Nat.Neurosci. **7**, 333–334.
Ruggero, M.A. 2004. Comparison of group delay of 2f1-f2 distrotion product otoacoustic emissions and cochlear travel times. ARLO 5, 143-147
Shera, CA, Bergevin, C 2012. Obtaining reliable phase-gradient delays from otoacoustic emission data J Acoust Soc Am 132, 927–43
Shera, CA, Guinan, JJ Jr 1999. Evoked otoacoustic emissions arise by two fundamentally different mechanisms: A taxonomy for mammalian OAEs. J Acoust Soc Am 105, 782–798
Shera, CA, Guinan, JJ Jr 2003. Stimulus-frequency-emission group delay: a test of coherent reflection filtering and a window on cochlear tuning. J Acoust Soc Am 113, 2762–72
Shera, C.A., Guinan, J.J., Jr., Oxenham, A.J. 2002. Revised estimates of human cochlear tuning from otoacoustic and behavioral measurements. Proceedings of the National Academy of Sciences of the United States of America 99, 3318-3323.
Shera, C.A., Guinan, J.J., Jr., Oxenham, A.J. 2010. Otoacoustic estimation of cochlear tuning: validation in the chinchilla. J Assoc Res Otolaryngol 11, 343-65.
Shera, CA, Tubis, A, Talmadge, CL, Guinan, JJ Jr 2004. The dual effect of "suppressor" tones on stimulus-frequency otoacoustic emissions Assoc Res Otolaryngol Abstr 27, Abs 776
Shera, CA, Tubis, A, Talmadge, CL 2008. Testing coherent reflection in chinchilla: Auditory-nerve responses predict stimulus-frequency emissions. J Acoust Soc Am 123, 3851
Siegel, JH, Temchin, AN, Ruggero M 2003. Empirical estimates of the spatial origin of stimulus-frequency otoacoustic emissions J Assoc Res Otolaryngol 26, 172 (#679)
Siegel JH, Cerka AJ, Recio-Spinoso, A, Temchin, AN, van Dijk, P, Ruggero, M 2005. Delays of stimulus-frequency otoacoustic emissions and cochlear vibrations contradict the theory of coherent reflection filtering J Acoust Soc Am 118, 2434–2443
Sisto R, Sanjust F, Moleti A 2013. Input/output functions of different-latency components of transient-evoked and stimulus-frequency otoacoustic emissions J Acoust Soc Am 133, 2240–53
Talmadge, CL, Tubis, A, Long, GR, Tong, C 2000. Modeling the combined effects of basilar membrane nonlinearity and roughness on stimulus frequency otoacoustic emission fine structure. J Acoust Soc Am 108:2911–2932
Tognola, G., Ravazzani, P., and Grandori, F. 1997. Time-frequency distributions of click-evoked otoacoustic emissions. Hear. Res. 106, 112–122.
Versnel H, Prijs VF, Schoonhoven R, 1990.Single-fibre responses to clicks in relationship to the compound action potential in the guinea pig. Hear Res 46:147–160.
Wit, H. P., van Dijk, P., and Avan, P., 1994. Wavelet analysis of real ear and synthesized click evoked otoacoustic emissions. Hear. Res. 73, 141–147.
Withnell, R.H.,Shaffer, L.A., Talmadge, C.L., 2003. Generation of DPAOEs in the guinea pig. Hear. Res. 178, 106-117

Zweig G, Shera CA, 1995. The origin of periodicity in the spectrum of evoked otoacoustic emissions J Acoust Soc Am 98, 2018–2047

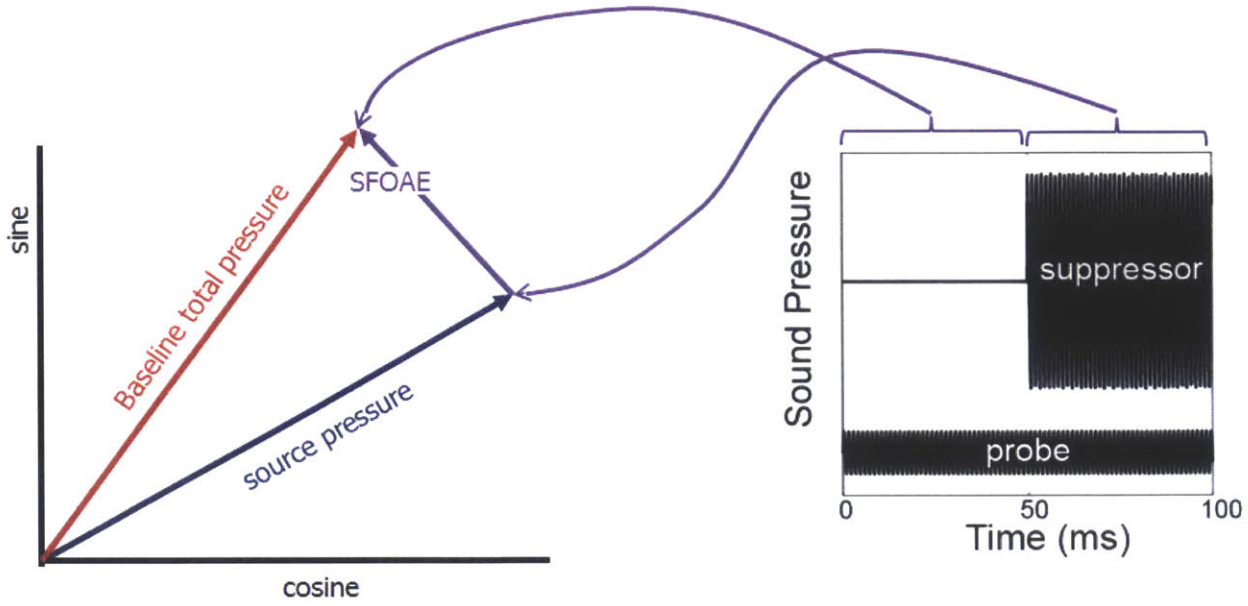

Figure 2.1: Measurement of SFOAEs using the Suppression Method.
Suppressor tones (50 ms every 100 ms) at 50 Hz above the probe frequency were superimposed on continuous probe tones (right panel). The SFOAE was calculated as the vector difference between the probe frequency sound pressure during the 50 ms of probe tone alone and the 50 ms of probe tone and suppressor together (left panel).

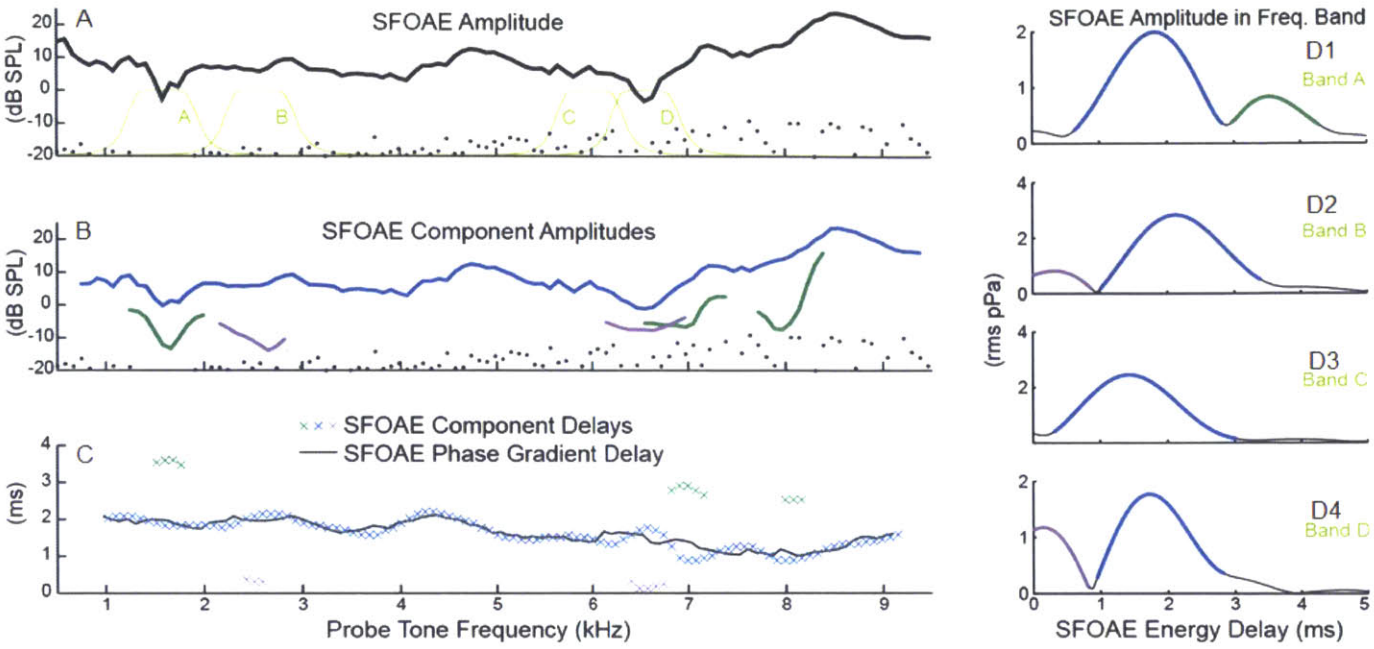

Figure 2.2 Time-Frequency Analysis of SFOAEs & Separation of SFOAEs into Components.

A: *Thick black line* = SFOAE magnitude, *dots* = noise levels, *thin green lines* = four windows that selected SFOAE frequency regions that were Inverse Fourier Transformed (IFFTed) and shown in panels D1-D4. The window-filter dB scales are filter pass-bands in dB, not re SPL.

B: SFOAE-component amplitudes. SFOAEs were separated into components based on the delays obtained by time-frequency (TF) analysis (these delays are shown in Panel C). *Blue line* = the magnitude of the component whose group delay agrees with the phase gradient delay; *green and purple line*s = magnitudes of components whose group delays are longer or shorter, respectively, than the component that agrees with the phase-gradient-delay-latency.

C: Group delays obtained from phase-gradients (*solid black line)* and from TF analysis (x's). *Blue* x = group delays that agree with the phase gradient delay; *green* x = delays that are longer than phase gradient delay; *purple* x = delays that are shorter than phase gradient delay.

D1-D4: Four examples of impulse response functions. IFFTs of windows A through D in Panel A produce the impulse response functions shown in panel D1 through D4, respectively. In each panel: the peaks in *blue* have delays (shown on the x-axis) that agree with the corresponding phase gradient delay, peaks in *green* have delays that are longer than the corresponding phase gradient delay and peaks in *purple* have delays that are shorter than the corresponding phase gradient delay.

Data from GP108R.

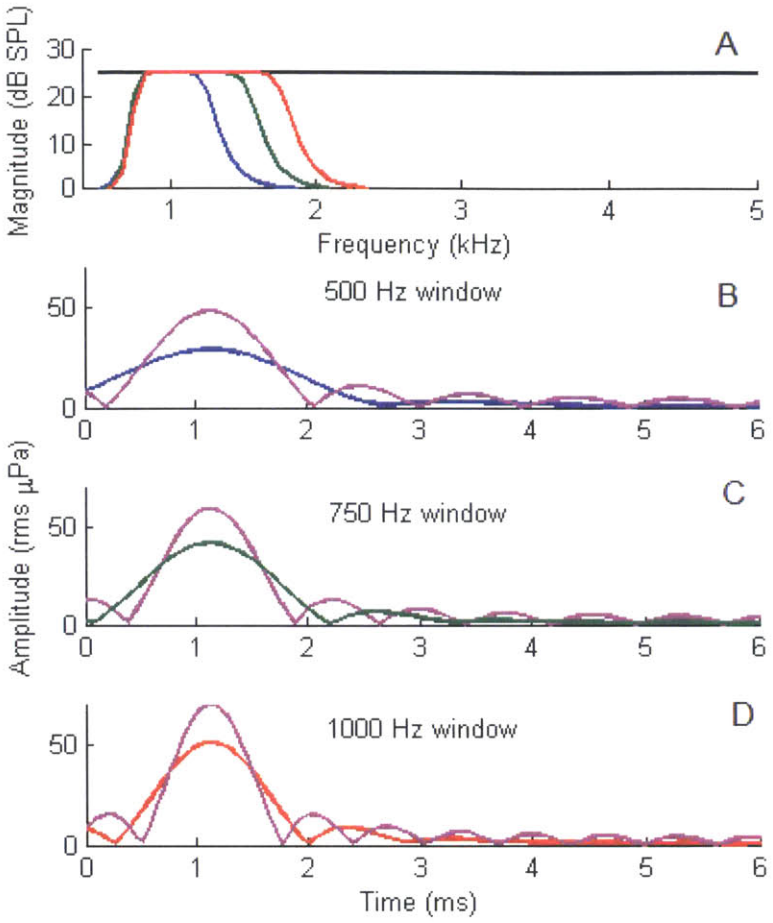

Figure 2.3: The Effects of Butterworth vs. Rectangular-Window Shapes on Impulse Response Functions.

A: *Thick black line* = Magnitude vs. frequency of a simulated set of SFOAEs with constant 25 dB SPL magnitudes and a 1.3 ms phase-gradient delay across frequency; *blue, green and red lines* = the shapes of the SFOAE segements after application of modified Butterworth windows with 0.5, 0.75 and 1 kHz pass bands. All Butterworth filters had 0 dB attenuation pass bands, and 0.6 kHz wide attenuation bands with 30 dB attenuation at their outer edge. **B, C and D:** *Blue, green and red lines* are impulse response functions from frequency segments windowed with the 0.5, 0.75, and 1 kHz modified Butterworth windows; *pink lines* are impulse response functions of SFOAE frequency segments windowed with 0.5, 0.75, and 1 kHz rectangular windows, respectively.

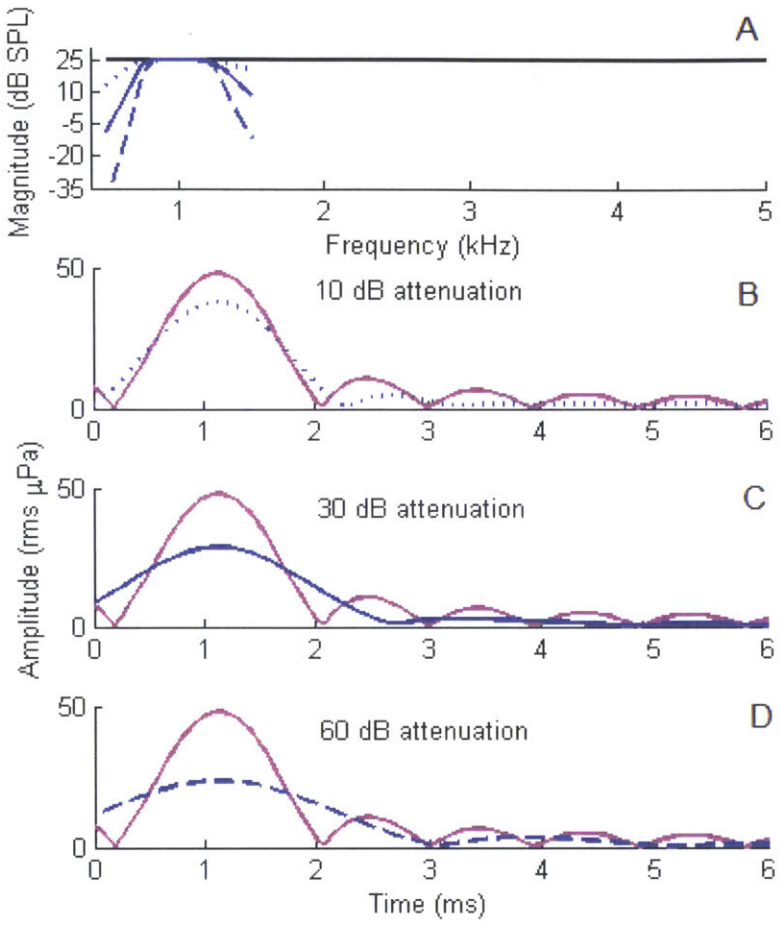

Figure 2.4: The Effects of Butterworth-Shaped Windows with Different Attenuations on Impulse Response Functions.

A: *Thick black line* = Magnitude vs. frequency of a simulated set of SFOAEs with constant 25 dB SPL magnitudes and a 1.3 ms phase-gradient delay across frequency; *blue dotted, solid and dashed line*s = the shapes of the SFOAE segments after application of modified Butterworth windows with 0.5 kHz pass-bands and 10, 30 and 60 dB attenuations. All Butterworth filters had 0 dB pass bands and 0.6 kHz attenuation bands on both sides of the pass band. Note that resulting filters are asymmetric, i.e. for all three filters, the specified attenuation is not quite achieved at the upper edge of the upper attenuation band. **B, C and D**: *Blue dotted, solid and dashed lines* are impulse response functions of segments windowed with modified Butterworth shaped windows that have 10, 30 and 60 dB attenuations respectively (as shown in Panel A); *pink lines* are the impulse response function of the SFOAE frequency segment windowed with a 0.5 kHz rectangular window.

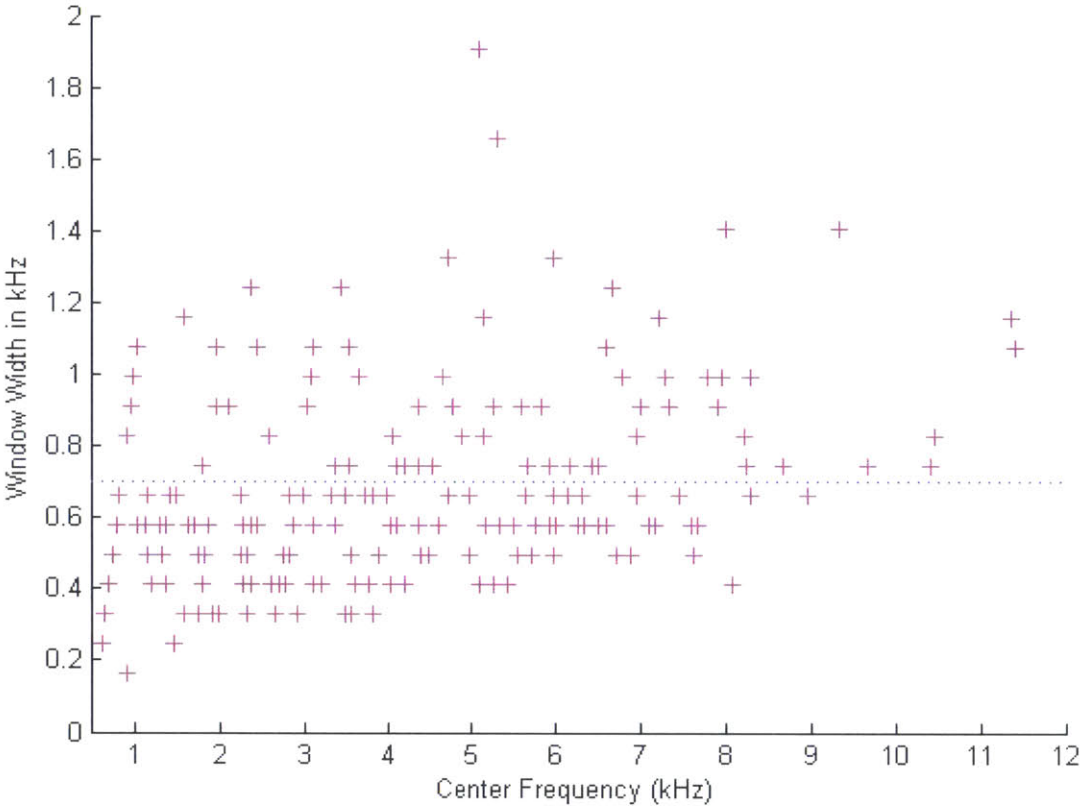

Figure 2.5 The Frequency Widths of SFOAE Segments over which SFOAE Phase Accumulated One Cycle vs. the Center Frequency of the Segment.
Pink + = width of SFOAE frequency segments over which one cycle of phase change was accumulated vs. the center frequency of that SFOAE segment. *Dotted blue line* = mean width of the data. Data from 17 guinea pig ears.

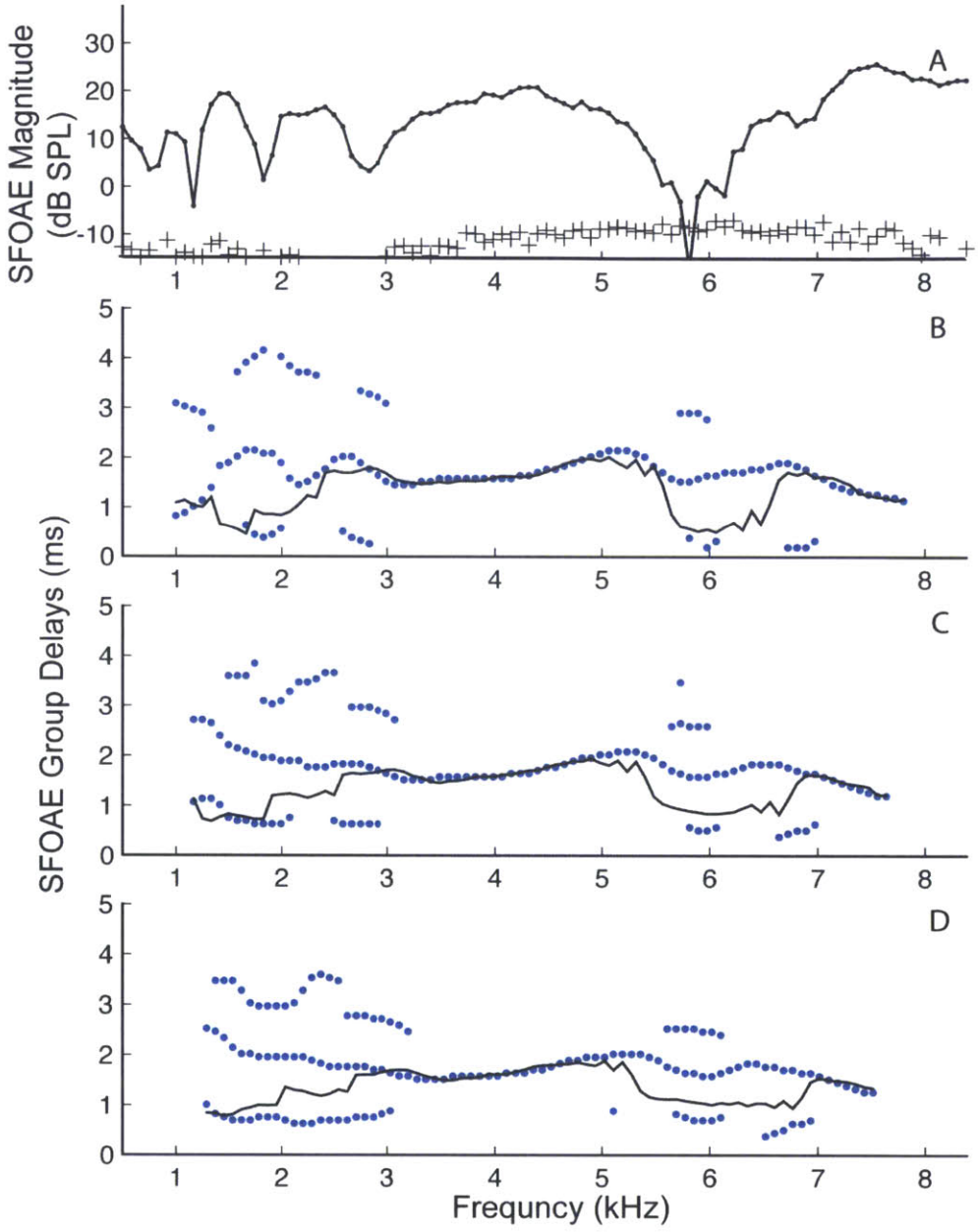

Figure 2.6: The Effects of Three Frequency-Window Lengths on Group Delays in the resulting Impulse Response Functions.

A: *Black line with dots* = SFOAE magnitude versus frequency from a representative subject, *crosses* = noise levels. **B, C and D**: Blue dots = Group delays of the peaks obtained using time-frequency analyses with window lengths of 0.5, 0.75 and 1 kHz, respectively, applied to the SFOAEs shown in Panel A; *dashed black lines* = group delays obtained from the phase-gradients measured over the same window lengths as the time-frequency analysis. Data from GP116L.

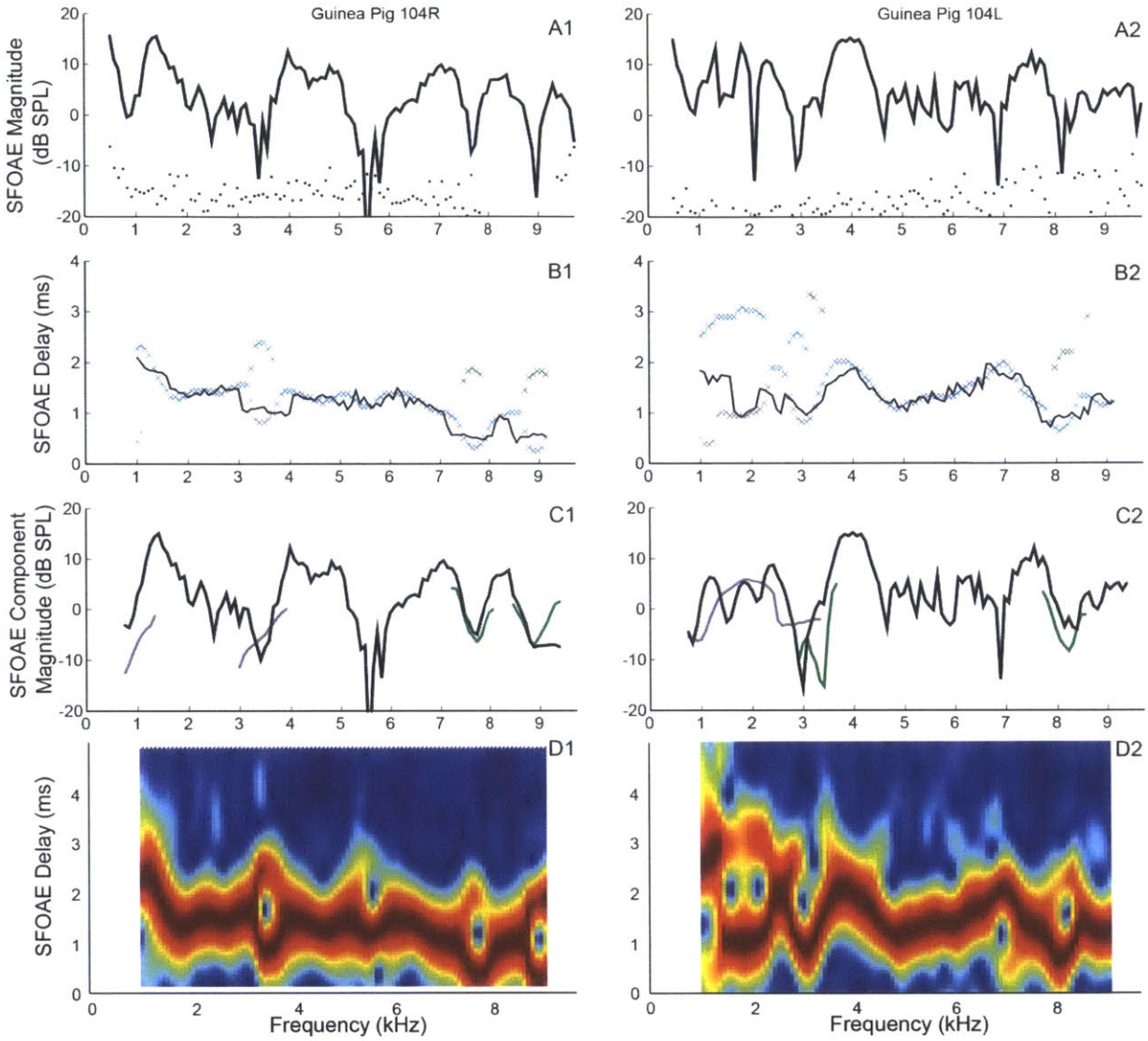

Figure 2.7: Time-Frequency Analysis of SFOAEs from Two Representative Ears.

The Left and Right columns show data from two different ears. In each column: **A**: The solid *black line* = SFOAE magnitude vs. frequency, *dots* = noise levels. **B:** *solid black line* = group delay obtained from the phase-gradient; x's = Group delays obtained from time-frequency analysis of the SFOAEs shown in Panel A; blue x's = group delays that agree with the phase gradient delay; green x's = delays that are longer than phase gradient delay; purple x's = delays that are shorter than phase gradient delay. **C:** magnitudes of SFOAE components separated by their delays from the time-frequency analysis. The black line is the magnitude of the component whose group delay agrees with the phase gradient delay; green and purple lines = the magnitudes of components group delays that are longer or shorter than the component that agrees with phase gradient delay. **D**: Plot of impulse response functions versus frequency, with color indicating the energy at various delays. At each frequency, the maximum energy was scaled to 100% and colored red, while dark blue shows the minimum energy.

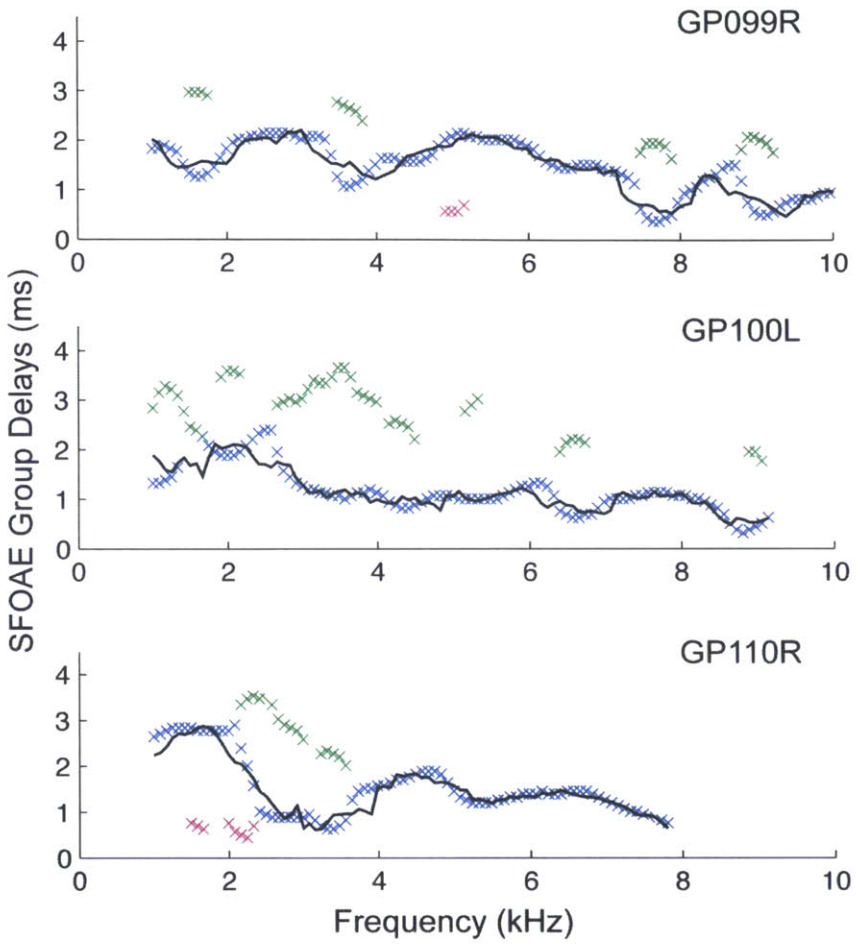

Figure 2.8: Classifying SFOAE Components by their Delays Relative to the Phase-Gradient Delay.

Each panel shows the SFOAE components from a different ear. *Solid black line* = the phase-gradient delay; x's = Group delays obtained from the time-frequency analysis; blue x's = group delays that agree with the phase gradient group delay (within ±0.6 ms of measured phase gradient delay); green x's = delays that are longer than the phase gradient delay; purple x's = delays that are shorter than the phase gradient delay.

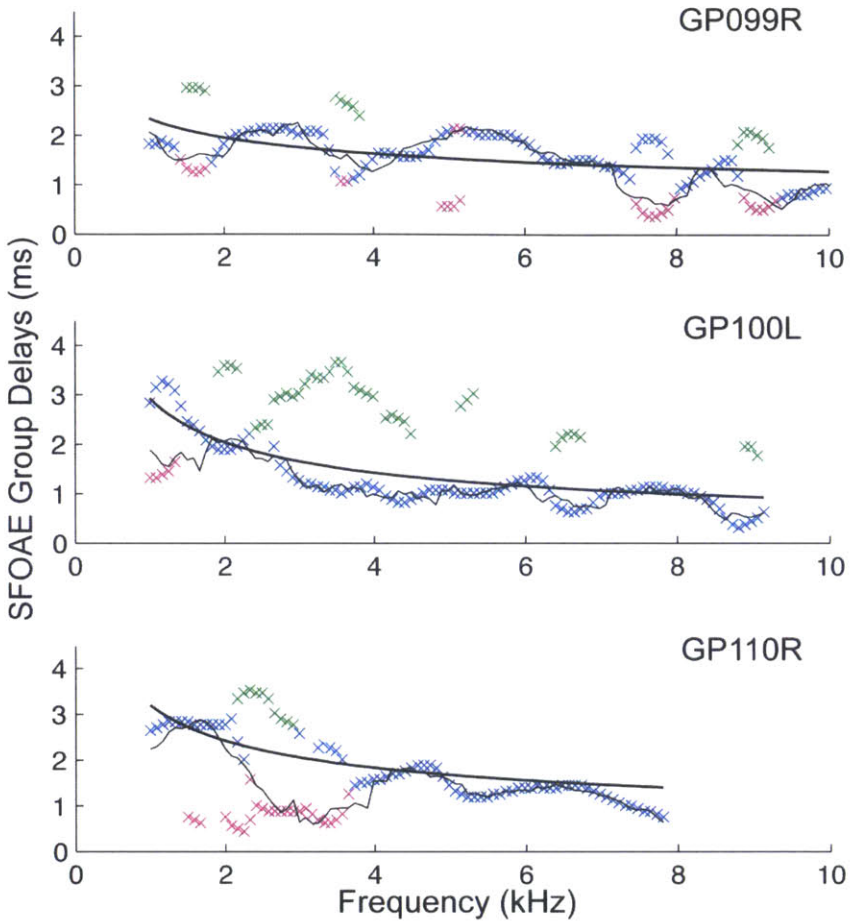

Figure 2.9: Classifying SFOAE Components by their Delays Relative to a Negative-Power-Law Fit to the SFOAE data.

Each panel shows the SFOAE components from a different ear. *Solid black line* = negative power-law fit to the distribution of energy in the time-frequency plane; x's = Group delays obtained from the time-frequency analysis; blue x's = group delays that agree with the negative power-law fit (within ±0.6ms of delay of fit); green x's = delays that are longer than the fit; purple x's = delays that are shorter than the fit.

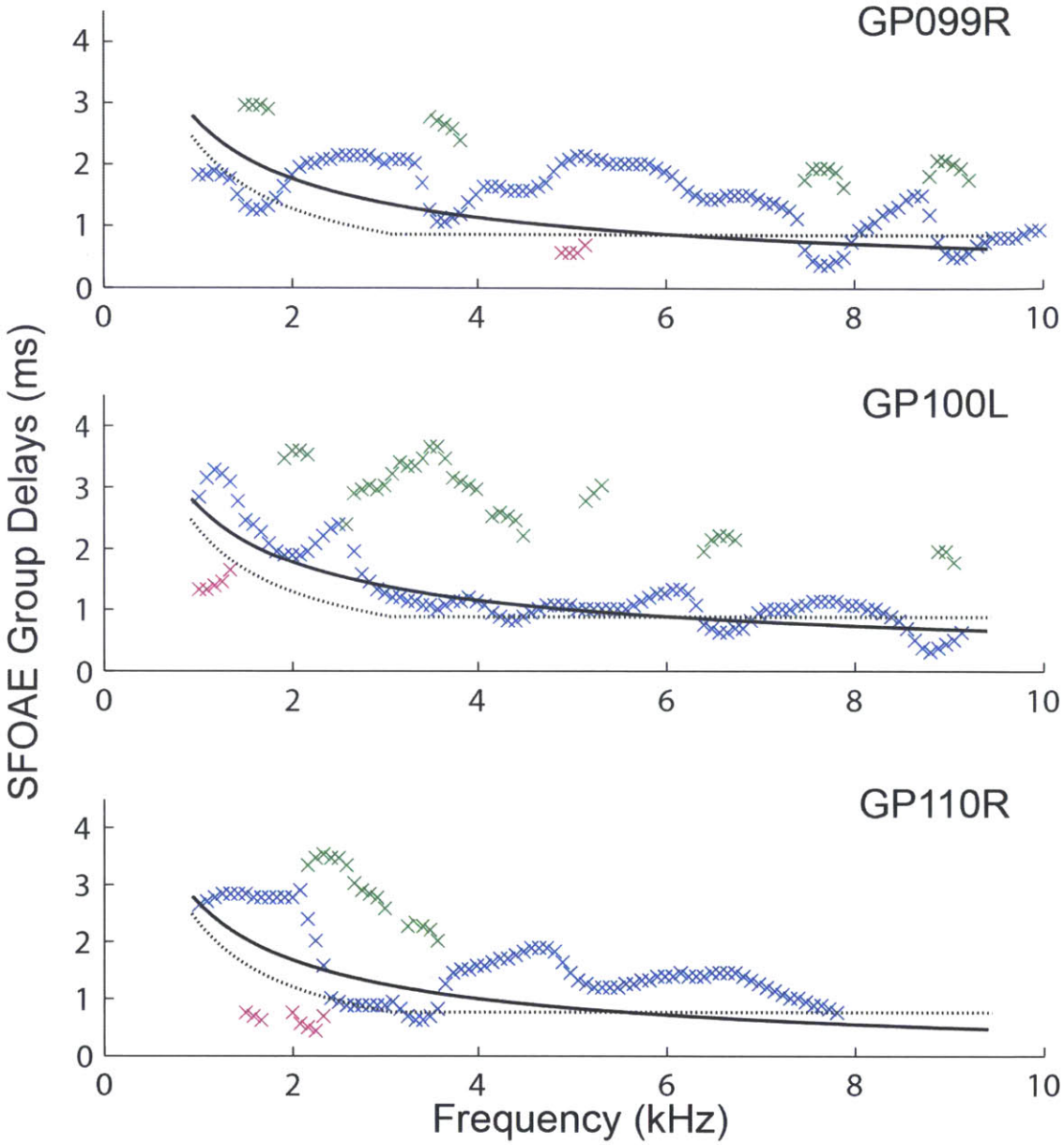

Figure 2.10: Classifying SFOAE Components by their Delays Relative to the Expected SFOAE Delay based on Auditory-Nerve Response Latencies.

Each panel shows the SFOAE components from a different ear; Dashed line = twice the value of the two-line fit to Versnel et al. (1990) data; solid black line = twice the value of the single-line fit to the Versnel et al. (1990) data. x's = Group delays obtained from time-frequency analysis; blue x's = group delays identified as being from the main component (i.e., the component whose delay agrees with twice the neural delay), green x's = delays that are longer than the main component, purple x's = delays that are shorter than the main component.

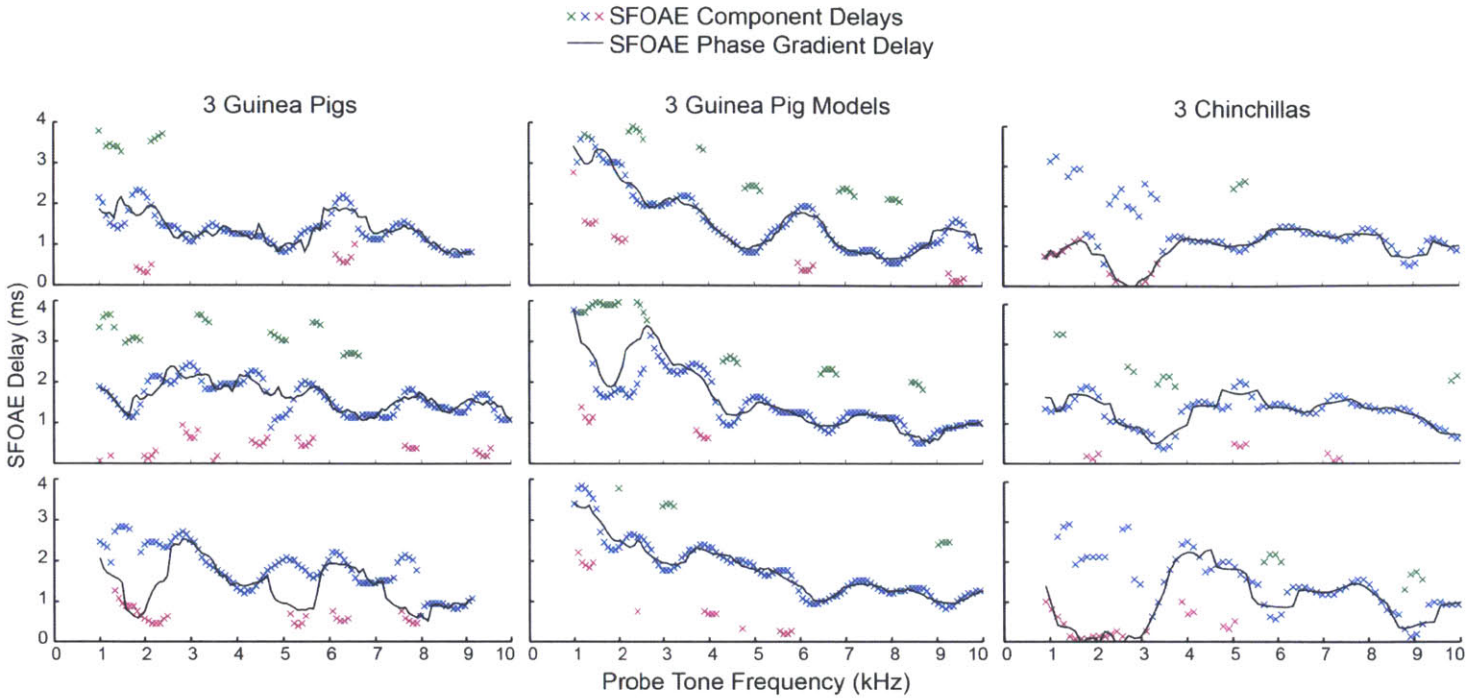

Figure 2.11: SFOAE Group Delays from Time-Frequency Analysis of Representative Guinea-Pig, Model and Chinchilla Ears.

Left, Center and Right columns shows the SFOAE components obtained from a time-frequency analysis of SFOAEs from three representative guinea-pig ears, three guinea-pig-model ears and three chinchilla ears, respectively. In each column, each panel is from a different ear; *solid black lines* = group delays from phase gradients; x' = Group delays obtained from time-frequency analysis; blue x's = group delays identified as the main component, i.e. the component whose delay agrees with the neural delay, green x's = delays that are longer than main component, purple x's = delays that are shorter than main component.

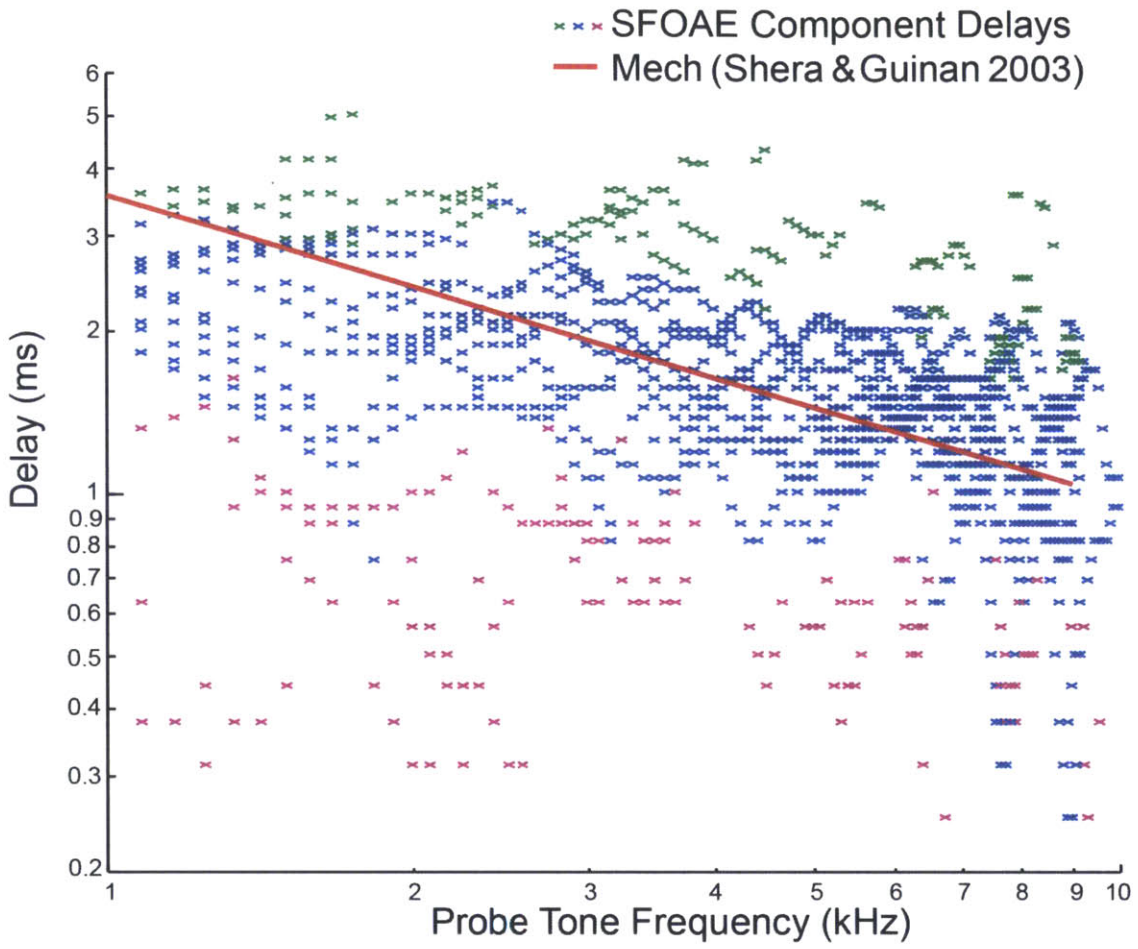

Figure 2.12: SFOAE-Component Group Delays from Time-Frequency Analysis compared to the SFOAE Delay estimated from Mechanical Data.

Red line = estimate of the SFOAE delay based on guinea pig mechanical data (from Shera and Guinan, 2003, Table I); x's = Group delays from time-frequency analysis; blue x's = group delays of components identified as the main component, i.e. those whose latencies agree with the SFOAE latencies expected from neural delays; green x's = delays that are longer than delays of the main component; purple x's = delays that are shorter than delays of the main component.

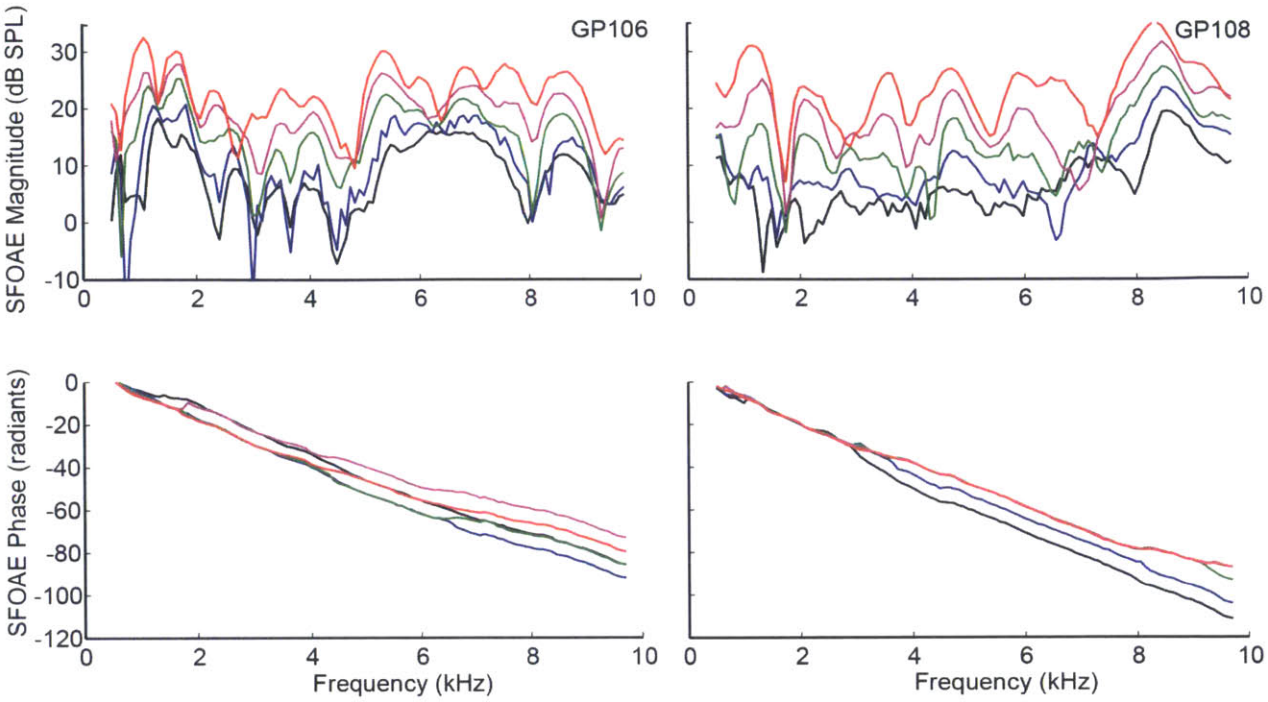

Figure 2.13: SFOAE Magnitude and Phase at Different Sound Levels for Two Ears.
Left and Right columns show SFOAE data from two different ears. Black, blue, green, maroon and red lines = SFOAE data collected with 35, 40, 45, 50 and 55 dB SPL probe tones, respectively. Top Panels: = SFOAE magnitudes; Bottom Panels: = SFOAE unwrapped phases in radians.

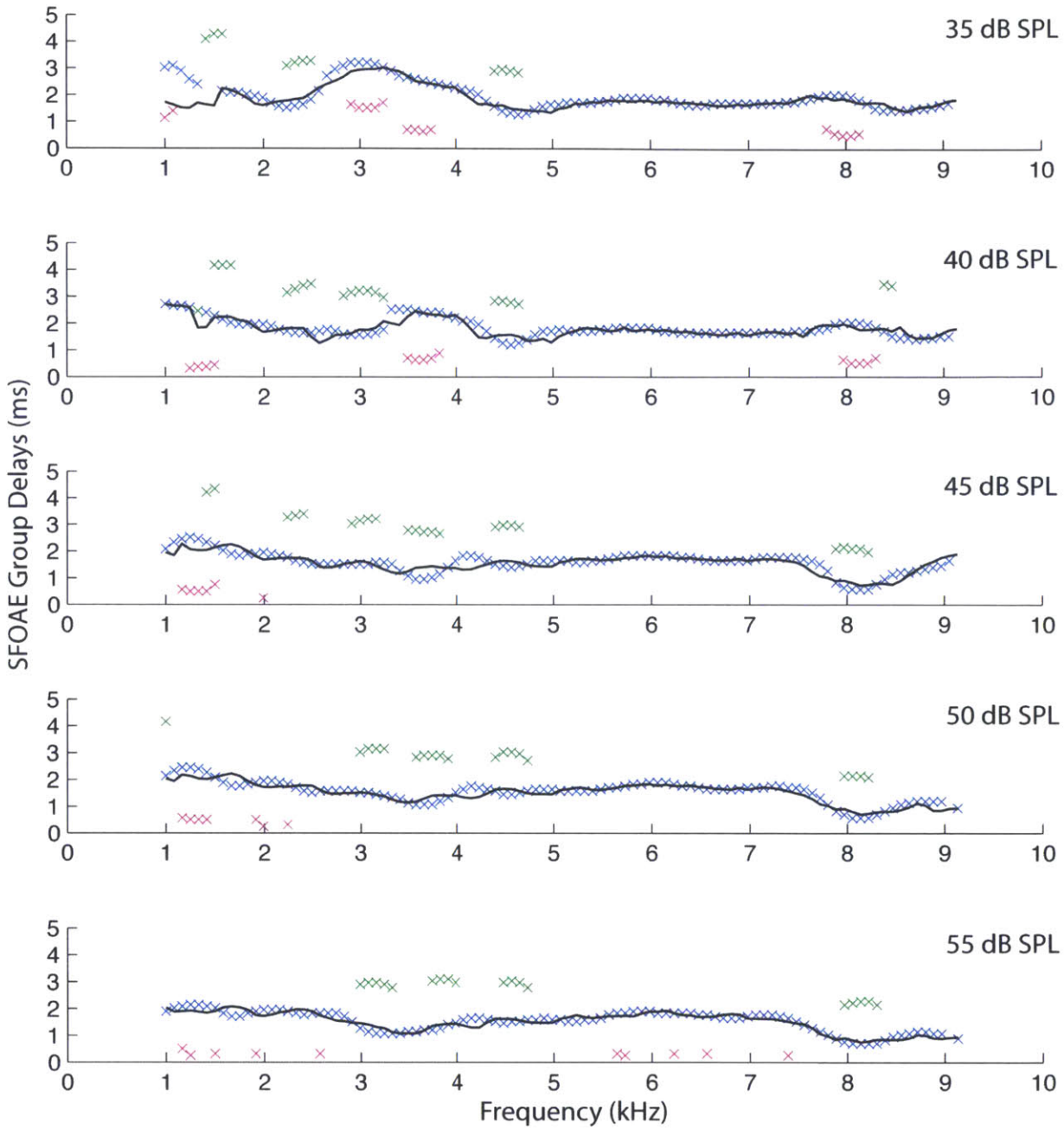

Figure 2.14: SFOAE Group Delays at Different Sound Levels from Guinea Pig 106R.
Each panel shows SFOAE group delays at a different probe-tone level (indicated at the right). The suppressor tone was always 50 Hz higher in frequency and 20 dB higher in level than the probe tone. In each panel: *solid black line* = group delay from the phase-gradient; x's = group delays from TF analysis; blue x's = group delays identified as main component (i.e. a component that agrees with neural delays), green x's = delays that are longer than the main component, and purple x's = delays that are shorter than the main component.

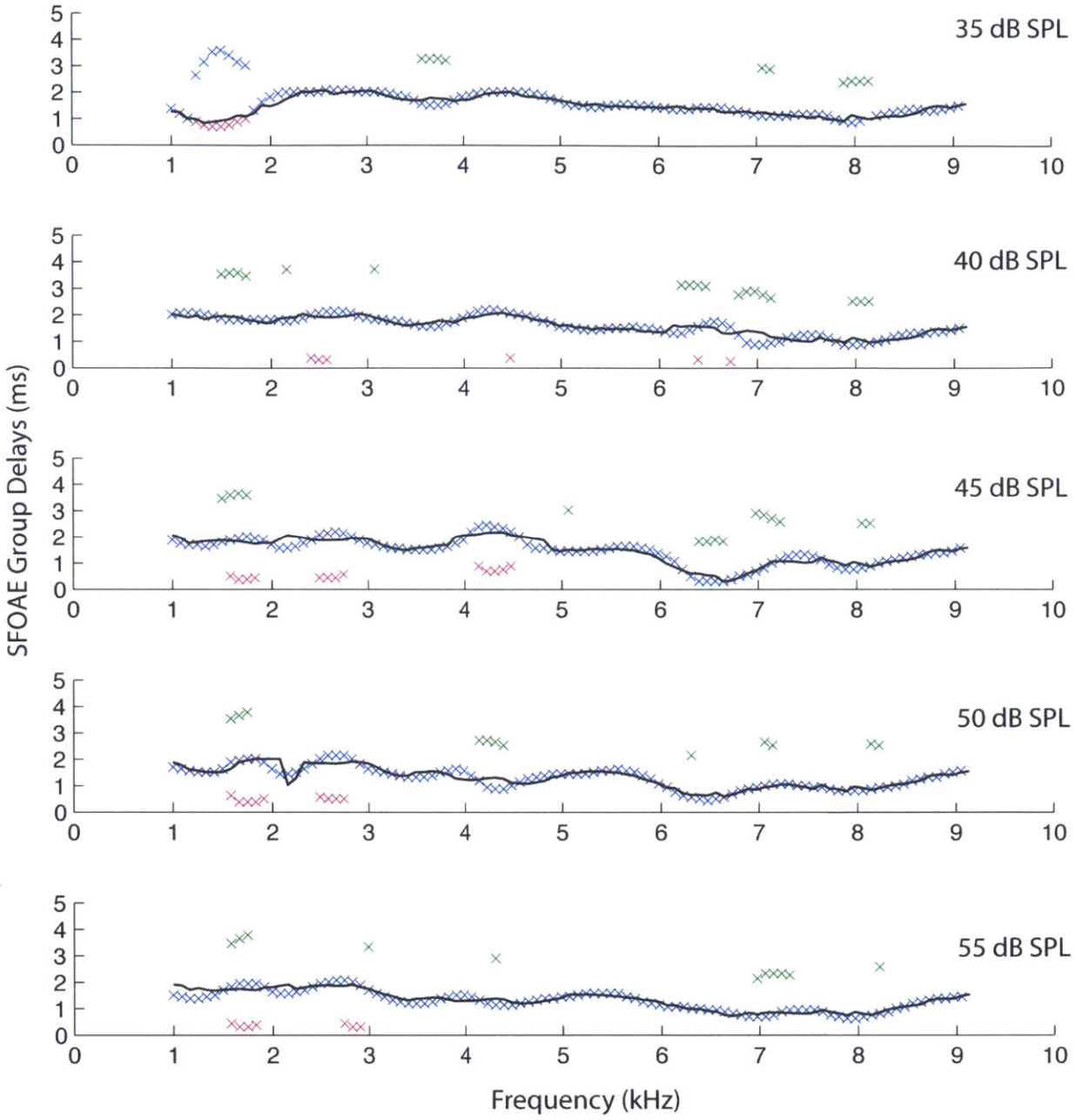

Figure 2.15: SFOAE Group Delays at Different Sound Levels from Guinea Pig 108R.
Each panel shows SFOAE group delays at a different probe-tone level (indicated at the right). The suppressor tone was always 50 Hz higher in frequency and 20 dB higher in level than the probe tone. In each panel: *solid black line* = group delay from the phase-gradient; x's = group delays from TF analysis; blue x's = group delays identified as main component (i.e. a component that agrees with neural delays), green x's = delays that are longer than the main component, and purple x's = delays that are shorter than the main component.

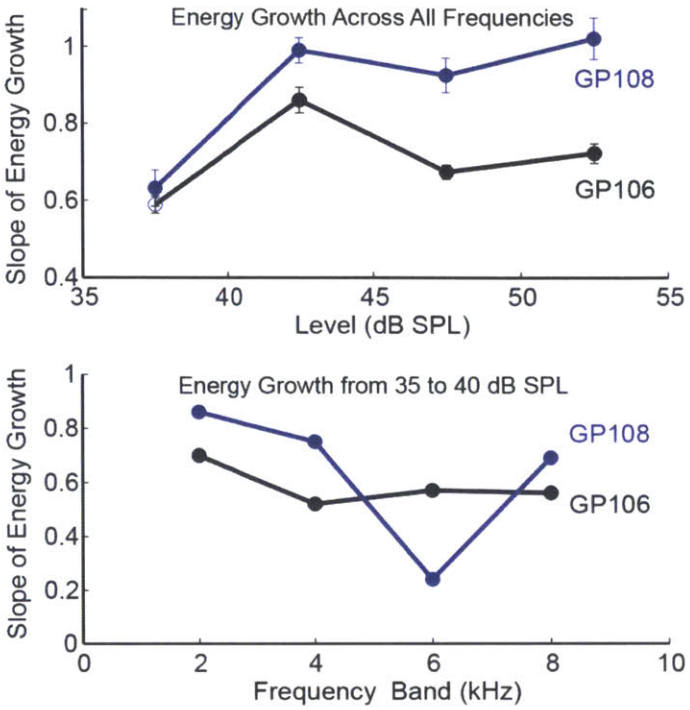

Figure 2.16 Growth of SFOAE Energy Across Level and Frequency.
Top panel: Growth of SFOAE energy across level in two ears (*blue and black solid lines with standard error bars*). *Bottom panel*: Growth of SFOAE energy from 35 dB SPL to 40 dB SPL level in four frequency bands:1-3, 3-5, 5-7 and 7-9 kHz.

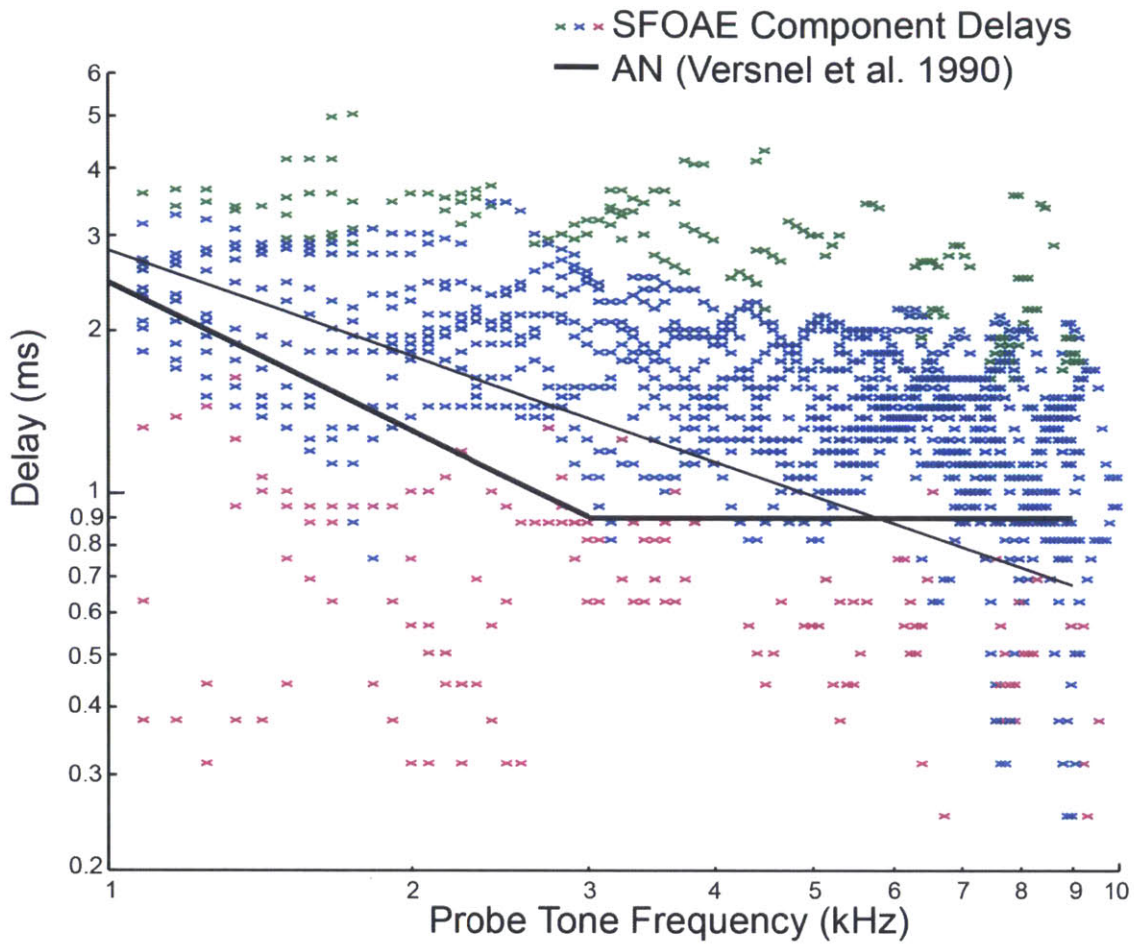

Figure 2.17: SFOAE Group Delays from Time-Frequency Analysis vs. SFOAE Delay Estimated from Neural Data.

*Thin and thick black line*s = estimates of SFOAE delay from single-line and two-line fits to single-auditory-nerve-fiber delays to high level clicks (Versnel 1990). x's = Group delays from time-frequency analysis; blue x's = group delays of components identified as the main component; green x's = delays that are longer than delays of the main component; purple x's = delays that are shorter than delays of the main component;.

Chapter 3: Medial Olivocochlear Efferent Effects on SFOAEs in Guinea Pigs.

3.1 Introduction

Understanding medial olivocochlear (MOC) effects on SFOAEs is valuable for providing a basic understanding of the mechanisms of SFOAE generation. Although it is generally accepted that SFOAEs come from cochlear irregularities that coherently reflect energy in the peak region of the traveling wave (Zweig and Shera 1995), arguments have been made that some SFOAE components arise from the basal part of the traveling wave (Siegel et al., 2005; Choi et al., 2008). Cochlear regions an octave or more basal to the traveling wave peak do not receive cochlear amplification so any SFOAE components that originate from these basal regions should be little-affected by stimulation of MOC efferents.

The fact that SFOAEs can be non-invasively measured in humans means that there is also a clinical usefulness for understanding MOC effects on SFOAEs. There is evidence that MOC efferents have an important role in the protection of hearing from damage due to traumatic sounds and in reducing the effects of auditory aging (Kujawa and Liberman, 2009; Liberman et al., 2014). Because this protection depends on the strength of the MOC reflex, there is clinical interest in the development of techniques for evaluating the strength of MOC efferents. Such tests may be able to discern individuals who are particularly susceptible to damage due to loud sounds so that they can be counseled to avoid noisy conditions or to employ adequate hearing protection. Evaluation of MOC effects on SFOAEs may provide a way of assessing MOC strength. However, before we can determine how well MOC effects on SFOAEs assess MOC strength and predict MOC protection from acoustic trauma, there is a need to understand how MOC efferents affect SFOAEs in the first place.

In this chapter we present data on the effects produced by electrical MOC activation on SFOAEs and SFOAE components with different group delays measured across a wide frequency range in guinea pig ears. There are no comparable data on SFOAEs that we could find in the literature.

3.2 Methods

Albino guinea pigs were anesthetized with Nembutal, followed by Fentanyl and Haloperidol (initial dose of 25mg/kg, 0.2 mg/kg and 10mg/kg respectively). Anesthesia was maintained with supplementary doses of Fentanyl and Haloperidol (every 30 min or when there was a toe-pinch

withdrawal reflex) and Nembutal (every 5 hours or when there was a toe-pinch withdrawal reflex that involved more than the paw pinched). Animals were tracheotomized and mechanically ventilated. The heart-rate, expelled CO_2, body temperature and electroencephalogram (EEG) were continuously monitored. The rectal temperature was maintained at approximately 37°C. The bulla was opened dorso-laterally and a silver wire electrode placed near the round window was used to monitor auditory-nerve compound action potentials (AN CAPs). The cerebellum was aspirated over the floor of fourth ventricle and an MOC stimulating electrode was placed near where the olivocochlear bundle (OCB) crosses the midline. When necessary, animals were paralyzed using Gallamine to eliminate spontaneous middle ear muscle (MEM) contractions and/or MEM contractions due to electrical shocks delivered at floor of fourth ventricle. The strength of the MOC efferent activation was monitored by the shift along the sound-level axis of the growth of AN CAPs in response to clicks that were increased in level in 5 dB steps from below to above the CAP threshold. Experimental protocols were approved by the Mass. Eye & Ear Animal Care Committee.

SFOAE frequency sweeps with MOC stimulation were collected for probe tone frequencies from 0.5 to 9 kHz in 83 Hz steps. To minimize the effects of response drift on the sound level functions, this frequency range was divided into eight blocks each containing 16 frequencies, e.g. the first block had 16 probe-tone frequencies that spanned the 0.5 to 1.8 kHz frequency region and the seventh block had 16 probe-tone frequencies from 7.15 to 8.5 kHz. For each block of frequencies, measurement with and without MOC stimulation were done separately but close in time. The collection of a single block of data included three randomized presentations of the frequencies within the block. At each frequency the average of the three trials was used. To control for drift in the strength of the MOC effect, MOC effects on click level functions were measured before and after every block of data with MOC stimulation. We only considered data from animals and frequency regions that (1) had hearing thresholds below or at 40 dB SPL before and after the data were collected (2) had measurable and stable MOC effects (i.e. MOC effects were present and didn't change by more than 1.5 dB during collection of single block of data), (3) showed no motion and no spontaneous or shock-induced MEM contractions (some animals were paralyzed using Gallamine to eliminate MEM contractions). The presence of spontaneous MEM contractions was assessed by monitoring the ear-canal sound pressure as a

function of time while presenting a continuous low-level, low-frequency (typically a 40 dB, 1000 Hz) tone. Spontaneous MEM contractions produced quasi-periodic, large, brief (~1/2 s) changes in the ear-canal sound pressure that were easily seen. For some of the frequencies within a data-gathering block, a suppressed-OAE test (Lilaonitkul and Guinan, 2009) was done to check that the shocks did not produce MEM contractions. In this test, the suppressor tone was included throughout the measurement so that the SFOAE was suppressed. The result of this is that because the SFOAE was suppressed, any change seen in the ear-canal sound pressure could be attributed to MEM contractions or to motion of the animal in response to the shocks.

A custom-made, three prong. platinum, electrode was used to stimulate MOC efferents at the floor of forth ventricle. Voltage pulses were coupled to two of the prongs via a transformer with a series resistor (usually 2 kΩ). AC coupled, 0.3 ms electrical pulses at a 200/s rate were used as the electrical stimulus. The shock voltage was adjusted to be just below the level which caused muscle movement (except that very weak whisker twitches and eye movements were allowed).

MOC-induced changes in SFOAEs were measured in two steps. First, for every probe frequency, the baseline SFOAE (i.e. the SFOAE without MOC stimulation) was measured by a suppressor paradigm (as in Fig. 3.1B). To do this, a continuous probe tone was played throughout a 100 ms repetition period, and a suppressor tone 50 Hz and 20 dB above the probe tone was presented from 50 ms to the end of each 100 ms period (Fig. 3.1B). 20 responses were averaged and 3-4 averages were obtained, yielding 60 to 80 responses averaged per test condition. Fast Fourier transforms (FFTs) were applied in appropriate time windows to extract the Baseline Total Pressure and the Probe Source Pressure at the probe frequency. The vector difference between Baseline Total Pressure and the Probe Source Pressure (Fig. 3.1A) is the baseline SFOAE without MOC stimulation. In the second step, MOC-induced changes in SFOAEs were measured by presenting a continuous probe tone along with 500 ms duration bursts of MOC shocks every 1500 ms (Fig. 3.1C). Note that the sound was only a probe tone; no suppressor tone was present. 4 to 8 responses were averaged. FFTs were applied in appropriate time windows to extract the Baseline Total Pressure and the MOC-induced total pressure at the probe frequency (Fig. 3.1B). The vector difference between these two measures is the change in SFOAE magnitude (ΔSFOAE) due to MOC stimulation (Fig. 3.1A). The magnitude of the

SFOAE with MOC stimulation (SFOAEmoc) is the vector addition of the baseline SFOAE and the ΔSFOAE (Fig. 3.1A).

CAPs were evoked by 5-ms tone pips with 0.5 ms rise/fall times, spaced every 100 ms throughout a 1500 ms long repetition period. MOC shocks were the same as for measuring MOC effects on SFOAEs. 4 to 8 responses were averaged. The tone-pip-evoked CAP amplitude was measured as the N1-P1 peak-to-peak amplitude. The MOC effect was quantified as the horizontal level shift, i.e., the MOC-induced shift to higher sound levels of the CAP sound-level function. The MOC effect on CAPs was measured at single level, usually 30 or 35 dB SPL, e.g. we determined the interpolated sound level *with-shocks* required to produce a CAP amplitude equal to the CAP amplitude from 30 dB SPL tone pips *without-shocks*. The level shift was the number of dB the *with-shocks* sound level was above the *without-shocks* sound level. The measurement was only done for levels at which the horizontal-shift had well-defined end points, i.e. in the *with-shocks* tone-pip level function, the CAP amplitudes bracketed the *without-shocks* CAP value from 30 dB tone pips, but was not non-monotonic and did not bracket the CAP value *without-shocks* more than once. The overall strength of the MOC effect at a particular shock level was evaluated by obtaining a similar average horizontal level shift on click level functions. The strength of the MOC effect was taken to be the average of the horizontal level shifts across several sound levels, usually 30 to 45 dB SPL.

The time-frequency analysis described in the methods of Chapter 2 was applied to the SFOAE sweeps using the SFOAE measurements averaged over windows that corresponded to times with and without MOC stimulation. The MOC effect on SFOAEs was measured as difference in SFOAE level, i.e. difference between the SFOAE magnitude with MOC stimulation (dB SPL) and the SFOAE magnitude without MOC stimulation (dB SPL).

3.3 Results

Data from 12 ears of 10 animals satisfied all of the control criteria described in Methods. A total of 37 data blocks were collected. In 4 blocks the drift in the strength of the MOC effect was approximately 1 dB, while the rest of blocks had drift in MOC strength less than 0.5 dB. Data for low frequencies (<3 kHz) were collected in 5 ears: the average strength of the MOC effect on clicks across these ears was 3.85 dB horizontal level shift (averaged over 35-45 dB SPL click levels), the standard deviation was 1.1 dB, the range was 2.15 to 5 dB. Data for high frequencies

(>3 kHz) were collected in 9 ears: the average strength of the MOC effect on clicks across these ears was 3.4 dB, averaged over 35-45 dB click levels, the standard deviation was 0.94 dB, the range was 1.97 to 4.49 dB. In many animals, data could not be obtained at mid-frequencies because the threshold at these frequencies was above 40 dB SPL.

SFOAEs from low and high frequency regions collected with and without MOC stimulation from one representative ear are shown in Figures 3.2 and 3.3. MOC stimulation produced both inhibitions and enhancements of SFOAEs (top and bottom panels Fig 3.2). Enhancement in SFOAE dip regions was expected but enhancement in frequency regions with broad SFOAE peaks was surprising (e.g. the 3-4 kHz region in Fig 3.2A, C; see Discussion). In this ear, the MOC effect on SFOAE phase was small (Fig 3.2, B). Time-frequency analysis was applied to the SFOAE data with and without MOC stimulation from this ear. Different latency components observed in the SFOAE data (not shown) were manually classified as either a *main component* or as a component with a longer, or shorter, delay than the main component. The main component was defined as the component whose latency agreed with the SFOAE latency calculated from the two-line fit to the measured single-fiber delays from single guinea-pig auditory-nerve-fiber responses to clicks (Versnel et al., 1990). The single-fiber delays minus the neural conduction times are assumed to equal the forward delay, and were doubled because SFOAEs have both forward and backward travel delays (This is described in more detail in Chapter 2). The main components from SFOAE data with and without MOC stimulation are shown in panel B of Figure 3.3. SFOAE components with and without MOC stimulation, and with delays longer and shorter than the main component, are shown in Figure 3.3C. The MOC effect on the main component was almost always similar to the MOC effect on the whole SFOAE, i.e. the main component was inhibited over regions where the SFOAE was inhibited and was enhanced in regions where the SFOAE was enhanced. Components other than the main component were also affected by MOC stimulation, however, in regions where the overall SFOAE was enhanced or inhibited, there was no consistent pattern as to whether a non-main component was enhanced or inhibited.

Plots of the SFOAE data with and without MOC stimulation are shown in Figures 3.4-3.6 for all of the ears except for GP116L which was already shown in Figures 3.2-3.3. SFOAE magnitudes are shown in Figure 3.4, differences of SFOAE magnitude in Figure 3.5 and

differences of SFOAE phase in Figure 3.6. Small, MOC-induced SFOAE enhancements were observed in one out of five low-frequency segments (Figs. 3.4B-3.5B). At high frequencies, SFOAE enhancements due to MOC stimulation (excluding frequencies near SFOAE dips) were observed in six out of nine data segments (Panels H, J, F, K and L in Figs. 3.3- 3.5 as well in the ear shown in Fig 3.2 and 3.3).

MOC stimulation resulted in both SFOAE phase lags and phase leads relative to SFOAEs without stimulation (Figs. 3.5 - 3.6). A composite plot of SFOAE phase change versus SFOAE magnitude change for individual frequencies across all ears is shown in Figure 3.7. There was no strong relationship between the MOC induced changes in SFOAE phase and magnitude (correlation coefficient of -0.145, $p = 0.001$).

The changes in SFOAE magnitudes due to MOC stimulation as a function of sound frequency for all ears (Fig 3.8A) showed both enhancement and inhibition. To determine if the MOC enhancements might be due to MOC-induced enhancements in cochlear amplification, the data of Fig. 3.8A can be compared with MOC effects on tone-pip CAP level functions that were obtained in some animals. MOC effects on the tone-pips CAPs, measured as the horizontal level shift at 30 or 35 dB SPL, was always inhibitory (Fig 3.8B, plotted negative so that inhibition is down). Although the data showing MOC effects on SFOAEs and CAPs in Figure 3.8 were mostly collected from different ears, in one ear (shown in Figs. 3.4F and 3.5F) CAP level functions with and without MOC stimulation were obtained at frequencies where SFOAEs were enhanced (black circles in Fig 3.8). At frequencies where SFOAEs were enhanced, the MOC effects on CAPs were inhibitory, which indicates that the enhancement effect was limited to the mechanical SFOAE generating mechanism. It appears that the mechanisms that produce SFOAE enhancements don't translate into increased IHC stimulation and consequent neural enhancement.

In the previous chapter we showed that every guinea pig ear had regions over which a time-frequency analysis of the SFOAEs showed two, or sometimes three, SFOAE components with different delays. To visualize how MOC stimulation affected these SFOAE latency components when two or three components were present, the MOC effects on the main components were plotted against the corresponding MOC effects on components longer (Fig. 3.9A) or shorter (Fig 3.9B) than the main component. The results indicate that non-main components can be both

inhibited and enhanced, but the MOC effects on non-main components do not appear to be related to the MOC effects on the main component.

3.4 Discussion

MOC effects on SFOAEs can be both inhibitory and enhancing. Near SFOAE dips in plots versus sound frequency, the magnitude enhancement of an SFOAE can be due to a reduction in the cancellation of the out-phase components that produced the dips in the first place. However, this reduction-of-cancellation mechanism does not explain the increases at, and near, broad peaks in SFOAE magnitude. The fact that we never saw MOC stimulation produce an increase in the amplitude of auditory-nerve CAP responses to low-level tone bursts, suggest that SFOAE enhancement is not a result of an increase of cochlear amplification as seen by IHCs. Based on the MOC effects on CAP responses presented in this and the following chapter (and in other published work e.g. Gifford and Guinan 1987, Guinan 1996), we know of no evidence that MOC stimulation increases cochlear amplification as seen by IHCs.

Our working hypothesis is that MOC stimulation increases SFOAEs by increasing cochlear irregularities. Several lines of evidence are important for this hypothesis: (1) In unpublished work, McCue and Guinan studied the relationship between brainstem shock stimulation of MOC fibers and the responses of individual MOC fibers by recording responses of individual MOC fibers in the bundle of Oort while electrically stimulating MOC efferents at different shock levels and rates. Their data showed that shocks excited only a small fraction of MOC fibers, even though the shocks produced large (e.g. >10 dB) efferent inhibitions. In addition, they found that raising the shock level does not guarantee that all fibers will be excited because MOC fibers showed cathode-surround blocking. When an electrode near a fiber passes current into a fiber that locally depolarizes and excites the fiber, this current must flow out of the fiber on either side of the place where it flows in. If the current level is raised by a factor of 10 above threshold, then the current flowing out of the fiber produces enough local hyperpolarization of the fiber to block passage of the action potential out of the central, excited region. McCue and Guinan found that raising the shock level 20 dB above the level that initially excited an MOC fiber blocked excitation of the MOC fiber as seen by recording in the bundle of Oort. (2) In the experiments presented here, we did not require that data would be used only when the MOC shocks elicited large (e.g. >10 dB) inhibitions, because we wanted to include measurements with MOC

attenuations similar to those found with sound stimulation in humans (i.e. attenuations of a few dB). MOC fibers were excited with high-rate (200 per second) shocks, which is a much higher rate than they are expected to be excited by normal sounds. Nonetheless, exciting a small number of MOC fibers at high rates can produce sizable MOC effects that may be similar to those evoked by sounds that elicit low-rate firing in most or all MOC fibers. (3) A final important observation is that individual MOC fibers have very irregular innervation patterns along the length of the cochlea (e.g. Fig. 3.10; Brown 2014). Electrical stimulation of a few MOC fibers, each with an irregular innervation pattern, will inhibit scattered individual outer hair cells which can be expected to result in increased cochlear irregularity and therefore increased SFOAE amplitudes. In summary, our working hypothesis is that the shock-induced enhancement of SFOAEs is due to an increase in cochlear irregularities produced because only a few scattered OHCs are inhibited by the few MOC fibers activated by the shocks

It is possible that sound stimulation may excite all, or nearly all, MOC fibers at more uniform rates and not produce as much of an increase in cochlear irregularities, which is something that should be further investigated. It is useful to note that this is not the first time the hypothesis that MOC stimulation increases cochlear irregularities has been proposed. Backus and Guinan (2007) put forth this hypothesis to explain the variance in MOC effects on SFOAEs across closely spaced frequencies with sound stimulation in human subjects. More work on this issue is needed.

We examined the MOC effect on the various SFOAE delay components shown by our time-frequency analysis. In general, the main SFOAE component showed the same direction of MOC effect as the overall SFOAE at the same frequency, either increases or decreases. We saw no clear relationship between the direction of MOC effects on the main component, i.e. enhancement or inhibition, and the direction of MOC effects on additional components (Fig. 3.9). The fact that MOC stimulation affected the additional SFOAE delay components revealed by time-frequency analysis suggests that these components are not generated in the basal end of traveling wave, i.e. an octave or more away from peak of the traveling wave.

The fact that MOC stimulation may increase or change the pattern of cochlear irregularities and thereby affect the production of SFOAEs is a phenomenon that can be expected to lessen the correlation between the observed MOC effect on SFOAEs and the actual MOC effect in reducing cochlear amplification. This phenomenon can be expected to affect both SFOAEs and transient-

evoked otoacoustic emissions (TEOAEs). How important this phenomenon is in a clinical setting is unclear. Since sound may evoke activity in all MOC fibers, although at different firing rates (Liberman and Brown, 1986), sound-evoked MOC activity can be expected to produce smaller changes in cochlear irregularities than electrically-evoked MOC activity. This uncertainty just accentuates the need for experiments in humans to determine how well sound-evoked changes in SFOAEs, TEOAEs or DPOAEs provide a useful measure of MOC strength that may predict the degree of MOC protection from acoustic trauma or hearing aging.

3.5 References

Backus BC, Guinan JJ, 2007.Measurement of the distribution of medial olivocochlear acoustic reflex strengths across normal-hearing individuals via otoacoustic emissions. J. Assoc. Res. Otolaryngol. 2007;8:484–496

Brown MC, 2014. Single-unit labeling of medial olivocochlear neurons: the cochlear frequency map for efferent axons. J Neurophysiol 111:2177-2186

Choi YS, Lee SY, Parham K, Neely ST, Kim DO, 2008. Stimulus-frequency otoacoustic emission: measurements in humans and simulations with an active cochlear model J Acoust Soc Am 123, 2651–69

Guinan JJ., Jr. 1996. The physiology of olivocochlear efferents. In: Dallos PJ, editor. The Cochlea. Springer-Verlag; New York:. pp. 435–502.

Gifford ML, Guinan JJ., Jr, 1987. Effects of electrical stimulation of medial olivocochlear neurons on ipsilateral and contralateral cochlear responses. Hear Res.29:179–194.

Kujawa SG, Liberman MC, 2009. Adding insult to injury: cochlear nerve degeneration after "temporary" noise-induced hearing loss. J Neurosci. 29(45):14077–14085.

Liberman MC, Liberman LD, Maison SF, 2014. Efferent Feedback Slows Cochlear Aging. J Neurosci. 34(14):4599–4607.

Lilaonitkul W, Guinan JJ., Jr, 2009. Reflex control of the human inner ear: a half-octave offset in medial efferent feedback that is consistent with an efferent role in the control of masking. J Neurophysiol. 101:1394–406.

Siegel JH, Cerka AJ, Recio-Spinoso, A, Temchin, AN, van Dijk, P, Ruggero, M, 2005. Delays of stimulus-frequency otoacoustic emissions and cochlear vibrations contradict the theory of coherent reflection filtering J Acoust Soc Am 118, 2434–2443

Versnel H, Prijs VF, Schoonhoven R, 1990.Single-fibre responses to clicks in relationship to the compound action potential in the guinea pig. Hear Res 46:147–160.

Zweig G, Shera CA, 1995. The origin of periodicity in the spectrum of evoked otoacoustic emissions J Acoust Soc Am 98, 2018–2047

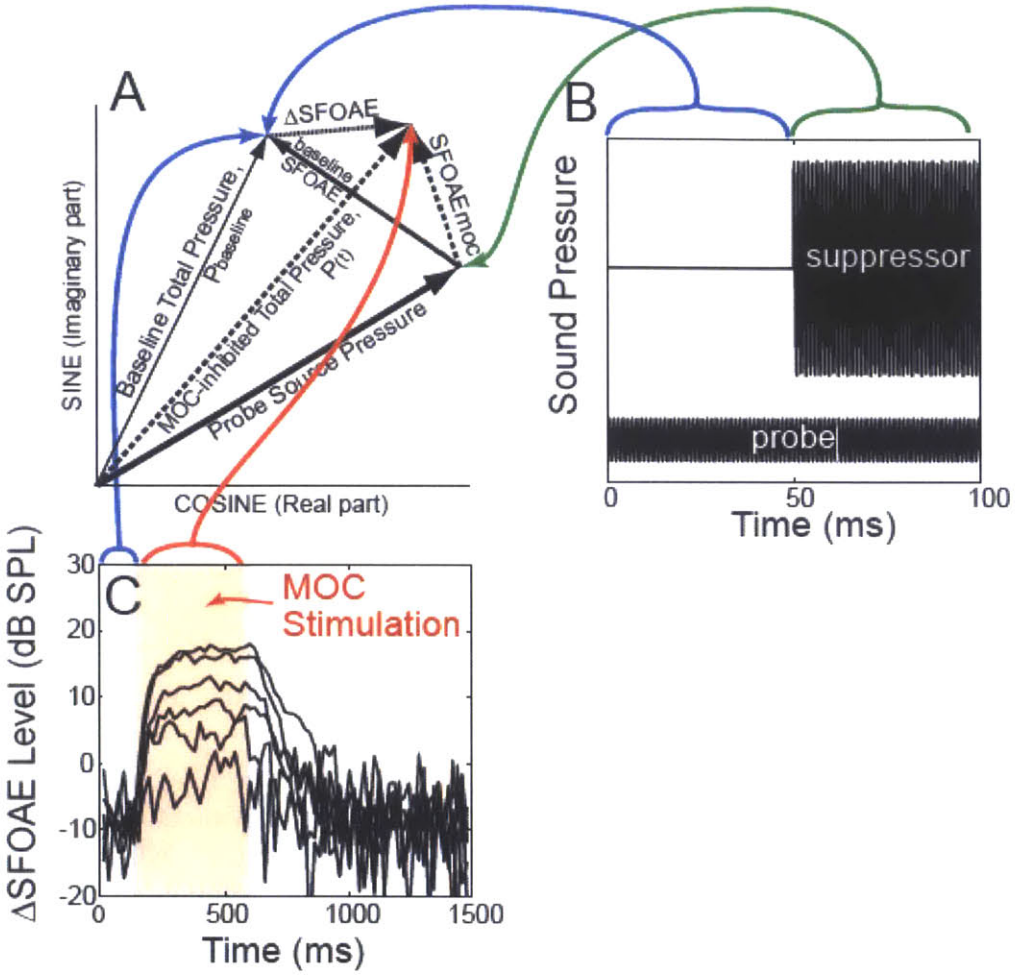

Figure 3.1: Measurement of SFOAE Changes Produced by MOC Stimulation

MOC-induced changes in SFOAEs were measured by presenting a continuous probe tone along with 500 ms duration bursts of MOC shocks every 1500 ms (panel C) The Baseline Total Pressure and the MOC-inhibited total pressure at the probe frequency (panel A) were extracted from the time waveforms (panel C) by fast Fourier transforms (FFTs). The vector difference between these two measurements is the change in the SFOAE (ΔSFOAE) due to MOC stimulation (panel A). The SFOAE with MOC stimulation (SFOAEmoc in panel A) is the vector addition of ΔSFOAE with the baseline SFOAE, which was obtained by the suppressor method (panel B).

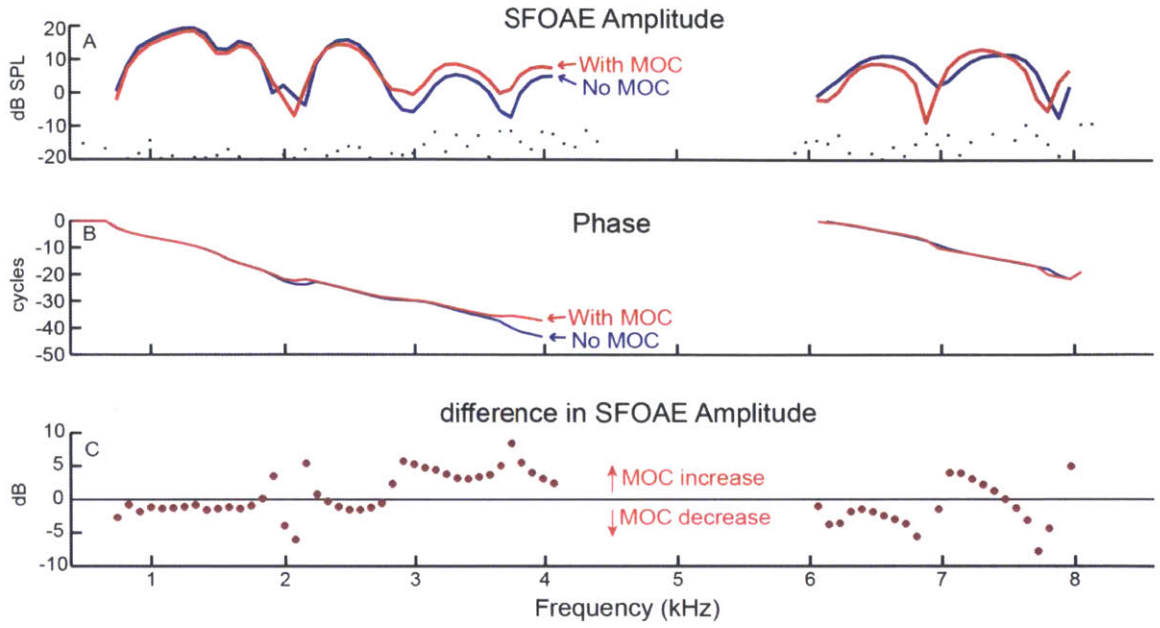

Figure 3.2: MOC Effects on SFOAE Magnitudes and Phases at Low and High Frequencies in one Ear

Panel A: SFOAE magnitudes without MOC stimulation (*blue line*) and with MOC stimulation (*red line*); *black dots* = noise floor. Panel B: SFOAE phase without MOC stimulation (*blue line*) and with MOC stimulation (*red line*). Panel C: *red filled circles* = MOC effects on the SFOAEs (the difference between the SFOAE magnitudes with and without MOC stimulation shown in the top panel). Data from GP116L.

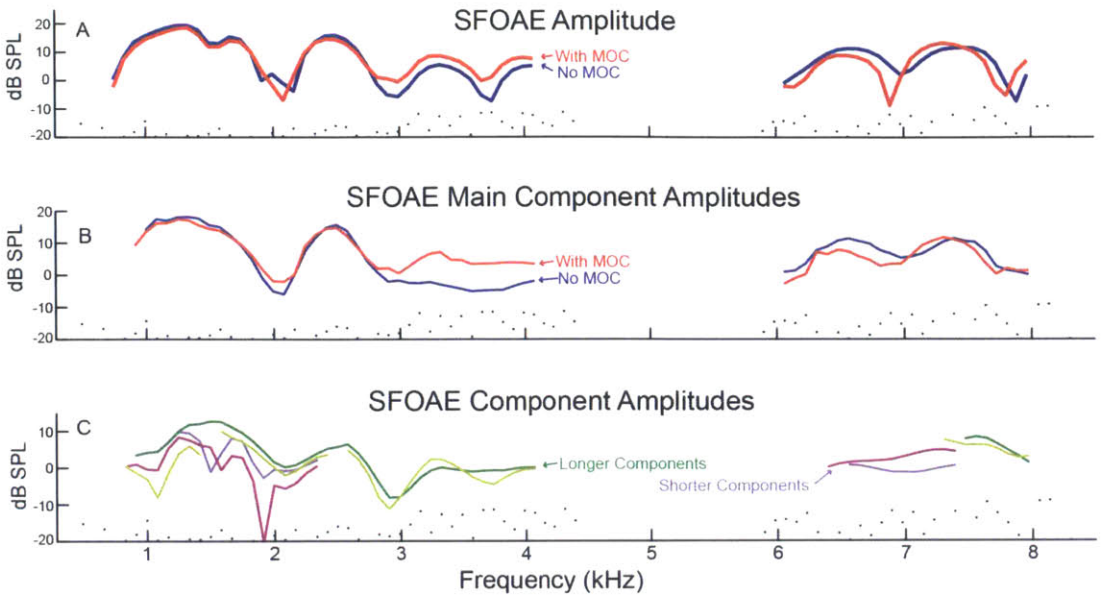

Figure 3.3: MOC Effects on SFOAE Delay Component Magnitudes

Panel A: SFOAE magnitudes without MOC stimulation (blue line) and with MOC stimulation (*red line*); *black dots* = noise floor (same as Fig. 3.2A). Panel B: Magnitudes of the main SFOAE delay components without MOC stimulation (blue line) and with MOC stimulation (*red line*); *black dots* = noise floor. Panel C: Magnitudes of SFOAE delay components longer than the main component without MOC stimulation (*light green line*) and with MOC stimulation (*dark green line*); Magnitude of SFOAE delay component shorter than main component without MOC stimulation (*light purple line*) and with MOC stimulation (*dark purple line*); *black dots* = noise floor. Data from GP116L.

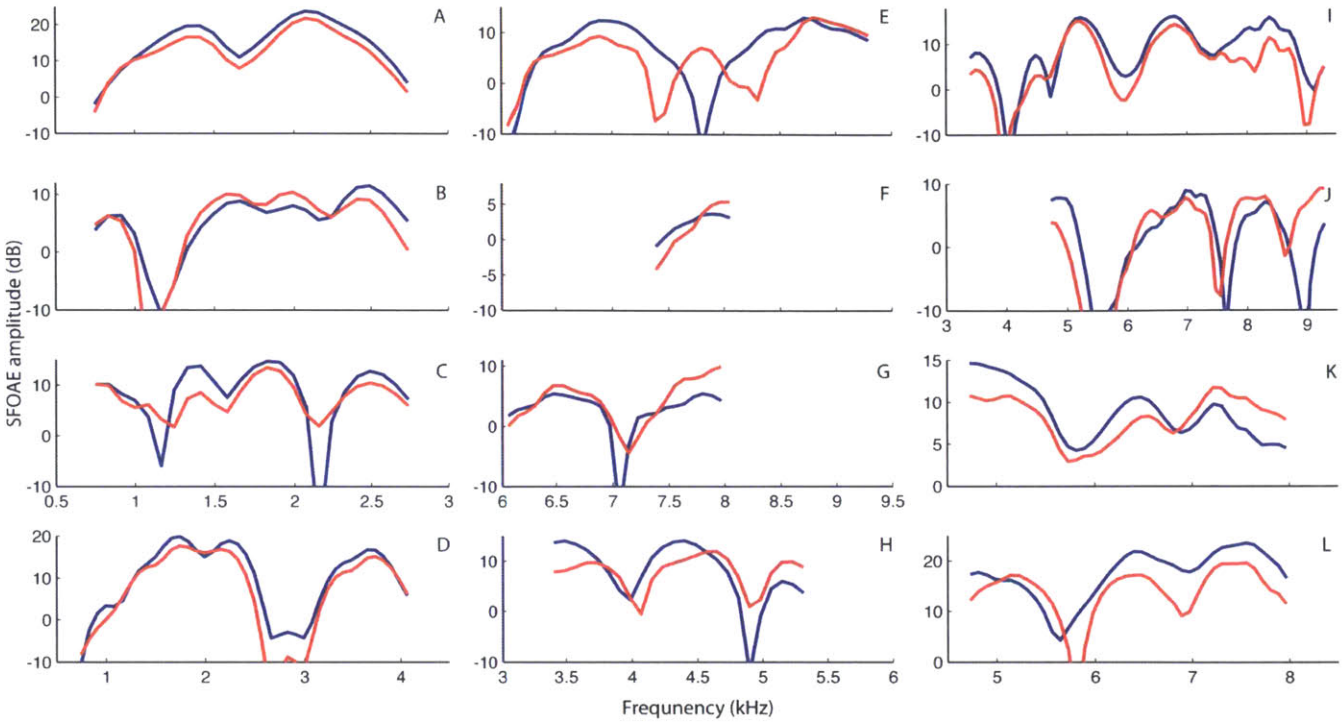

Figure 3.4: SFOAEs with and without MOC Stimulation across Ears and Frequencies

Shown are data from 9 ears in which there were 12 frequency regions over which SFOAEs were collected with and without MOC stimulation (the data in Figure 2.3 are not included). SFOAE without MOC stimulation (*blue lines*) and with MOC stimulation (*red lines*). The following panels have same x-axis: *(A,B,C), (D), (E,F,G), (H), (I,J) and (K,L).* SFOAEs from low frequencies are shown in the left column and in panel H. SFOAEs from high-frequency are shown in the right column and panels E-G.

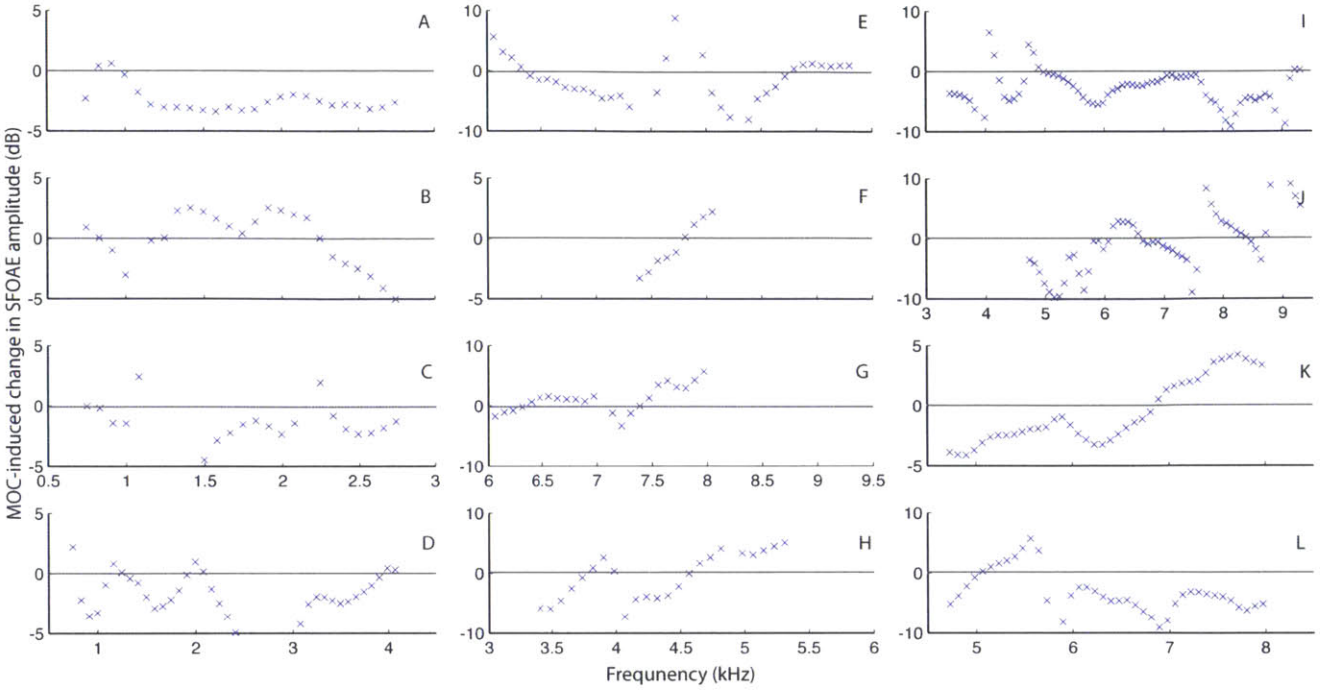

Figure 3.5: MOC Effects on SFOAE Magnitudes Corresponding to the Data in Figure 3.4

Each panel shows difference between the SFOAEs magnitudes with and without MOC stimulation for data shown in Figure 3.4. Panel order is the same as in Figure 3.4. The MOC effect is the difference between the SFOAEs with and without MOC stimulation.

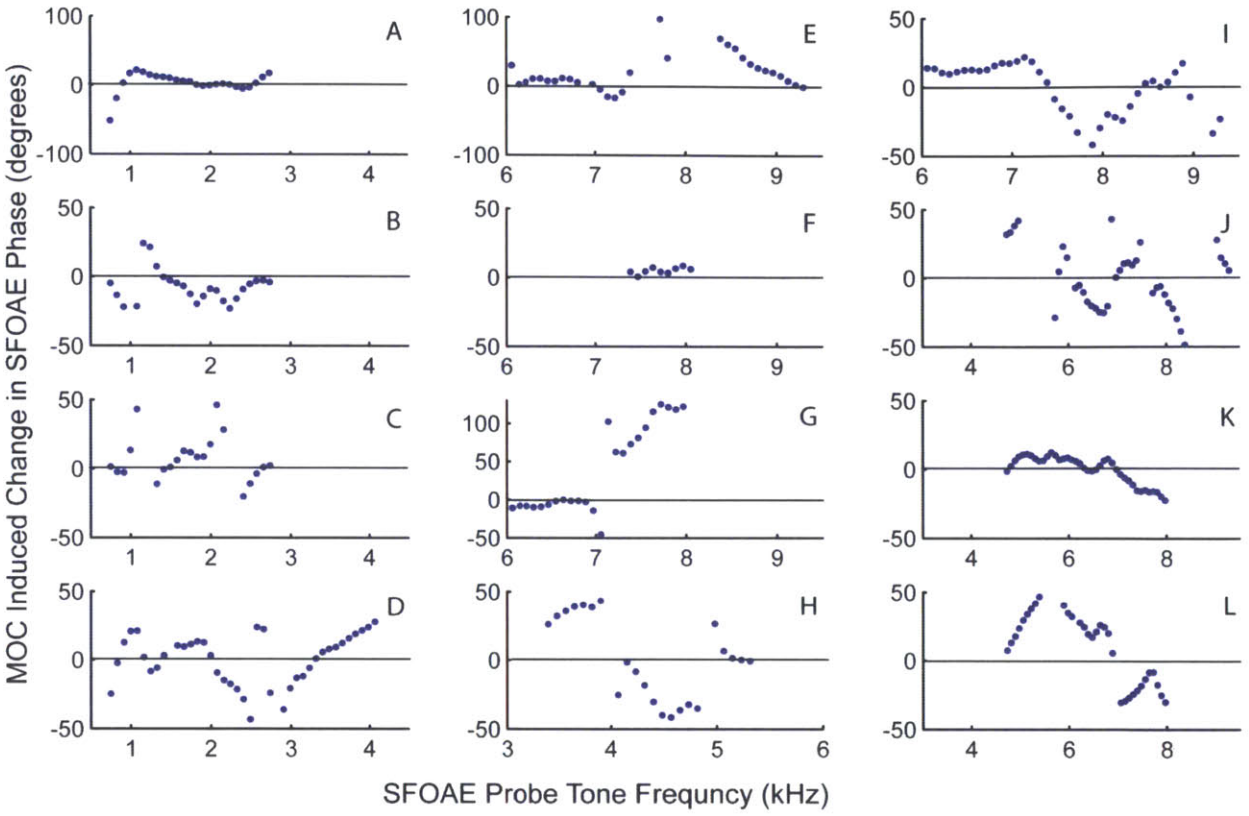

Figure 3.6: MOC Effects on the Phase of the SFOAEs Shown in Figure 3.4

Each panel shows the MOC effect (*blue dots*) on the SFOAE phase. Panel order the same as in Figures 3.4 and 3.5. The MOC effect on phase was the difference between the phase of SFOAEs with and without MOC stimulation.

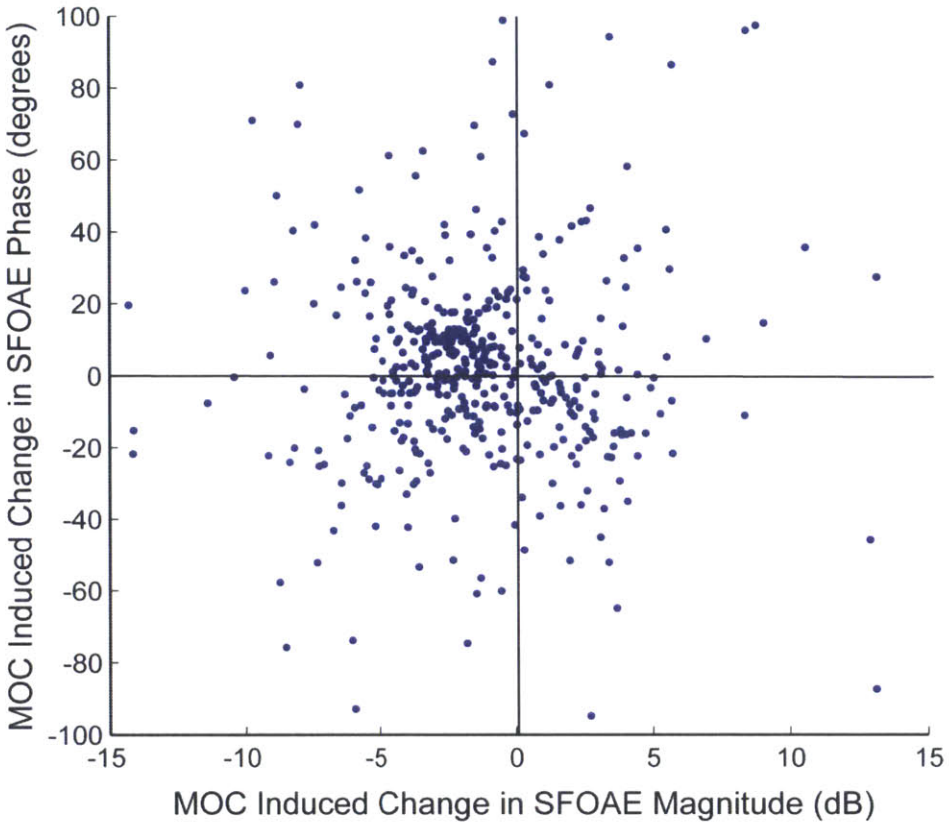

Figure 3.7: The Relationship between MOC Effects on SFOAE Phase and Magnitude

For all frequencies and ears in which SFOAEs with and without MOC stimulation were collected, the MOC effects on SFOAE phase versus the MOC effect on the SFOAE magnitude is plotted (blue dots).

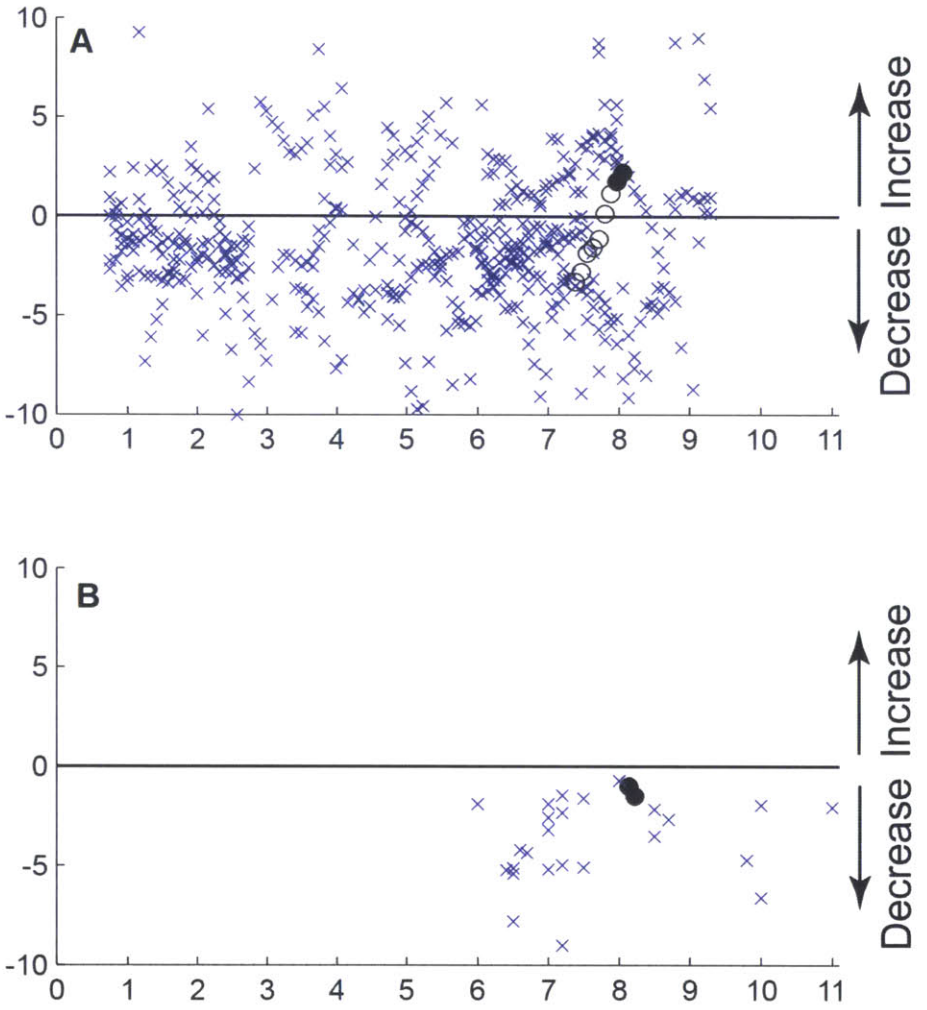

Figure 3.8: MOC Effects on SFOAEs across Frequencies from 10 ears

Panel A: *blue x*'s = MOC effects on SFOAE. *circles* = MOC effects on SFOAEs from ear 120R; *filled black circles* = frequencies at which MOC effects on SFOAEs and CAPs were both evaluated (also shown as black filled circles in the bottom panel). Y-axis is MOC induced change in SFOAE magnitude. Panel B: MOC effects (horizontal level shifts) on CAPs. Y-axis is MOC induced change horizontal level shift of CAP level function mostly at 30 or 35 dB SPL (4 points are at 40 dB SPL level.

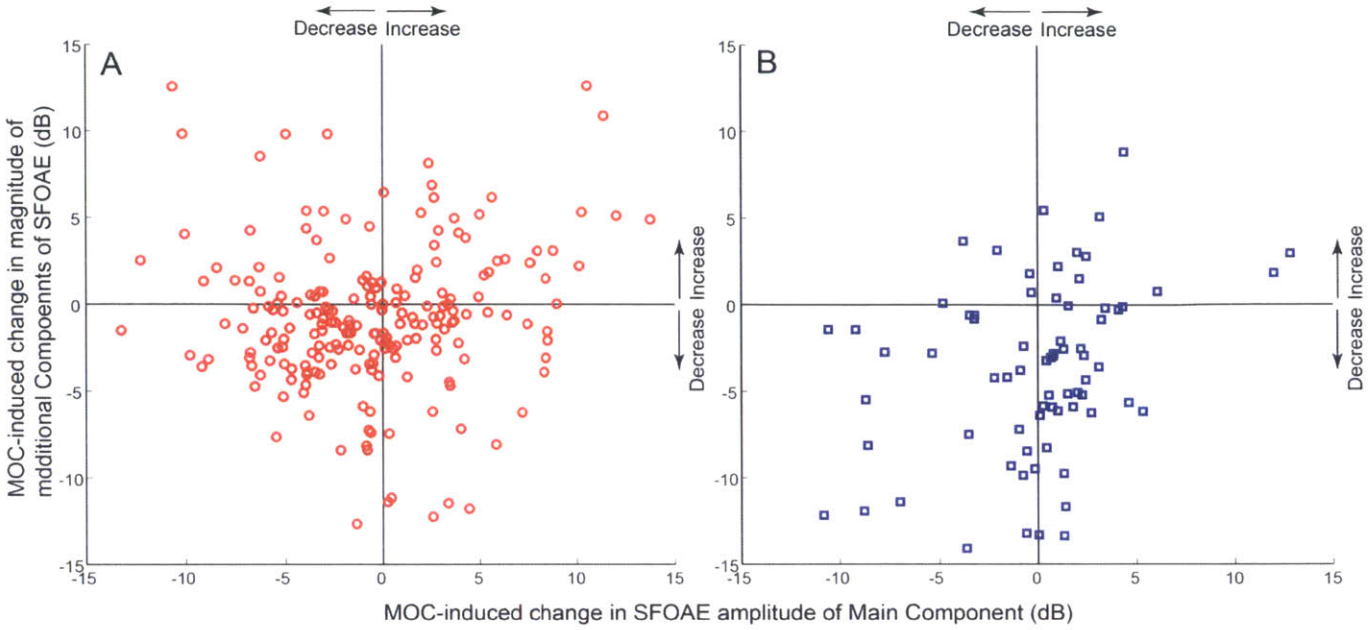

Figure 3.9: The Relationship among MOC Effects on SFOAE Delay Components

MOC effects on SFOAE components longer than the main component (*Red circles on Panel A*) and on SFOAE components shorter than the main component (*Blue squares on Panel B*) plotted versus the MOC effect on the main component.

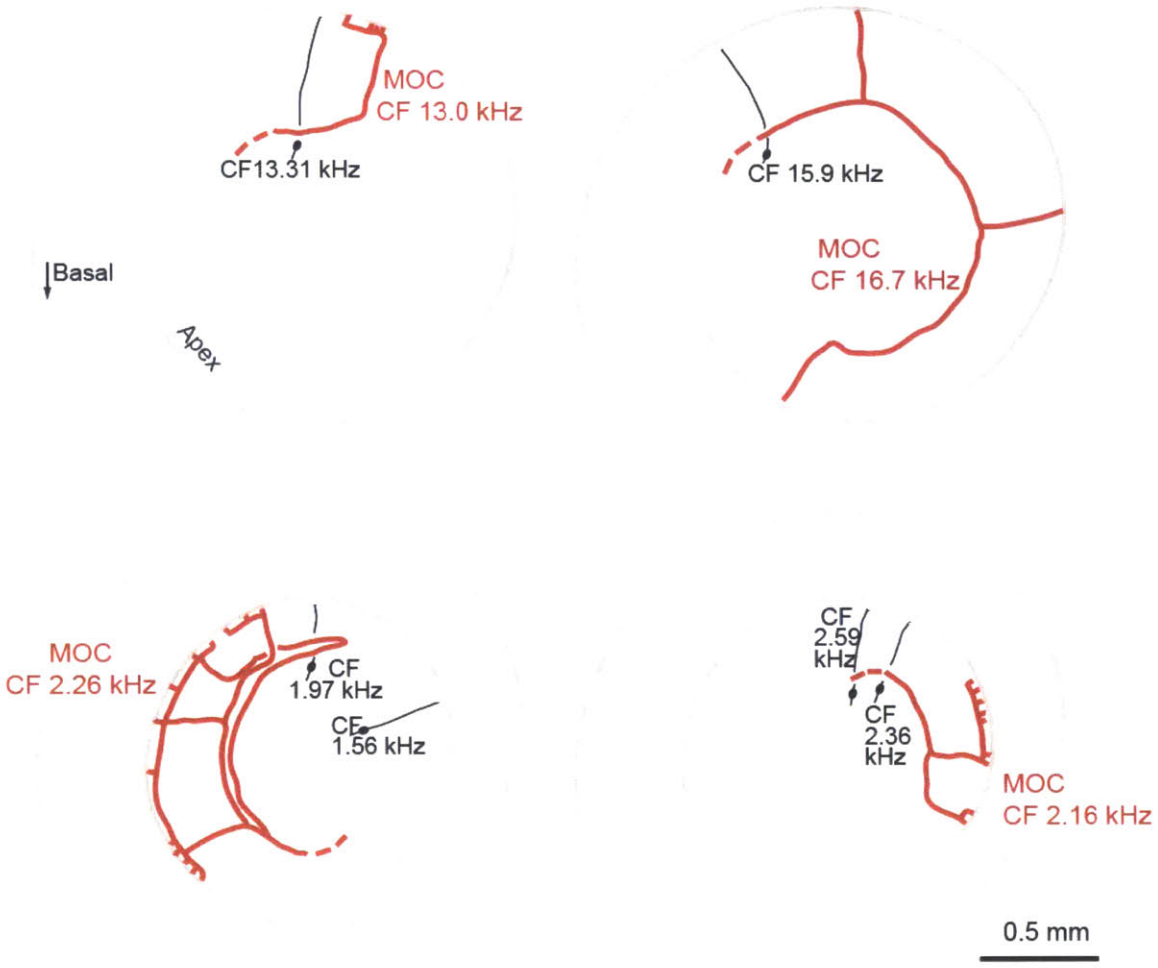

Figure 3.10: Examples of the irregular patterns of the MOC innervation of outer hair cells (OHCs)

Shown are four guinea-pig cochlear spirals (*gray spirals*) each showing a tracing of a single, labeled MOC fiber (*thick red lines*) with their central end shown as a dashed line and places where they innervate OHCs shown by the regions where the red lines end on the gray spirals. One or more labeled Type I auditory-nerve fibers provide characteristic frequency (CF) references. From Brown (2014).

Chapter 4: Medial Olivocochlear Efferent Effects on SFOAEs and CAPs in Guinea Pigs.

4.1 Introduction

Otoacoustic emissions (OAEs) have been used as a non-invasive way to assess the effects of medial olivocochlear (MOC) efferents in humans and laboratory animals. One reason for interest in MOC effects on OAEs is that MOC activity helps to prevent damage due to traumatic sounds, and individuals with weak MOC reflexes may be more susceptible to acoustic trauma. Although in humans MOC effects are most easily assessed by measuring the changes they induce in otoacoustic emissions, the MOC effect that is relevant for hearing is the inhibition of auditory-nerve (AN) fiber responses. There has been little work on the relationship between MOC effects on OAEs and neural responses. Puria et al., (1996) looked at distortion product OAEs (DPOAEs) and found a highly variable relationship between MOC effects on DPOAEs and neural responses. DPOAEs have two source modes which complicates the direct comparison of MOC effects on DPOAEs with those on tone-pip evoked CAPs. In contrast, stimulus frequency OAEs (SFOAEs) have only one source mode which may make them better assessors of cochlear mechanical changes.

Another reason for interest in the comparison of MOC effects on SFOAEs and CAPs, is that at threshold levels, the relationship can potentially be used in understanding the extent to which backward traveling waves are amplified. In some cochlear models, the gain of forward and backward traveling waves are nearly equal (e.g. Zweig, 1991), while in others the gain received by backward traveling waves is different from the gain received by forward traveling waves (e.g. Yoon et al., 2011). At CAP-threshold sound levels, the growth of basilar-membrane motion is approximately linear so the MOC inhibition of CAPs at threshold levels is representative of the gain reduction that forward traveling waves receive. In contrast, at threshold sound levels, the MOC effects on SFOAEs are expected to show how much the gain for both forward and backward traveling waves are reduced.

Testing theories of wave propagation is another reason for comparing MOC effects on SFOAEs and on CAPs. Although it is generally accepted that emissions propagate back to the stapes via slow backward traveling wave on basilar membrane, it has been proposed that

emissions propagate back via fast backward waves (Ren 2004, Ruggero 2004). Alternatively, it has also been proposed that emissions propagate back via waves on Reissner's membrane (Reichenbach et al., 2012). If SFOAEs were shown to receive more gain than CAPs, this would be evidence that SFOAEs were carried backward by slow (amplified) waves.

Stimulus frequency OAEs (SFOAEs) are used in this work because they are evoked by a single tone and may show the relationship between the MOC effects on SFOAEs and on tone-pip evoked CAPs better than DPOAEs (Puria et al 1996).

4.2 Methods

The methods for SFOAE measurements at different frequencies with and without MOC stimulation were described in Section 3.2 (Figure 3.1). Data in this chapter were collected in level function form, i.e. at a single probe tone frequency, SFOAEs with and without MOC situation were obtained over a series of sound pressure levels. Sound level was varied in 5 dB SPL steps over a 25 to 45-50 dB SPL sound range. The suppressor tone was 50 Hz higher in frequency and 20 dB SPL higher in magnitude than the probe frequency.

CAPs were evoked by 5-ms tone pips spaced 100 ms apart in a 1500 ms long repetition period, with MOC shocks the same as for measuring SFOAEs. 4 to 8 shock-burst responses were averaged. Tone pip-evoked CAP amplitudes were measured as the N1-P1 peak-to-peak amplitudes. MOC effect was quantified as the horizontal level shift, i.e., the MOC-induced shift to higher sound levels of either SFOAE or CAP level functions (Fig. 4.1). MOC effects on CAPs and SFAOEs were compared at a single sound level, usually 30 or 35 dB SPL; and in 3 cases in the second data batch, at 40 dB SPL. Comparison was done only at sound levels at which the horizontal shift had well defined end points (Fig 4.1). The strength of the MOC effect was evaluated numerous times throughout every experiment. The metric for the MOC strength was the MOC-induced sound level shift of CAP click level functions averaged across several sound levels (usually 30 to 45 dB SPL).

We compared MOC effects on CAPs and SFOAEs at the same frequency and at the same low sound level ($\leq$ 40 dB SPL), while monitoring the MOC strength to insure that it remained stable. We avoided comparison of MOC effects on CAPs and SFOAEs for sound levels above 40 dB SPL because above 40 dB SPL, SFOAEs grow non-linearly and the excitation of auditory-

nerve fibers that produces CAPs extends over broad regions along the cochlear partition. Most often data were collected in following sequence:

1) A SFOAE frequency sweep was done to identify probe-tone frequencies that had high-amplitude SFOAEs and unwrapped phases that were not near a phase jump. One such frequency was selected and the SFOAE and CAP comparison data were collected at that frequency.

2) As a stability control, the MOC strength, i.e. the MOC effect on click level functions, was measured (as in Fig. 4.1A, except using clicks instead of tone pips).

3) Tone-pip CAP level functions with and without MOC stimulation (Fig. 4.1 A) were collected at the probe-tone frequency identified in step 1. If a low sound level (usually 25- 35 dB SPL) was identified as a potential sound level at which a comparison of MOC effects on CAPs and SFOAE was possible (i.e. the signal-to-noise ratios (SNRs) of both appeared likely to be adequate), then data collection would proceed. If the MOC effect was small, this measurement was repeated several times and the results were averaged. If the CAP amplitude was above the noise floor (~10 μV) only at, or above, 35 dB SPL, then this frequency was considered as not sensitive enough, its data would be abandoned, and data collection would restart with step 1.

4) A SFOAE level function without MOC stimulation was collected that included the sound level identified in step (3). Next, a SFOAE level function at the same sound levels was collected with MOC stimulation. The data were visualized to see if there was indeed a low sound level (< 40 dB) at which a comparison of MOC effects on CAPs and SFOAEs could be made. If it was impossible to make a comparison of MOC effects on CAPs and SFOAEs for a sound level <40 dB SPL, then this frequency and its data would be abandoned and data collection would restart with step 1. After visualization, in the vast majority of times, SFOAE level functions with and without MOC stimulation would be collected at least another time before moving onto step 5. In the data collection for this chapter we avoided frequencies that showed MOC-induced enhancement, i.e. if MOC stimulation shifted SFOAE sound-level functions to lower sound levels, the data collection at that frequency was abandoned.

5) The MOC strength was measured again, to determine if it had changed.

6) Tone-pip level functions with and without MOC stimulation, the same as in step 3, were collected again.

In general it took about one half hour to do steps 1 through 6 at one frequency provided that the data collection did not need to be restarted at a different probe tone frequency at steps 3 or 4. The sound levels at which SFOAE and CAP level functions were collected were always randomized. In a few cases click-level CAP measurements were not done the second time (step 6). Data were not considered at frequencies that did not have MOC strength measurements before and after steps 3 and 4. Data were considered only from animals that had normal hearing before and after the data were collected and had no or few spontaneous MEM contractions at the beginning of experiment.

The data were obtained in two different batches. For both batches spontaneous MEM contractions and motion induced by shocks were monitored. All animals in the second data batch were paralyzed using Gallamine. Animals in first data batch were not paralyzed, but only shock levels that produced minimal (light whiskers twitch) to no motion were used. Another methodological difference between the two data batches is that in the second batch a test was done to check that the shock level used did not induce MEM contractions on every animal at some test frequency.

For Animal Surgery and Experimental Setup refer to previous Chapters. Lack of MEM contractions was controlled by modified version of middle-ear muscle contraction test in Lilaonitikul and Guinan (2009).

4.3 Results

The data were collected in two batches, the first with high-level shocks and the second with low-level shocks. The first data batch had an average MOC strength (the level shift in click-level functions) of 8.9 (SD 2.7) dB and consisted of 28 points from 8 animals and 22 unique probe tone frequencies from 2 to 15 kHz. For all first-batch data, the MOC effect on the CAP was greater or equal to the MOC effect on the SFOAE (Fig 4.2, top). To allow comparisons across frequency and MOC strength, we used the ratio of the MOC effect on the SFOAE to the MOC effect on the corresponding CAP which we call the "Level Shift Ratio". There does not appear to be any dependence of this ratio on probe tone frequency (Fig. 4.2 middle). There is a hint of a dependence of the ratio on MOC strength (Fig. 4.3 bottom).

MOC effects measured in humans with sound stimulation are almost an order of magnitude smaller (e.g. 0.5-2 dB SPL) than what has been typically evoked in animals with electrical stimulation, and so it was of interest to see how MOC effects on CAPs and SFOAEs compared at lower MOC-stimulation shock levels. In one animal, we acquired CAP and SFOAE level functions at the same frequency and four shock levels. Mean SFOAE magnitude and phase level functions for 7.2 kHz tones with and without MOC stimulation for the four shock levels are shown in Figure 4.3. MOC stimulation shifted the sound-level functions to higher sound levels with the MOC effect increasing as MOC shock level increased. The phase of SFOAEs with MOC stimulation lagged the phase of SFOAEs without MOC stimulation and this lag increased with increases in MOC shock level (Fig. 4.3, bottom). Corresponding CAP level functions with and without MOC stimulation at this frequency and these shock levels are shown in Figure 4.4. As with SFOAEs, MOC stimulation shifted the CAP sound-level functions to higher sound levels with the MOC effect increasing as MOC shock level increased. The MOC effects on CAPs and SFOAEs, as functions of shock level, are compared at 30 dB SPL in Figure 4.5. At the highest shock level, the MOC effect was greater on the CAP than on the SFOAE, which is consistent with the data we collected in the first data batch. However at the next two lower shock levels, the pattern reversed and MOC effects were greater on SFOAEs than on CAPs. At the lowest shock level, the MOC effects on both measures were smaller than the range of observed values so the measurements were effectively in the noise. Overall, these data suggested that there was a need to investigate how MOC effects on SFOAEs and CAPs compare at low shock levels, so a second data batch was collected.

The second data batch had an average MOC strength of 3.7 (SD 1.6) dB and consisted of 25 points from 9 animals and 13 unique frequencies that covered approximately the same frequency range as the first batch (Fig. 4.6, center). For the second batch, 8 out 25 points had MOC effects on CAPs greater than MOC effects on SFOAEs. The rest of the points had MOC effects on SFAOEs greater than on CAPs (Fig. 4.6, top). Similar to the first batch, there was no obvious dependence of the level-shift ratio on frequency (Fig. 4.6, middle), but there appears to be a dependence on MOC strength (Fig. 4.6 bottom).

The two data batches are plotted together in Figure 4.7. Overall, the figure shows that the relationship of MOC effects on SFOAEs and CAPs can go either way, meaning that MOC effect

on SFOAE can be larger, smaller or near equal to MOC effect on CAP (Fig. 4.7, top). This appears to be true for all frequencies that were studied (Fig. 4.7, middle). The plot also shows that the Level Shift Ratio depends on the strength of MOC stimulation (Fig. 4.7, bottom). MOC effects on CAPs can be larger than MOC effects on SFEs for the entire studied range of MOC stimulation (points below 1 in Fig. 4.7, bottom). On the other hand, MOC effects on SFOAEs are larger than MOC effects on CAPs only for the lower shock levels (points above 1 in Fig. 4.7, bottom). Overall the Level Shift Ratio was significantly correlated with shock strength ($\rho = -0.56$, $p<0.001$).

4.4 Discussion

Our data show that the ratio of the MOC effects on CAPs relative to the MOC effects on SFOAEs strongly depends on the strength of MOC stimulation (Fig 4.7). MOC stimulation of varying strength was achieved by varying the shock level. The shock level itself is not a meaningful measure because it is highly dependent on the electrode placement. Small movements of the electrode can require large changes in the shock level to achieve the same MOC strength. For shocks that produced MOC strengths less than about 6 dB, the MOC effects were greater on SFOAEs than on CAPs for most of the points (points from the second data batch). For shock levels that produced MOC strengths greater than about 6 dB, MOC effects were greater on CAPs than on SFOAEs for all but three of the points (most of the points from the first data batch). With both batches taken together, there was a highly significant ($p<0.001$) correlation between the Level Shift Ratio and the strength of MOC stimulation. Several possible hypotheses can be considered that may explain why this ratio varies with MOC strength.

The first hypothesis for why the Level Shift Ratio depends on the MOC strength is that the change in this ratio is due to changes in the gain of backward traveling waves which would only affect SFOAEs and not CAPs. The Level Shift Ratio would be near two if backward-traveling SFOAE components receive the same gain as forward-traveling SFOAE components, and if MOC stimulation inhibits both gains equally. For low shock levels, some Level Shift Ratios are near two, consistent with the hypothesis that the forward and backward waves of SFOAEs both receive the same gain and the MOC effects on these gains are similar. However, one ratio point is much greater than two, and the overall ratio decreases as MOC strength increases so that it becomes less than one. To account for this would require a tremendous change in the ratio of the

MOC effects on forward versus reverse traveling waves. There is no known mechanism by which MOC effects would be different on the gain received by forward vs. reverse traveling waves, but such a mechanism cannot be ruled out. Note also that the original goal of using the Level Shift Ratio to determine whether backward traveling waves receive gain is compromised by the fact that this ratio depends on the MOC strength. This goal was also compromised by the hypothesis of the previous chapter that MOC activity can increase cochlear irregularity and thereby increase SFOAEs, because such an increase in SFOAEs would not correspond to an increase in cochlear amplification.

A second hypothesis is that the change in the Level Shift Ratio with shock level is a result of changes in cochlear irregularity produced by the MOC stimulation. Electrical stimulation excites only a small fraction of MOC fibers (McCue & Guinan, unpublished) and MOC fibers have highly irregular cochlear innervation patterns (Brown, 2014), so electrical MOC stimulation may increase cochlear irregularities by inhibiting only a few scattered OHCs (explained more fully in Chapter 3). It seems likely that the ratio of the increase in cochlear irregularities to the MOC inhibition produced is highest at low shock levels (since more MOC fibers excited produce more inhibition and more irregularities, but the irregularities may have less effect because they fill in gaps in OHC inhibitions). Since irregularities increase SFOAE amplitudes and lessen the apparent MOC inhibition, an increase in cochlear irregularities at low shock levels would produce a trend opposite to what is needed to explain the increase in the Level Shift Ratio at lower MOC strengths. However, changes in cochlear irregularities with shock level may play some role in the change in Level Shift Ratio with MOC strength.

A third hypothesis is that MOC fibers are heterogeneous and have heterogeneous effects in the cochlea, and that high-level shocks excite some kind of MOC fiber that low-level shocks do not. There are two known ways in which MOC fibers differ: there are crossed and uncrossed MOC fibers, and within each of these groups the MOC fibers range in size. It is well established that larger myelinated fibers have lower thresholds to extracellular electrical stimulation than smaller fibers. Also, larger MOC fibers are likely to produce more ending within the cochlea than smaller fibers (Brown 1987; Brown, 2014). For the hypothesis that differences in shock excitation of large vs. small MOC fibers produce the dependence of the Level Shift Ratio on MOC strength, larger fibers would have to produce a smaller Level Shift Ratio than smaller

fibers. This might come about because the innervation patterns of larger MOC fibers produce smaller increases in cochlear irregularity than smaller MOC fibers. It is also possible that there are other, unknown differences between larger and smaller MOC fibers.

The MOC-shock electrode was placed at the midline and is therefore closer to crossed MOC fibers than to uncrossed MOC fibers. Thus, as shock level is increased, the crossed MOC fibers are expected to be excited before the uncrossed MOC fibers. Differences between crossed and uncrossed MOC fibers might therefore be responsible for the decrease in the Level Shift Ratio as shock level is increased. One ipsi/contra difference is that relative to ipsi MOCR fibers, contra MOCR fibers have an apical offset in their OHC terminations and a larger span of innervation (Brown, 2014). MOC fibers also terminate on type II auditory nerve fibers within the organ of Corti, and, in some species, on spiral-ganglion cells. Both of these are places where ipsi and contra MOC innervation may be different. To explain the Level Shift Ratio becoming less as MOC strength increases, the uncrossed MOC fibers would have to produce smaller changes in SFOAEs than on CAPs relative to the changes produced by crossed MOC fibers. What anatomical difference between these groups would produce such changes is unknown.

None of these hypothesis are exclusive: all may be contributing to the effects we observed. This work points to several important questions that need to be pursued in future research. First, there are clear anatomical and physiological indications that MOC fibers are heterogeneous and understanding what that heterogeneity is in more detail and what purpose it serves is important for overall understanding of role of MOC efferents. Second, there is a need to understand the differences in electrical vs. acoustic stimulation of MOC fibers. With electrical stimulation a small fraction of the MOC fibers are stimulated at a high rate whereas with sound stimulation a large fraction (perhaps all) MOC fibers are stimulated at much lower rates. Comparisons of MOC effects from electrical vs. sound stimulation are needed to understand the consequences of this difference. Finally, both of these considerations may affect the clinical use of SFOAEs, TEOAEs (which are produced by the same mechanisms as SFOAEs) and even DPOAEs in such things as predicting MOC protection from damage due to traumatic sounds.

4.5 Conclusions

The ratio of the MOC effect on the SFOAE to the MOC effect on the CAP showed a highly-significant decrease ($p<0.001$) as the strength of MOC stimulation was increased. This

observation was unexpected and precludes using the Level Shift Ratio to determine the amount of gain received by backward traveling waves. However, it shows that our understanding of how MOC fibers affect SFOAEs is incomplete and points to their possibly being significant differences in the effects of different populations of MOC fibers, e.g. crossed vs. uncrossed MOC fibers.

4.6 References

Brown, M. C. 1987. Morphology of labeled efferent fibers in the guinea pig cochlea. Journal of Comparative Neurology, 260(4), 605-618.

Brown, M.C. 2014. Single-unit labeling of medial olivocochlear neurons: the cochlear frequency map for efferent axons. J Neurophysiol 111, 2177-86.

Gifford, M.L., Guinan, J.J., Jr. 1987. Effects of electrical stimulation of medial olivocochlear neurons on ipsilateral and contralateral cochlear responses. Hearing Res. 29, 179-194.

Guinan, J.J., Jr., Stankovic, K.M. 1996. Medial efferent inhibition produces the largest equivalent attenuations at moderate to high sound levels in cat auditory-nerve fibers. J Acoust Soc Am 100, 1680-90.

Puria, S., Guinan, J.J., Jr., Liberman, M.C. 1996. Olivocochlear reflex assays: Effects of contralateral sound on compound action potentials vs. ear-canal distortion products. J Acoust Soc Am 99, 500-507.

Reichenbach, T., Stefanovic, A., Nin, F., Hudspeth, A.J. 2012. Waves on Reissner's membrane: a mechanism for the propagation of otoacoustic emissions from the cochlea. Cell Rep 1, 374-384.

Ren, T. 2004. Reverse propagation of sound in the gerbil cochlea. Nat.Neurosci. 7, 333–334.

Reichenbach, T., Stefanovic, A., Nin, F. & Hudspeth, A. J. 2012. Waves on Reissner's membrane: a mechanism for the propagation of otoacoustic emissions from the cochlea. Cell reports 1, 374–384.

Ruggero, M.A. 2004. Comparison of group delay of 2f1-f2 distrotion product otoacoustic emissions and cochlear travel times. ARLO 5, 143-147

Yoon, Y.J., Steele, C.R., Puria, S. 2011. Feed-forward and feed-backward amplification model from cochlear cytoarchitecture: an interspecies comparison. Biophys J 100, 1-10.

Zweig, G. 1991. Finding the impedance of the organ of Corti. J. Acoust. Soc. Am. 89, 1229-1254.

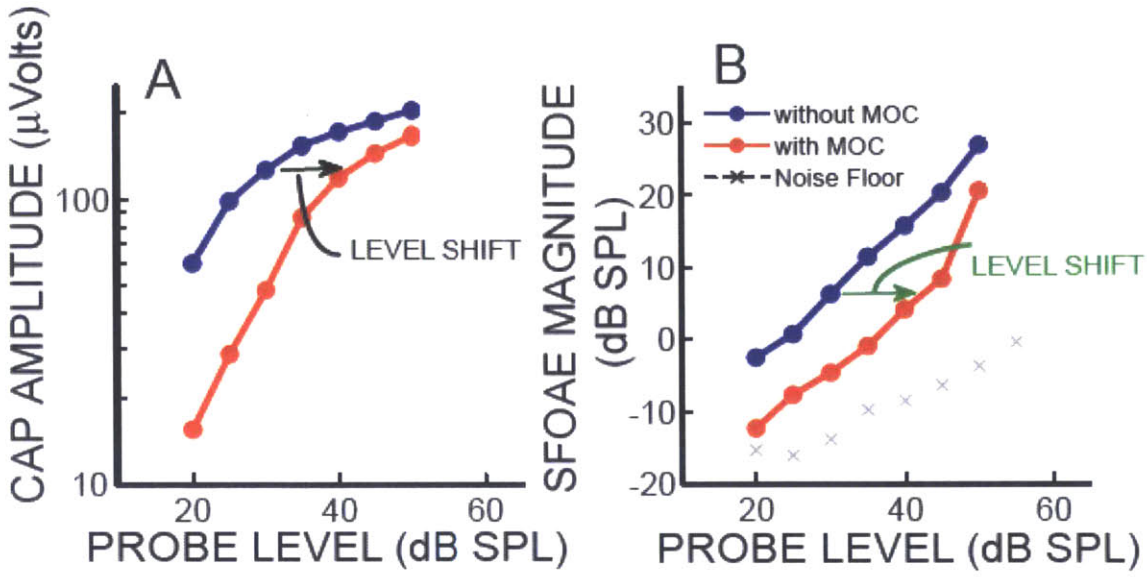

Figure 4.1 Quantification of MOC Effects on CAPs and SFOAEs by Level Shifts

The quantification of MOC-induced CAP (*A*) and SFOAE (*B*) level shifts at a probe level of 30 dB SPL. Blue and red traces represent data recorded at 8.75 kHz without and with MOC stimulation, respectively. CAP and SFOAE level shifts were measured as the increase in probe level needed to obtain a response with MOC stimulation equal to the response without MOC stimulation (horizontal black and green arrows in *A* and *B*). Level shift was defined only for levels that had a well defined end point, i.e. the end points was on a measured data point or on an interpolation between two data points without nonmonoticity producing multiple possible end points.

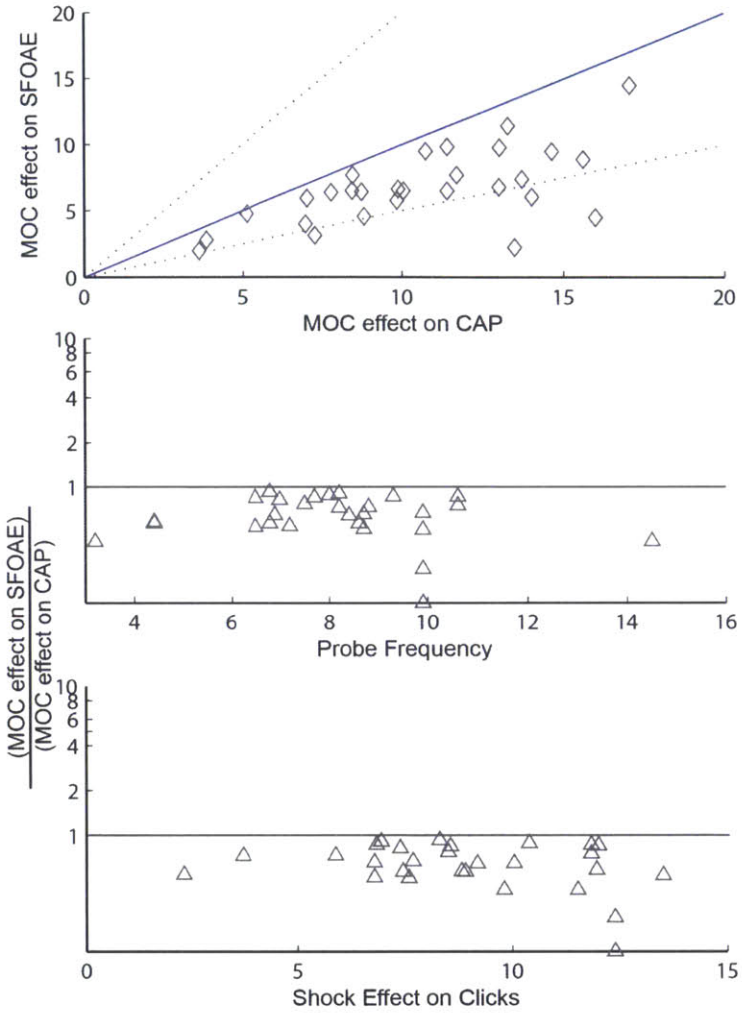

Figure 4.2 Comparison of MOC Effects on CAPs and SFOAEs for High-Level MOC Simulation (First Data Batch)

Top panel: (*Grey diamonds*) MOC effects on SFOAEs vs. MOC effects on CAPs, for different frequencies and animals. *Blue solid line* = Unity line, i.e. a line at which the MOC effect on both measures would be equal. *Dashed black lines* = Lines at which the MOC effect on CAPs is twice or half the MOC effect on SFOAEs.

Center panel: *Grey triangles* = The ratio of the MOC effect on the SFOAE to the MOC effect on the CAP vs. the frequency at which the comparison was made. (y-axis on log scale).

Bottom Panel: *Grey triangles* = The ratio of the MOC effect on the SFOAE to the MOC effect on the CAP vs. the MOC strength, i.e. the MOC effect on clicks at the time the data were collected. (y-axis on log scale).

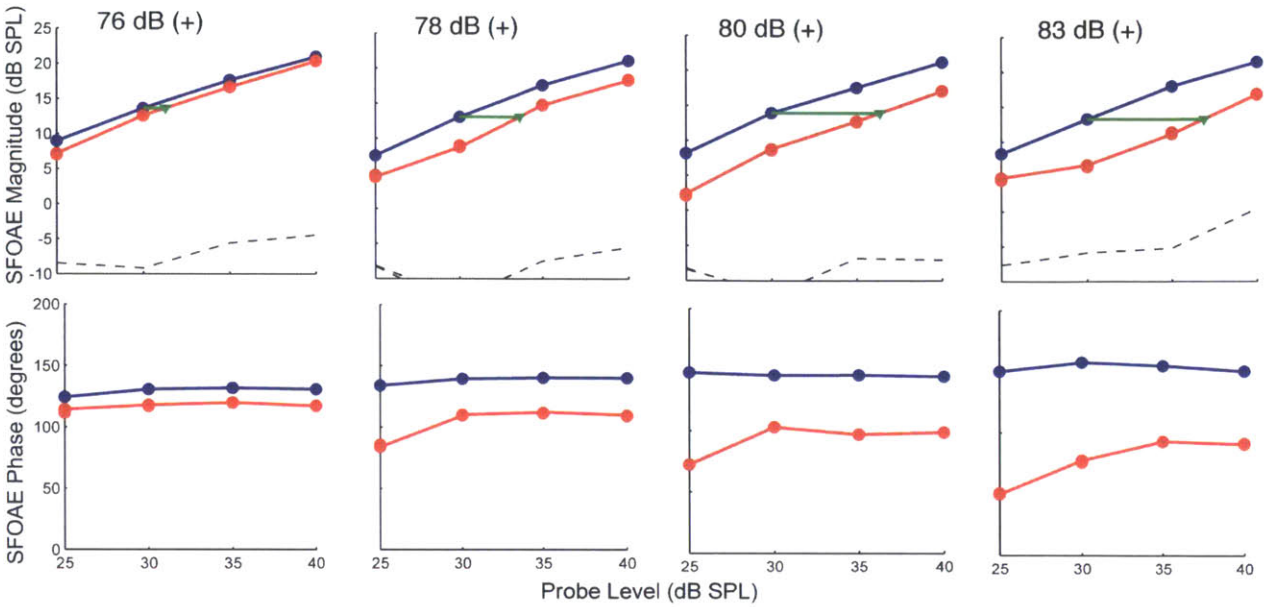

Figure 4.3: MOC Effects on 7.2 kHz SFOAE Level Functions for Different Shock Levels

Top row: SFOAE Magnitude vs. sound-level functions with (*red*) and without (*blue*) MOC stimulation for four shock levels (indicated above each panel, the "+" indicates positive shocks). Black dashed lines are noise floor measurements. The MOC induced level shift in the SFOAE was measured at 30 dB SPL (*Green Solid lines*)

Bottom row: SFOAE Phase vs. level functions with (*red*) and without (*blue*) MOC stimulation for four shock levels

At every shock level the SFOAE level functions with and without MOC stimulation are averages of two measurements. Data from GP84.

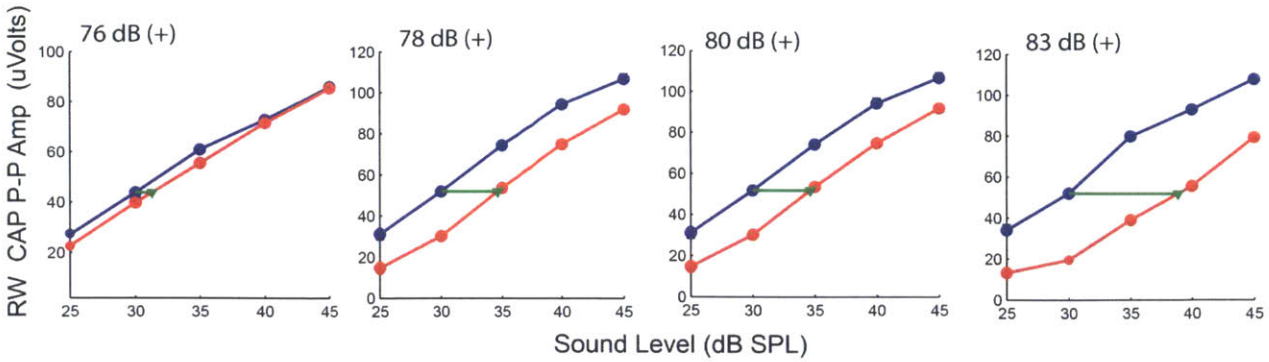

Figure 4.4: MOC Effects on 7.2 kHz CAP Level Functions for Different Shock Levels

CAP Amplitude vs. sound-level functions with (*red*) and without (*blue*) MOC stimulation for four shock levels (indicated above each panel). The MOC induced level shift in the CAP was measured at 30 dB SPL (*Green Solid lines*). At the two highest shock levels, CAP levels functions are averages of two measurements, while at the two lowest shock levels, CAP level functions are averages of 3 and 4 measurements. Data from GP84.

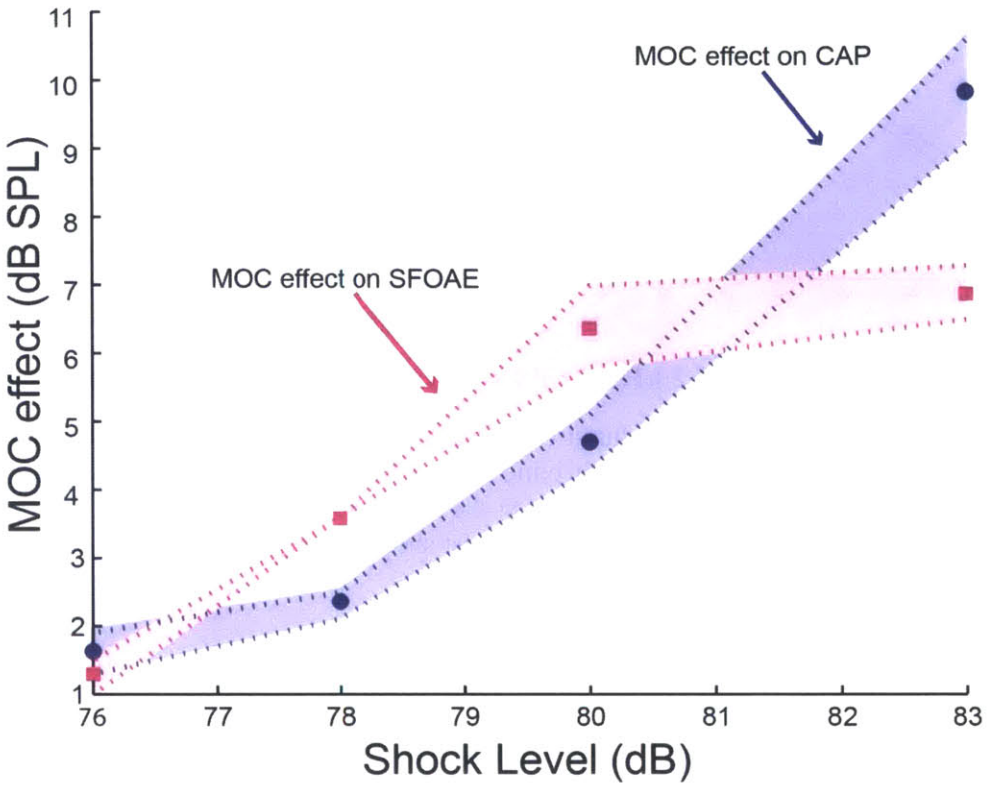

Figure 4.5 MOC Effects on CAPs and SFOAEs as a Function of Shock Level at one frequency.

Red squares = Mean MOC effects on SFOAEs at 30 dB SPL and four shock levels. *Blue circles* = Mean MOC effects on CAPs at 30 dB SPL and four shock levels. *Pink dashed lines* = At every shock level the highest and lowest measured MOC effect on the SFOAEs were used to construct the upper and lower lines, respectively. The area between two lines that defines the range of measured values is shaded pink. At the 78 dB shock level, the same MOC effect on SFOAEs was measured at 30 dB SPL in two different instances. *Blue dashed lines* = At every shock level the highest and lowest measured MOC effect on CAPs were used to construct the upper and lower lines, respectively. The area between two lines that defines the range of measured values is shaded blue. Data from GP84.

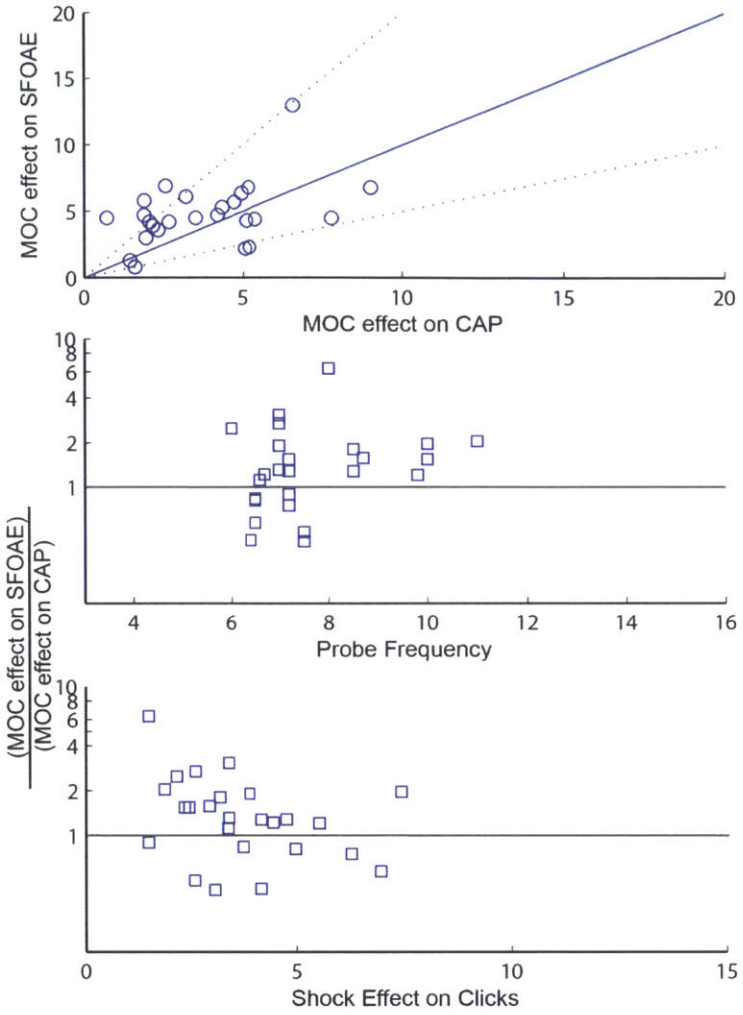

Figure 4.6 Comparison of MOC Effects on CAPs and SFOAEs for Low-Level MOC Simulation (Second Data Batch)

Top panel: *Blue circles* = MOC effects on SFOAEs vs. MOC effects on CAPs for different frequencies and different animals. *Blue solid line* = Unity line, i.e. a line at which the MOC effect on both measures would be equal. *Dashed black line* = Lines at which the MOC effect on CAPs is twice or half the MOC effect on SFOAEs.

Center panel: *Blue squares* = The ratio of the MOC effect on the SFOAE to the MOC effect on the CAP vs. the frequency at which the comparison was made. (y-axis on log scale)

Bottom Panel: B*lue squares* = The ratio of the MOC effect on the SFOAE to the MOC effect on the CAP vs. the MOC strength, i.e. the MOC effect on clicks at the time the data were collected. (y-axis on log scale)

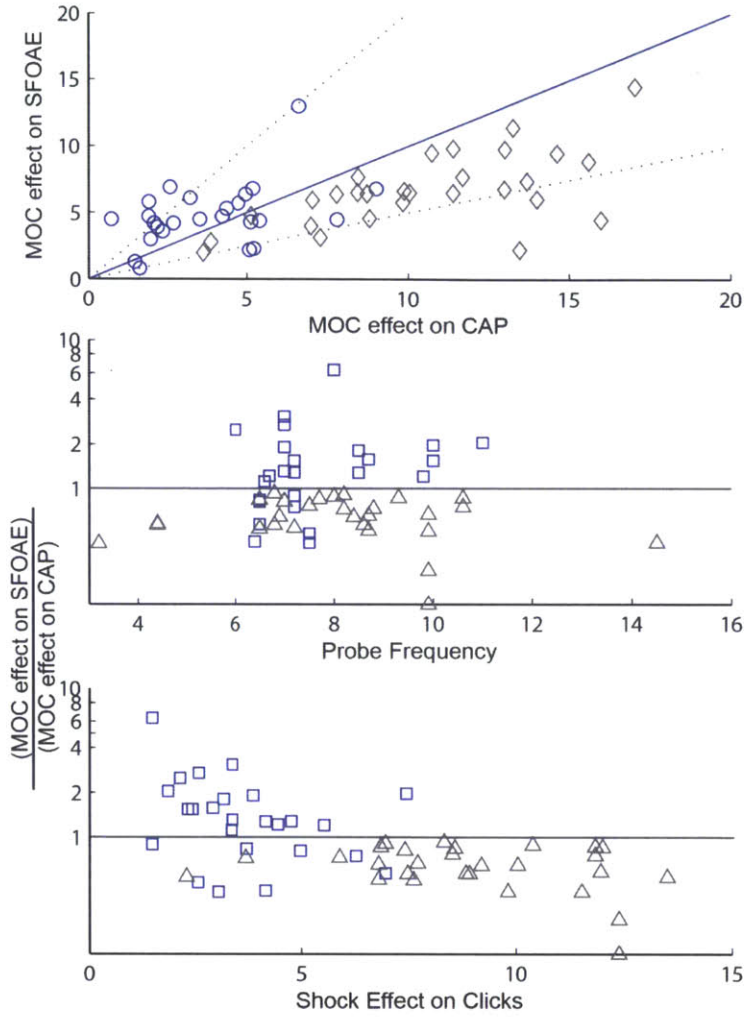

Figure 4.7 Comparison of MOC Effects on CAPs and SFOAEs for All Data

Throughout: *Blue circles and squares* = 2nd batch, *grey diamonds and triangles* = 1st batch. Top panel: MOC effects on SFOAEs vs. MOC effects on CAPs for different frequencies and different animals. *Blue solid line* = Unity line i.e. a line at which MOC effect on both measures would be equal. *Dashed black line* = Lines at which the MOC effect on CAPs is twice or half the MOC effect on SFOAEs.

Center panel: The ratio of the MOC effect on the SFOAE to the MOC effect on the CAP vs. the frequency at which the comparison was made. (y-axis on log scale).

Bottom Panel: The ratio of the MOC effect on the SFOAE to the MOC effect on the CAP vs. the MOC strength, i.e. the MOC effect on clicks at the time the data were collected. (y-axis on log scale).

Chapter 5: Discussion

The three key observations of this dissertation are: (1) time-frequency analyses of SFOAE responses showed multiple latency components in regions near SFOAE-magnitude dips, (2) shock stimulation of MOC efferents resulted in both inhibitions and enhancements of SFOAEs, and (3) the ratio of MOC effects on SFOAEs to the MOC effects on CAPs depended on the strength of the MOC shock stimulation. In this chapter the implications of these observations are discussed and suggestions for further research are made. This is followed by a discussion of some clinical implications of this work as a whole.

5.1 SFOAE Multiple Latency Components

Time frequency analysis of SFOAEs suggests that near the dips in SFOAE-magnitude vs. stimulus-frequency functions, SFOAEs often have two (or rarely three) components with different group delays. Such multiple delays were seen for SFOAEs from guinea pig and chinchillas as well as for SFOAEs simulated by a cochlear model that included coherent reflection (the model described by Shera and Bergevin, 2012, updated for guinea pig delays). We propose that the simple cancellation of wavelets reflected from irregularities within the peak region of the traveling wave can result in multiple SFOAE delay components. Coherent reflection theory predicts that such cancelations will occur and are a major cause of the dips in the SFOAE magnitude vs. frequency functions (Zweig and Shera 1995). When energy from the traveling-wave peak region is canceled, what remains is energy coming from the edges of the peak region. This energy is what produces SFOAE components with shorter and longer delays than the delay that would have originated from reflections from the traveling-wave peak. This mechanism for multiple delay generation should be further evaluated using more detailed cochlear modeling.

At frequencies an octave or more below the best frequency of the cochlear location, motion of the basilar membrane grows linearly with sound level and does not receive cochlear amplification (Robles and Ruggero 2001). Responses at such low frequencies are often referred to as being in the basal part or the "tail" of the traveling wave. It has been proposed that significant SFOAE components are generated in the basal part of the traveling wave (Siegel 2005, Choi 2008). In contrast, we conclude that it is unlikely that any of the SFOAE components revealed by our time-frequency analysis are generated in basal part of the traveling wave.

Electrical stimulation of MOC efferents affected all components of guinea pig SFOAEs, which indicates that all of the SFOAE components arose in regions that received cochlear amplification. In addition, analysis of SFOAEs simulated by a cochlear model with coherent reflection revealed short-latency SFOAE components at frequencies near SFOAE dips; even though the model was constructed in a way that produces essentially no emissions from the basal part of the traveling wave. This demonstrates that the observation of short latency SFOAE components does not imply that the components are generated in basal end of the traveling wave.

Using data from humans, a time-frequency analysis of SFOAEs has suggested that there are two main SFOAE components: the one with the longer latency originating from the peak of the traveling wave, and the one with the shorter latency originating approximately 1/3 of an octave basal to the peak of the traveling wave (Moleti et al., 2013; Sisto et al., 2013). These authors have referred to the shorter-latency component as a component from the "basal" part of the traveling wave; however we believe that this is poor naming, since the so-called "basal" component still arises from within amplified peak region of the traveling wave. Overall, we see no good evidence that any substantial part of the energy in SFOAEs arises far basal (>1 octave) of the peak of the traveling wave.

5.2 Shock Stimulation of MOC Efferents Results in both Inhibition and Enhancement of SFOAEs

We observed that electrical stimulation of MOC efferents resulted in either enhancement or inhibition of SFOAEs depending upon the sound frequency. It is of interest to understand whether similar effects occur in other species, but in the published literature, we could not find a data set comparable to the shock-evoked MOC-effects on SFOAEs collected for this dissertation. Because of the possible clinical use of SFOAEs, it is of particular interest to understand if the phenomenon of MOC-induced SFOAE enhancement (1) occurs with sound activation of MOC and (2) occurs in humans.

We hypothesized the following scenario for how SFOAEs are enhanced by MOC shock stimulation: (1) electrical stimulation of MOC efferents excites only a few MOC fibers, (2) because individual MOC fibers have patchy patterns of OHC innervation (Brown 2014), this results in inhibition of only a few scattered OHCs, which (3) cause a net increase in the cochlear irregularities that produce SFOAEs. Sound stimulation has been reported to activate all, or at

least many, MOC fibers (Liberman and Brown, 1986), which might result in a smoother inhibition pattern, and so it is possible that there would be little or no enhancement of SFOAEs due to sound activation of MOC efferents. This question should be addressed both experimentally and theoretically. There is a need for experimental work that studies sound-evoked MOC effects on SFOAEs over broad frequency regions. Even better would be research aimed at understanding the differences in MOC-induced enhancement versus inhibition of SFOAEs due to electrical versus sound stimulation with both measured in the same animal. It is also of interest to better understand the differences in MOC fiber activation with electrical stimulation versus with sound stimulation. This would require studying responses of MOC fibers with varying shock stimulation and with sound stimulation in same animal. In addition, modeling should be done to understand the extent to which activation of different numbers of MOC fibers with realistic irregular patterns of OHCs innervation can produce SFOAE enhancement or inhibition.

5.3 MOC Effects on CAP and SFOAE Amplitudes Depend on the Strength of MOC Stimulation

The goal of the last thesis aim was to study how MOC effects on auditory-nerve CAPs and on SFOAE amplitudes compare at same frequency and same probe tone level in a given ear. MOC efferents were activated using electrical shocks at the floor of the 4^{th} ventricle, and shock level was varied to produce MOC effects of different strengths. The effects of MOC stimulation were measured by the sound-level shift of CAP and SFOAE level functions. The level shift is a dimensionless, equal-response measure that removes, or reduces, the effects of nonlinearities, thereby making it possible to directly compare MOC effects on CAPs and SFOAEs. The data indicate that the ratio of the MOC-induced changes in SFOAEs to the MOC-induced changes in CAPs depends on the strength of MOC stimulation (The strength of MOC stimulation was measured by the shock-induced level shift in click-evoked CAP responses). This unexpected dependence of the ratio on the strength of the MOC effect was present with high statistical significance. It is conceivable that ratio of the MOC effects on SFOAEs and on neural responses does not depend on the strength of MOC stimulation when MOC activity is elicited using sound, but this remains to be seen. A study is needed of how MOC effects on SFOAEs and neural responses compare when MOC activity is elicited with sound.

It is of interest to understand why the ratio of MOC effects on SFOAEs to those on CAPs depends on the strength of MOC stimulation. If we assume that electrical stimulation activates only a few MOC fibers, then some kind of heterogeneity within the population of MOC efferent fibers could potentially account for the observed dependence. Crossed and uncrossed MOC efferents are one of the likely candidates for different classes of MOC fibers that are differentially activated by electrical shocks in our experimental setup. In all experiments the MOC stimulating electrode was positioned above the *midline* of the floor of the 4th ventricle, so it is likely that at low shock levels only crossed MOC efferent fibers were activated, and as shock level was increased more uncrossed MOC fibers were stimulated. Many anatomical experiments that looked at where on OHCs MOC fibers terminate and what neurotransmitter is used, did not distinguish between crossed and uncrossed fibers. As a result it is unknown if crossed and uncrossed fibers differ in their patterns of OHC innervation. However, uncrossed MOC fibers do have an apical offset in their OHC termination and have larger span of innervation relative to crossed MOC fibers (Brown, 2014). It should be mentioned that we do not believe that our shocks resulted in activation of lateral olivocochlear efferent (LOC) fibers (Gifford and Guinan, 1987).

Another factor to consider in trying to understand why MOC effects on SFOAEs and CAPs were not proportional is our poor understanding of how basilar-membrane and OHC motion are coupled to the mechanical drive to IHCs. MOC effects on CAPs (measured as level shifts) can be thought of as proportional to MOC effects on cochlear amplification as seen by the IHCs. MOC effects on SFOAEs can be thought of as proportional to MOC effects on cochlear amplification delivered by OHCs. The coupling of energy delivered by OHCs into the mechanical stimulation seen by IHCs, and how MOC activation affects this coupling, are not understood (Guinan, 2012). The variability in the ratio of MOC effects on CAPs and MOC effects on SFOAEs across frequencies and across MOC stimulation levels may arise from some variability in how MOC effects on OHCs couple into IHC stimulation. The unexpected dependence of the ratio of MOC-induced changes in SFOAEs relative to changes in CAPs really emphasizes the need for understanding how OHC activity couples into motions of structures in organ of Corti, and more importantly how OHC activity couples into IHC stimulation. According to the traditional view of cochlear mechanics, the structures in organ of Corti move in phase and the motion of basilar

membrane defines the mechanical input to OHCs and IHCs. In recent years there has been a surge of experimental evidence indicating that this traditional view is overly simplistic. While the basilar membrane has a unimodal vibration pattern (Cooper, 1999; Ramamoorthy et al 2014), the reticular lamina and basilar membrane sometimes move out of phase (Chen at el., 2011) and a comparison of motions along the reticular lamina in the radial direction shows evidence of at least two modes of vibration (Ramamoorthy et al 2014). Additionally, the motion of the reticular lamina near the apical part of the OHCs is different from BM motion in tuning and growth with sound level (Zha et al. 2012). These findings indicate that there is a complex a coupling between OHCs and IHCs which is yet to be fully understood. Changes in this coupling could affect the ratio of MOC effects on SFOAEs to MOC effects on CAPs.

5.4 The use of SFOAEs in the Clinic

In this thesis SFOAEs in guinea pigs were studied, however the observations are applicable to mammalian reflection-source emissions in general.

Results from the first and second aims of this thesis (Chapters 2 & 3) contributed to our understanding of how reflection source emissions are generated. In particular this work suggest that reflection source emission appear to have multiple components, however these components are likely to be generated by same reflection mechanism within the amplified peak region of the traveling wave. We studied SFOAEs, and although SFOAEs are not yet used in clinic, TEOAEs are used for determining hearing status and have potential to be used in estimating hearing thresholds (Goodman et al., 2009, Mertes and Goodman 2013). Since TEOAEs, like SFOAEs, are generated by a reflection source mechanism our results likely apply to TEOAEs. Multiple components (short and long latency) have been observed in TEOAEs of normal-hearing human subjects (Goodman et al., 2011) and are likely generated in the same way as multiple components of SFOAEs in guinea pigs. Our finding that the additional, short-latency components are not generated in the basal, non-amplified part of traveling wave is consistent with the observation that both short- and long-latency TEOAE components predicted hearing thresholds when TEOAEs filtered at a certain frequency were used to predict thresholds at that same frequency, but were not predictive of the thresholds at higher frequencies (Mertes and Goodman 2013). This is consistent with all reflection-source components originating near the peak region of the traveling wave and not from more basal, high frequency regions.

The potential use of SFOAEs for the purpose of evaluating the strength of the MOC reflex was one of the motivations for studying MOC effects on SFOAEs (Chapter 3). MOC effects on SFOAEs may be used to estimate how susceptible an individual is to loud sounds that cause permanent threshold shifts. The main goal of the Chapter 3 work was simply to study shock induced MOC effects on SFOAEs. Our work showed that MOC effects on SFOAEs can have both an inhibitory and an unexpected enhancement effect. Clinical application of SFOAEs requires further investigation and understanding of SFOAE enhancement due to MOC excitation. SFOAE enhancement may be a result of the peculiar pattern of MOC fibers excited by electrical stimulation of MOC fibers, thus sound-evoked, rather than shock evoked, MOC effects on SFOAEs may be a better indicator of trauma protection, however that is something that needs to be studied. The use of SFOAEs to estimate the amount of protection from acoustic trauma provided by the MOC system requires experiments in which trauma protection and the change in SFOAEs due to MOC activation are both measured in the same preparation.

MOC efferents may also protect from long-term permanent loss of auditory nerve fibers (auditory-nerve neuropathy) caused by exposure to sounds that produce temporary elevations in threshold (temporary threshold shifts, or "TTS"). Acoustic over stimulation that causes TTS also results in swelling and bursting of auditory nerve terminals on IHCs, and eventually to auditory-nerve neuropathy. Activation of MOC efferents can reduce auditory nerve stimulation by reducing OHC motility and thereby reducing IHC mechanical drive. MOC effects on SFOAEs can potentially be used as a non-invasive measure of how much protection from TTS and from auditory-nerve neuropathy the MOC reflex offers. Since auditory-nerve neuropathy is due to excessive excitation of the auditory nerve, the same factors that influence the ratio of MOC effects on SFOAEs to MOC effects on CAPs may influence how well MOC stimulation reduces the drive to IHCs and thereby reduces auditory-nerve neuropathy. In order to use SFOAEs to non-invasively evaluate how much protection the MOC system offers from TTS and from auditory-nerve neuropathy, there is a need for understanding the relationship between MOC effects on SFOAEs and MOC effects on auditory nerve responses. In this thesis we have started exploring this relationship by systematically measuring shock-induced MOC effects on SFOAEs and on CAPs (Chapter 4). The results show an unexpected relationship between MOC effects on SFOAEs and CAPs that depends on the strength of MOC stimulation. This work is the first

demonstration of this relationship. There is a need for further investigation, including experiments in which sound-evoked MOC effects on SFOAEs and CAPs are studied. Understanding the relationship between MOC effects on SFOAEs and CAPs will help enable experiments that study how MOC effects on SFOAEs are related to the long-term loss of auditory-nerve fibers in animals subjected to TTS. Such experiments can lead to the development of metrics that use MOC effects on SFOAE to predict the protection that MOC activation provides from TTS and auditory-nerve neuropathy.

5.5 References

Brown M.C.,2014. Single-unit labeling of medial olivocochlear neurons: the cochlear frequency map for efferent axons. J Neurophysiol 111:2177-2186

Chen F, Zha D-J, Fridberger A, Zheng J, Choudhury N, et al., 2011. A differentially amplified motion in the ear for near-threshold sound detection. Nat Neurosci. 14:770–774

Choi Y.S., Lee S.Y., Parham K., Neely S.T., Kim D.O., 2008. Stimulus-frequency otoacoustic emission: measurements in humans and simulations with an active cochlear model J Acoust Soc Am 123: 2651–69

Cooper, N.P. 1999. Radial variation in the vibrations of the cochlear partition. In: Wada, H., Takasaka, T., Ikeda, K., Ohyama, K., (Eds.), Recent Developments in Auditory Mechanics. World Scientific, Singapore, NJ.

Gifford ML, Guinan JJ., Jr., 1987. Effects of electrical stimulation of medial olivocochlear neurons on ipsilateral and contralateral cochlear responses. Hear Res.29:179–194.

Goodman, S.S. and Fitzpatrick, D.F. and Ellison, J.C. and Jesteadt, W. and Keefe, D.H., (2009) High-frequency click-evoked otoacoustic emissions and behavioral thresholds in humans. J Acoust Soc Am, 125, 1014-1032,

Goodman, S.S., Mertes, I.B., Scherer, M.P., 2011. Delays and growth rates of multiple TEOAE components In: Shera CA, Olson ES, (eds) What Fire is in Mine Ears: Progress in Auditory Biomechanics, Vol 1403 American Institute of Physics, Melville, New York, USA pp. 279–285

Goodman, S. S., Mertes, I. B., Lewis, J. D., & Weissbeck, D. K., 2013. Medial Olivocochlear-Induced Transient-Evoked Otoacoustic Emission Amplitude Shifts in Individual Subjects. J. Assoc. Res. Otolaryngol. 14, 829-842.

Guinan J.J.Jr. 2012.How are inner hair cells stimulated? Evidence for multiple mechanical drives. Hear.Res. 292, 35–50

Kujawa S.G., Liberman M.C., 2009. Adding insult to injury: cochlear nerve degeneration after "temporary" noise-induced hearing loss. J Neurosci. 29(45), 14077–14085.

Liberman M.C., Brown M.C., 1986. Physiology and anatomy of single olivocochlear neurons in the cat Hear. Res., 24, 17–36

Mertes, I.B. and Goodman, S.S., 2013. Short-latency transient-evoked otoacoustic emissions as predictors of hearing status and thresholds J Acoust Soc Am, 134, 2127-2135

Moleti, A, Mohsin Al-Maamury, A, Bertaccini, D, Botti, T, Sisto, R., 2013. Generation place of the long-and short-latency components of transient-evoked otoacoustic emissions in a nonlinear cochlear model. J Acoust Soc Am 133, 4098–108

Ramamoorthy, S., Zha, D., Chen, F., Jacques, S. L., Wang, R., Choudhury, N., Fridberger, A., 2014. Filtering of Acoustic Signals within the Hearing Organ. The Journal of Neuroscience, 34(27), 9051-9058.

Robles L and Ruggero M.A., 2001. Mechanics of the mammalian cochlea. Physiol Rev 81,1305–*1352.*

Shera, C.A., Bergevin, C., 2012. Obtaining reliable phase-gradient delays from otoacoustic emission data J Acoust Soc Am 132, 927–43

Siegel J.H., Cerka A.J., Recio-Spinoso, A., Temchin, A.N., van Dijk, P., Ruggero, M., 2005. Delays of stimulus-frequency otoacoustic emissions and cochlear vibrations contradict the theory of coherent reflection filtering J Acoust Soc Am 118, 2434–2443

Sisto R, Sanjust F, Moleti A., 2013. Input/output functions of different-latency components of transient-evoked and stimulus-frequency otoacoustic emissions J Acoust Soc Am 133, 2240–53

Zha, D., Chen, F., Ramamoorthy, S., Fridberger, A., Choudhury, N., Jacques, S.L., et al., 2012. In vivo outer hair cell length changes expose the active process in the cochlea. *PLoS One* 7, e32757.

Zweig G, Shera C.A., 1995. The origin of periodicity in the spectrum of evoked otoacoustic emissions J Acoust Soc Am 98, 2018–2047